Università degli Studi di Ferrara

DOTTORATO DI RICERCA IN SCIENZE CHIMICHE

CICLO XXII

COORDINATORE Prof. Gastone Gilli

PHOTOINDUCED PROCESSES IN SUPRAMOLECULAR SYSTEMS FOR SOLAR ENERGY CONVERSION

Settore Scientifico Disciplinare CHIM/03

Dottorando
Dott. Orlandi Michele

_____

Tutore
Prof. Scandola Franco

_____

Anni 2007/2009

Abstract

Artificial photosynthesis, defined as the conversion of solar energy into fuels, could provide a solution to the problem of the intermittent avalaibility of sunlight, one of the key issues to overcome in order to implement widespread use of solar energy. Among the possible applications of artificial photosynthesis, particularly interesting are photochemical water splitting, a possible way to solar hydrogen generation, and the photocatalytic reduction of CO_2 to CO, HCOOH, CH_3OH or CH_4, important industrial intermediates or fuels.

In a biomimetic approach, a generic artificial photosynthetic device consists of an antenna system, a charge-separating reaction center, an oxidation catalyst and a reduction catalyst. Antenna systems absorb visible photons, thus converting them to electronic excitation energy which is then conveyed via energy transfer processes to the reaction center where it drives electron transfer processes leading to charge separation. The photogenerated electrons and holes provide to the catalysts the oxidizing and reducing equivalents necessary to drive redox reactions on a substrate.

In this work, a number of systems proposed as possible components of an artificial photosynthetic device or as models for the investigation of related key processes are studied. The systems described here are designed organizing molecular components in spatially defined architectures, following the principles of supramolecular chemistry.

In particular, Chapter 3 describes a triad for charge-separation obtained by self-assembling of a Ru-porphyrin electron donor, an Al-porphyrin as the photoexcitable chromophore and a naphtalenebisimide electron acceptor. The intrinsically asymmetric nature of triad systems required the development of assembling strategies based on molecular recognition between the subunits, implemented exploiting highly selective metal-ligand interactions. Photoinduced charge-separation was demostrated by a detailed photophysical and electrochemical characterization.

In Chapter 4, a Sn-porphyrin component and a Ru-porphyrin component are combined in a series of tri-, penta- and heptanuclear supramolecular arrays. A number of photoinduced intercomponent electron-transfer processes, leading to a common charge-separated state, could be identified by use of time-resolved UV-Vis absorption and emission spectroscopy and their kinetics rationalized in terms of standard electron-transfer theory.

Chapter 5 describes a model complex of the [FeFe] hydrogenase enzyme active site, tested as a reduction catalyst for photochemical hydrogen production. High turnover numbers were obtained in a photocatalytic cycle using $Ru(bpy)_3^{2+}$ as photosensitizer and ascobic acid as sacrificial electron donor.

In Chapter 6, a kinetic study on $[Ru_4(\mu\text{-}O)_4(\mu\text{-}OH)_2(H_2O)_4(\gamma\text{-}SiW_{10}O_{36})_2]^{10-}$, a recently proposed Ruthenium Polyoxometalate catalyst for the oxygen-evolving side of water splitting, is presented. Hole transfer from photogenerated oxidants to the catalyst has been investigated by means of nanosecond laser flash photolysis, both in solution and at a sensitized TiO_2 surface. The very fast rates observed open the possibility to include $[Ru_4(\mu\text{-}O)_4(\mu\text{-}OH)_2(H_2O)_4(\gamma\text{-}SiW_{10}O_{36})_2]^{10-}$ in photochemical water splitting devices.

Chapter 7 describes the photophysical investigation of supramolecular systems containing a Zn-porphyrin chromophore and the $[fac\text{-}Re(CO)_3(bpy)]^+$ fragment as components. Polypyridine-Re(I)-tricarbonyl complexes are known to catalyze CO_2 reduction, opening the possibility to exploit them for photocatalysis. The results obtained provided guidelines for the realization of new adducts to be tested in photocatalytic cycles.

A side-project in the field of molecular electronics is also reported in Chapter 8. Photoinduced electron transfer is demonstrated here as the working principle of a prototype photochromic switch for non-destructive read-out optical memory systems. The system proposed is composed of a diarylethene as photochromic unit and a perylene bisimide as fluorophore.

In memory of Marco.
Maybe we'll meet again
as highly improbable events
in an highly improbable universe

Table of Contents

Chapter 1

Introduction

1.1 Energy from the sun

According to a recent estimate[1] more energy from sunlight strikes the earth in 1 hour (4.3 * 10^{20} J) than all of the energy consumed by mankind on the planet in 1 year (4.1 * 10^{20} J). The energy to power life on the planet, the fraction intercepted by plants and converted into chemical bonds in the process of photosynthesis, is only a small part of this huge amount. The remaining part represents an incredible opportunity of development for humanity. Besides the scientific and technological advancements already coming from related research, adding sunlight to the pool of our energy sources could provide benefits from a social point of view and help to solve the environmental issues coming from a fossil fuels-based society.

Increasing energy demand and the uneven distribution of energy resources like coal, natural gas and oil shaped our history and our world. Control over strategic resources, energy resources priming among them, has been the cause, although frequently not overt, of wars, occupations, oppression and revolutions. Relying largely on carbon-based sources to meet the increasing energy demand led also to environmental problems. Besides global warming and the climate change, which are finally gathering widespread public attention,[2] pollution has always been the dark side of our energy consumption model, bringing along ecosystem alterations and health-related issues.

Considerations of this nature are forcing a change in the way we produce and use energy that would have been unavoidable in any case, since fossil fuels are not renewable resources, although the actual and estimated reserves could sustain the energy demand increase for centuries to come[3]. There is a growing number of alternatives proposed to implement this change and in the near future the solution will probably be to generate energy in as many different ways as we can, increasingly exploiting renewable and carbon-free sources[4]. In this scenario, solar energy has great potential both as short-term contributor to the energy mix and as a long-term solution, being abundant, clean and carbon-free (except in the case of biomass). Furthermore, solar radiation reaches the whole planet, and is therefore suitable for an highly distributed production model, even to the point of personalized energy,[5] offering the possibility of a secure energy supply not only to rich countries but also to developing countries.

According to a recent estimate,[3] this potential is still largely inexpressed: electricity generated from solar sources accounts for less than 0.1 % of the total, while the figure for

fuels is less than 1.5 % including biomass. In order to implement a widespread use of sunlight as an energy source, two major problems must be solved: costs and the discontinuous nature of solar irradiation.

The current semiconductor-based technology is still expensive[6] when confronted with fossil-fuels based generation methods, altough it must be pointed out that pollution from fossil fuels consumption comes with substantial costs in healtcare and environmental damage which are generally not taken into account4. The quest for alternative materials represents a wide and active research field and in the last decade different approaches emerged, like photoelectrochemical dye-sensitized solar cells,[7,8] generally with still low efficiencies but good perspectives in terms of reducing costs.

Whatever the technology employed for conversion, the intermittent avalaibility of sunlight still makes the development of storage methods a necessity. Phototrophic organisms solved the very same problem using energy from sunlight to drive the synthesis of higly energetic molecules in the process of natural photosynthesis. Following this guideline offered by nature in a biomimetic approach, artificial photosynthesis could represent a long-term solution and thus constitutes an interesting and very active research field.

1.2 Artificial Photosynthesis

In the last decades, investigation of natural photosynthesis and the understanding of some of its basic principles at a molecular level[9] led to the concept of artificial photosynthesis, defined as the conversion of solar energy into fuels.

A generic artificial photosynthetic device requires four functional units: an antenna system, a charge-separating reaction center, an oxidation catalyst and a reduction catalyst. Antenna systems absorb visible photons, thus converting them to electronic excitation energy which is then conveyed via energy transfer processes to the reaction center where it drives electron transfer processes leading to charge separation. The photogenerated electrons and holes provide to the catalysts the oxidizing and reducing equivalents necessary to drive redox reactions on a substrate.

The functions performed by each unit and their coupling in a working device ultimately consists of a number of energy and electron transfer steps, resulting in an energy and charge flow. Controlling the competition between all the possible energy or electron

trasfer processes, in order to direct the flow towards the desired result, represents one of the intrinsic difficulties to overcome in the design of an artificial photosynthetic system. Another problem of central importance is how to couple one-electron reactions (as is the case for photoinduced charge-separation, which is a one photon-one electron process) to the multi-electron reactions generally required for substrate transformation.

The concepts of artificial photosynthesis find a particularly interesting application in photochemical water splitting, that represents a possible way to solar hydrogen generation.[10,11] Being a clean and carbon-free fuel, molecular hydrogen is possibly the best candidate for the role of tomorrows energy vector, replacing oil derivatives as the fuel of choice for transports. However, most of the hydrogen produced today comes from the steam reforming of methane,[12] again a fossil source with all related problems. Instead, photochemical water splitting produces hydrogen in a clean and zero emission process, using sunlight and water as a substrate. A generic water splitting process is reported in equation 1:

$$2H_2O \rightarrow 2H_2 + O_2 \hspace{4cm} \text{eq. 1}$$

this reaction is highly endergonic with $\Delta G° = 474$ kJ/mol. The standard potential $\Delta E°$ for eq. 1 is given by:

$$\Delta E° = -\Delta G°/4F = -1.23 \text{ V} \hspace{4cm} \text{eq. 2}$$

in the framework of artificial photosynthesis eq. 1 can be rewritten as the sum of two redox half-reactions:

$$2H_2O \rightarrow O_2 + 4H^+ + 4e^- \hspace{4cm} \text{eq. 3}$$
$$4H^+ + 4e^- \rightarrow 2H_2 \hspace{4cm} \text{eq. 4}$$

from eq. 3 and 4 is immediately evident the multi-electron nature of the process, hence, a photochemical water splitting system should not only provide the driving force required but also contain catalysts capable of stepwise storage of redox equivalents.

Another example of artificial photosynthesis currently drawing attention[13] is the photocatalytic reduction of CO_2 to CO, HCOOH, CH_3OH or CH_4, important industrial

intermediates, some of which can also be used as fuels ultimately being transformed back to CO_2 in a carbon-neutral cycle.

1.3 Supramolecular systems

The highly efficient molecular machinery behind many biological processes, including photosynthesis, relies on very specific supramolecular structures, the wondrous result of aeons of evolution. Mutuating its basic principles from nature, supramolecular chemistry offers the possibility to organize molecular components in spatially defined architectures through electronically weak interactions, so that single components retain their invidual properties largely unaltered and their combination in suitably designed systems causes intercomponent processes to occur. Through appropriate design it is possible to achieve the vectorial energy and electron transfer at the basis of an artificial photosynthetic device.

In the context of this discipline, a modular approach to artificial photosynthesis emerged.[14] As an example, Scheme 1 shows a generic system where the antenna function is performed by a multichromophoric array and charge-separation is accomplished by a triad system composed of a photosensitizer, an electron acceptor and an electron donor.
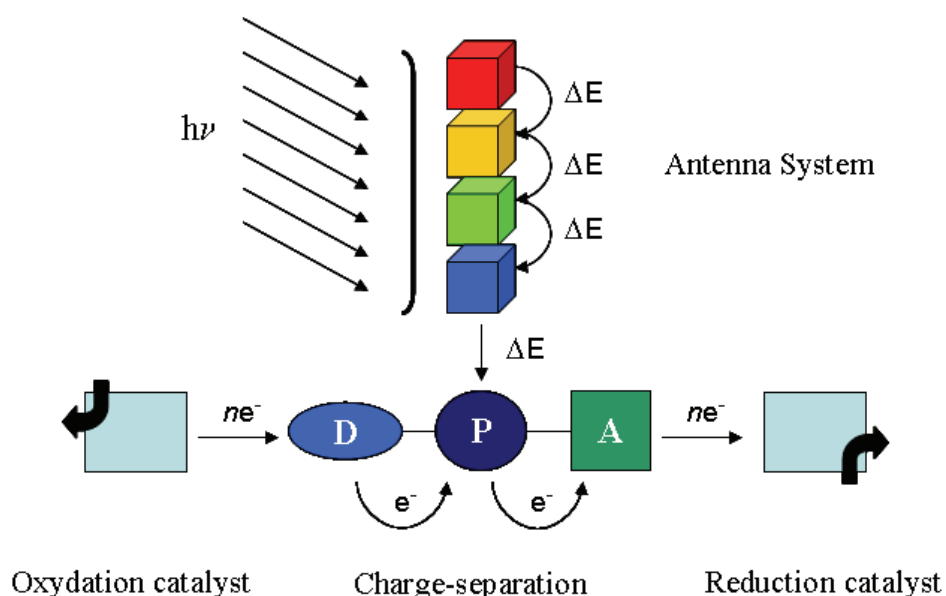
Scheme 1 - Layout for a generic modular artificial photosynthetic system.

1.4 Scope of the thesis

This thesis is a summary of the work done as a Ph.D. student on various supramolecular systems studied as possible components of an artificial photosynthetic device or as models for the investigation of basic properties in this field. Chapter 2 gives an overview of the experimental methods employed, chapter 3 and 4 deal with charge-separating functional units, chapter 5 and 6 with redox catalysts for photochemical water splitting and chapter 7 describes a system related to CO_2 reduction. A side-project in the field of molecular electronics is also reported in Chapter 8, where the same basic processes of electron and energy transfer are employed as working tools for a completely different application.

1.5 References

[1] United Nations Development Program (**2003**) World Energy Assessment Report: *Energy and the Challenge of Sustainability* (United Nations, NewYork).

[2] See the Copenaghen Accord of 18 december **2009**.

[3] N. Lewis, D. Nocera, *Proc. Natl. Acad. Sci. U. S. A.* **2006**, *103*, 15729.

[4] N. Armaroli, V. Balzani, *Angewandte Chemie Int. Ed.* **2007**, *46,* 52.

[5] D. Nocera, *Inorganic Chemistry,* **2009**, *48*, 10001.

[6] Energy Information Administration, *International Energy Outlook,* **2009** (U.S. Department of Energy, Washington DC).

[7] M. Grätzel, *Inorganic Chemistry,* **2005**, *44*, 6841.

[8] T. W. Hamann, R. A. Jensen, A. B. F. Martinson, H. Van Ryswyk, J.T. Hupp, *Energy Environ. Sci.*, **2008**, *1*, 66.

[9] B. Ke, *Photosynthesis: Photobiochemistry and Photobiophysics*; **2001**; Vol. 10. Kluwer Academic.

[10] J. H. Alstrum-Acevedo, M. K. Brennaman, T. J. Meyer, *Inorganic Chemistry*, **2005**, *44*, 6802.

[11] F. M. MacDonnell, *Molecular Approaches to Photochemical Splitting of Water* in *Solar Hydrogen Generation*, Chapter 6, K. Rajeshwar, R. McConnell, S. Licht Ed., **2008**, Springer.

[12] K. Rajeshwar, R. McConnell, K. Harrison, S. Licht *Renewable Energy and the Hydrogen Economy* in *Solar Hydrogen Generation*, Chapter 1, K. Rajeshwar, R. McConnell, S. Licht Ed., **2008**, Springer.

[13] A. J. Morris, G. J. Meyer, E. Fujita, *Acc. Chem. Res.,* **2009,** *42*, 1983.

[14] V. Balzani, F. Scandola, *Supramolecular Photochemistry*, **1991**, Ellis Horwood.

Chapter 2

Experimental Methods
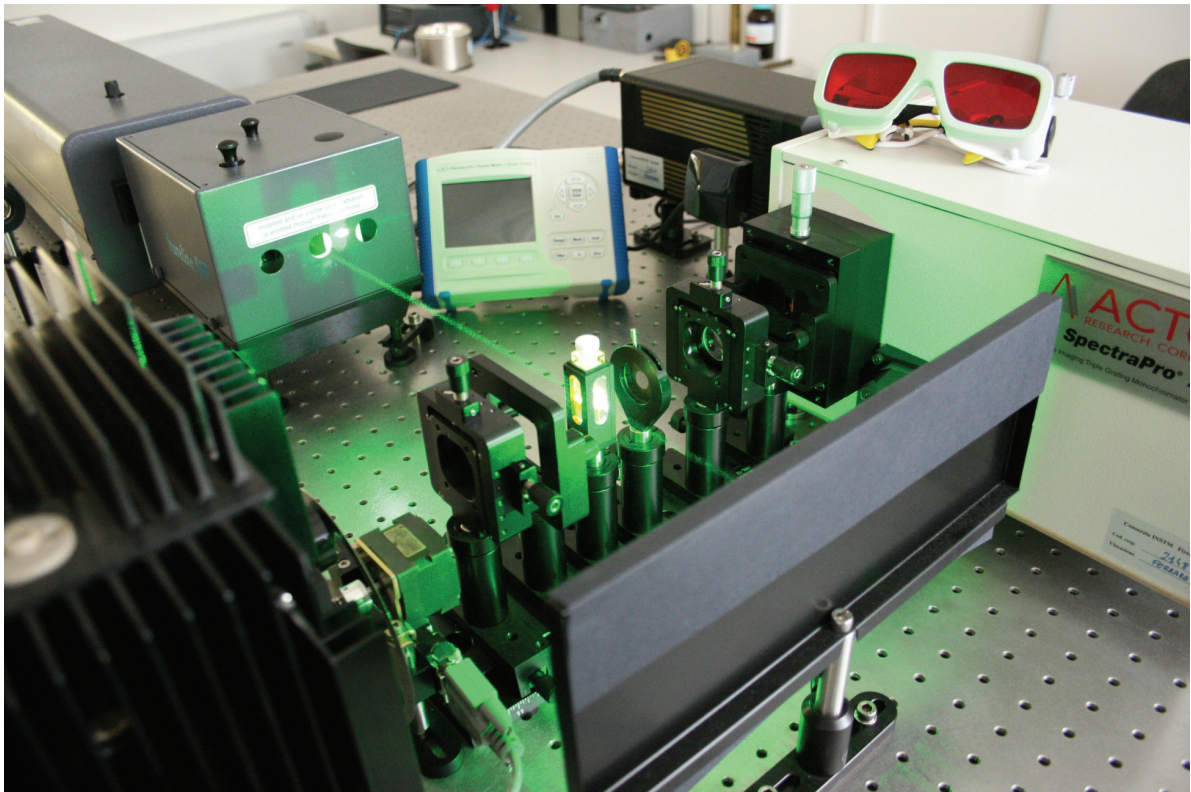
2.1 Electrochemistry

The redox properties of the systems object of this work were investigated by Cyclic Voltammetry (CV) and Differential Pulse Voltammetry (DPV).

The experiments were performed (if not otherwise stated) in a three-compartment cell, with glassy carbon as working electrode, a Pt wire as counter electrode and a Saturated Calomel Electrode (SCE) as reference electrode, using a PC-interfaced Eco Chemie Autolab/Pgstat 30 Potentiostat. Both the counter and the reference electrode were separated from test solution by a frit. In a typical experiment, test solutions were prepared dissolving the sample at a concentration between 10^{-4} M and 10^{-3} M in electrochemical grade solvents containing 0.1 M tetrabutylammonium hexafluorophosphate (TBAPF$_6$) and Ferrocene as an internal standard.

In both techniques the potential applied V is varied with time t and the resulting current i is measured. Plotting current versus potential gives a voltammogram, the analysis of which yields information about the formal potential $E^{0\prime}$ for the reduction or oxidation of an electroactive species, and about the reversibility of the process. Where the techniques differ is in how the potential varies with time: in CV, V is linearly swept back and forth between two set values at a prefixed rate (Figure 1a), while in DPV a series of voltage pulses is superimposed to a linear potential sweep (Figure 2a). The timescale of both experiments is determined by the scan rate.
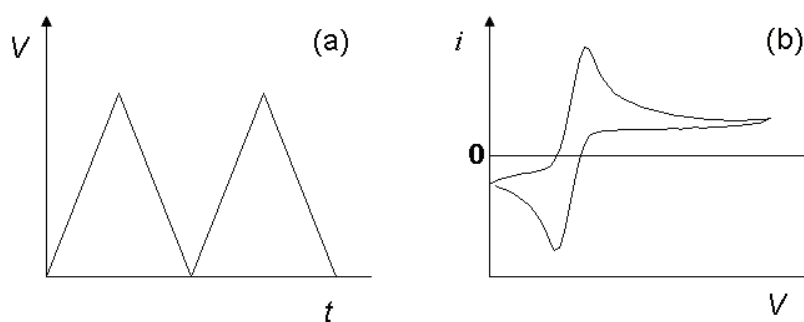

Figure 1. (a) CV waveform showing two cycles (b) CV voltammogram for a reversible process.
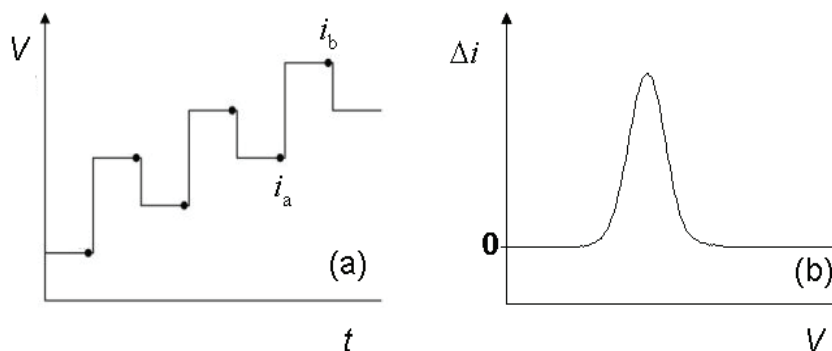
Figure 2. (a) DPV waveform (b) DPV voltammogram for a reversible process. $\Delta i = (i_b - i_a)$.

In the case of CV, a typical voltammogram, like the one shown in Figure 1b, is a plot of the measured current i vs. V, where oxidative current results in a positive wave with a maximum (anodic peak, at potential E_{pa}) and reductive current in a negative wave with a minimum (cathodic peak, at potential E_{pc}). If the process is reversible then current values at the two peaks are the same and $E^{0'} \approx E_{1/2}$ where $E_{1/2} = (E_{pa} + E_{pc})/2$. In the case of DPV (Figure 2b) instead the plot is of $\Delta i/V$, where Δi is the difference between currents sampled before and at the end of each potential pulse. For a reversible process the result is a symmetric peak for which holds the relation $E_{1/2} = E_{peak} + \Delta E/2$ where ΔE is the pulse potential.

An irreversible process is more easily identified from a CV voltammogram, while its potential is more accurately obtained from DPV. DPV provides also a superior peak resolution, useful in the case of two or more processes taking place at similar potentials.

2.2 UV-Vis Spectroscopy

Interaction with visible light has been studied employing conventional stationary techniques (UV-Vis absorption and emission spectroscopy) alongside time-resolved absorption and emission techniques. Except for the data of Chapter 5, UV-Vis absorption spectra were recorded with a Jasco V-570 UV/Vis/NIR spectrophotometer and emission spectra were taken on a Spex-Jobin Ivon Fluoromax-2 spectrofluorimeter, equipped with Hamamatsu R3896 photomultiplier tube. Time resolved methods will be described in some detail in the next sections.

19

Ultrafast transient absorption spectroscopy

Ultrafast transient absorption spectroscopy experiments were performed using a pump-probe setup based on the Spectra-Physics Hurricane laser source and the Ultrafast Systems Helios spectrometer.

A scheme for the setup used is shown in Figure 3. The laser source is a Spectra-Physics Hurricane Ti-sapphire regenerative amplifier system which employs a Mai-Tai Nd:YLF as seed laser. Radiation from this source is a 800 nm laser pulse with 1 mJ power, 1 kHz frequency and 100 fs duration (FWHM). The output beam is split in two different beams, one will become excitation light (pump) and the other analysis light (probe).

Excitation light with a wavelength in the range 320-700 nm is obtained from 800 nm light with an optical parametric amplifier (Spectra-Physics OPA 800), or in alternative 400 nm light is obtained from a second harmonic generator (SHG). The output beam is then directed on the sample after passing through a 30 Hz optical chopper (Scitec Instruments 320 C).

In order to obtain the analysis light the second 800 nm beam is directed into a delay line (Physik, Instrumente M-415 DG 150 mm linear positioning stage), a corner retroreflector mounted on a track and moved by a stepping-motor which introduces a variable delay on the time at which the probe beam hits the sample respect to the pump beam. The output from the delay line is directed on a sapphire plate (Crystal System Inc., HEMLUX grade) where it generates a white light beam which is then overlapped with the excitation beam on the sample.

Solution samples are studied in 1 mm or 2 mm optical path quartz cells, under continous stirring in order to minimize degradation. Transmitted light is analyzed with a spectrometer (Ocean Optics PC2000, 2048-element linear silicon CCD detector). Transient absorption spectra are obtained averaging 4000 experiments at every delay line position. A data acquisition software (Ultrafast System, DAQ) controls the spectrometer, the optical chopper and the delay line. Effective time-resolution is about 300 fs and temporal window of the experiment is about 1 ns.
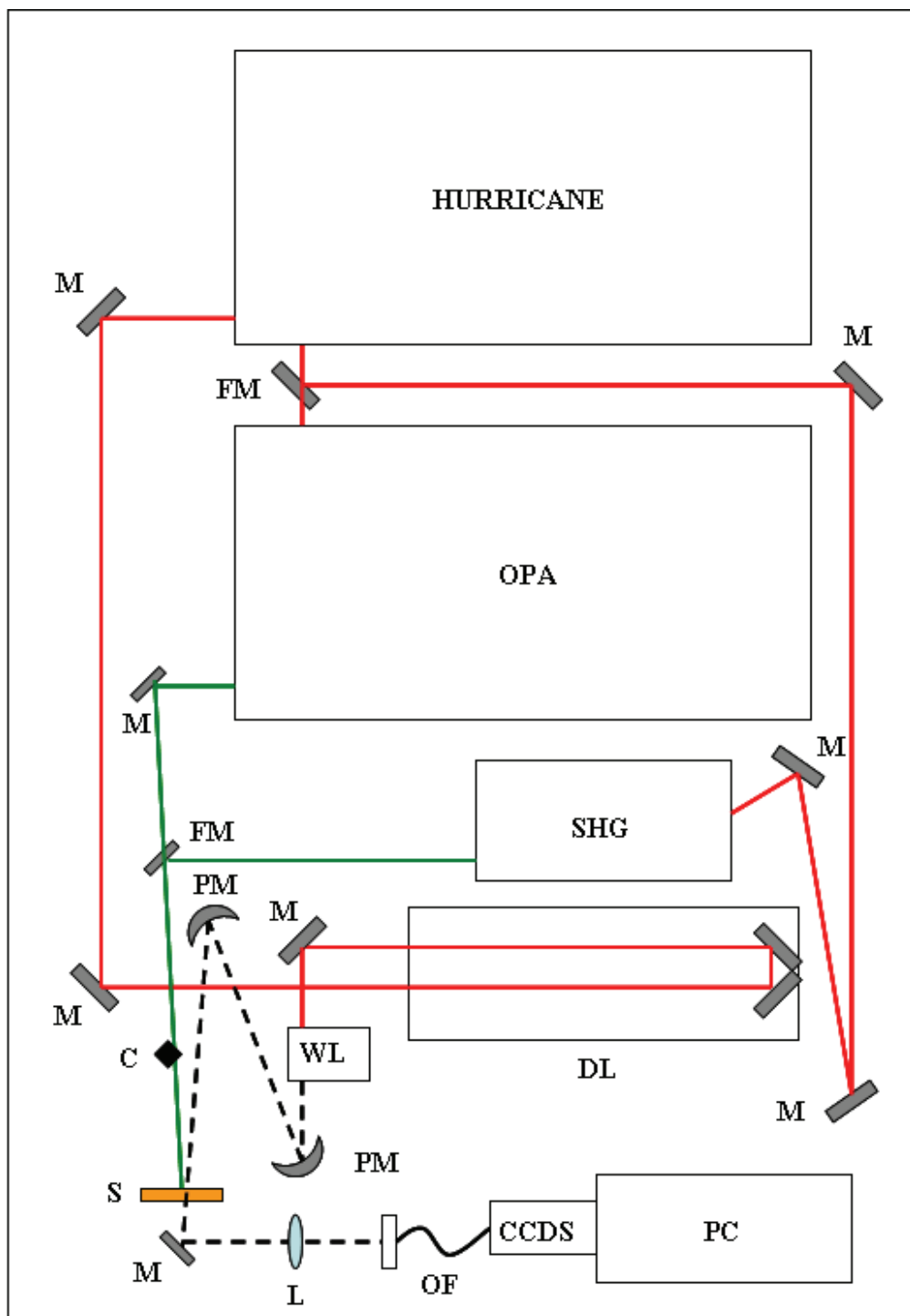
Figure 3. Ultrafast transient absorption spectroscopy setup. Red line, 800 nm; green line, pump beam; black dashed line, white light probe; M, mirror; FM, flipping mirror; PM, parabolic mirror; SHG, second harmonic generator; C, chopper; WL, white light generation; DL, delay line; S, sample; L, lens; OF, optical fiber; CCDS, CCD spectrometer.

Picosecond Time Correlated Single Photon Counting

Single photon counting is a time-resolved emission technique used to investigate luminescence lifetimes, usually in the ns timescale. The method is based on the possibility of detecting single photons and of measuring the time delay between excitation and emission of a photon.

The experiments were performed with a PicoQuant PicoHarp 300 system (Figure 4) equipped with subnanosecond pulsed LED sources (centered at 280 nm, 380 nm, 460 nm or 600 nm, 500-700 ps pulsewidth) powered by a PicoQuant PDL 800-B variable (2.5-40 MHz) pulsed power supply. Detection is performed by a photomultiplier (Hamamatsu PMA 185) equipped with a monochromator. Data processed by an integrated Time to Digital Converter (TDC) and Histogrammer is then analyzed by means of PicoQuant FluoFit Global Fluorescence Decay Analysis Software.

In a typical experiment, excitation pulse produces a start signal, while the first photon emitted from the excited sample produces a stop signal (count) when hits the photomultiplier detector. The time difference between the two signals is measured and recorded. The experiment is repeated at the set rate until a number of counts sufficient to define a decay probability histogram is accumulated. It can be demonstrated that the decay probability histogram matches the emission decay curve. Effective time-resolution is about 300 ps, temporal window of the experiment, depending on the repetition rate, can be up to 1 μs.
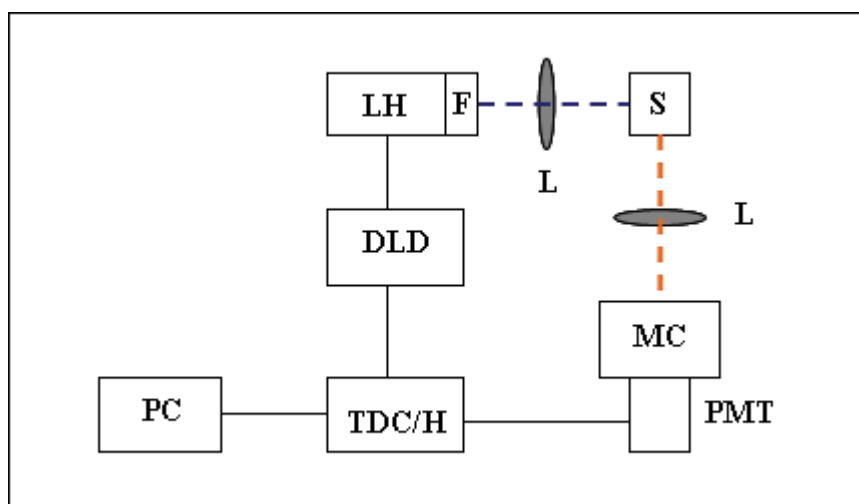
Figure 4. Picosecond Time Correlated Single Photon Counting setup. Blue line, exciting light; orange line, emitted light; TDC/H, time to digital converter and hystogrammer; DLD, diode laser driver; LH, laser head; F, filter; L, lens; S, sample; MC, monochromator; PMT, photomultiplier tube.

Nanosecond laser flash photolysis

Laser flash photolysis is a transient technique used both for absorption and emission spectroscopy in the time window from tens of ns to ms.

Except in the case of Chapter 5, all the measurements were performed with the setup shown in Figure 5. Excitation source is a Surelite Continuum II Nd:YAG laser (pulsewidth 6-8 ns) with frequency doubled, (532 nm, 330 mJ) or tripled (355 nm, 160 mJ) outputs.
For transient absorption measurements, analysis light is provided by a 150 W Xe lamp, equipped with a pulser (Applied Photophysiscs Model 410, 2 ms pulses) and a homemade rotating shutter.

When performing kinetic analysis, a Photomultiplier (Hamamatsu R3896) is used as detector and signals are processed by means of a LeCroy 9360 (600 MHz, 5 Gs/sec) digital oscilloscope. Transient spectra are alternatively recorded using as detection system a Princeton Instruments gated intensified CCD-Camera PI-MAX II equipped with an Acton SpectraPro 2300i triple grating flat field monochromator, an RB GenII intensifier, an ST133 controller and a PTG pulser. Switching between the two detection systems is obtained with a flipping mirror internal to the monochromator.

All the components are controlled by a custom LabVIEW software which provides also the requested signal synchronization. Transient spectra are acquired using the CCD-Camera detector by means of Princeton Instruments WinSpec software. Effective time-resolution is about 10 ns and temporal window of the experiment can be up to milliseconds.
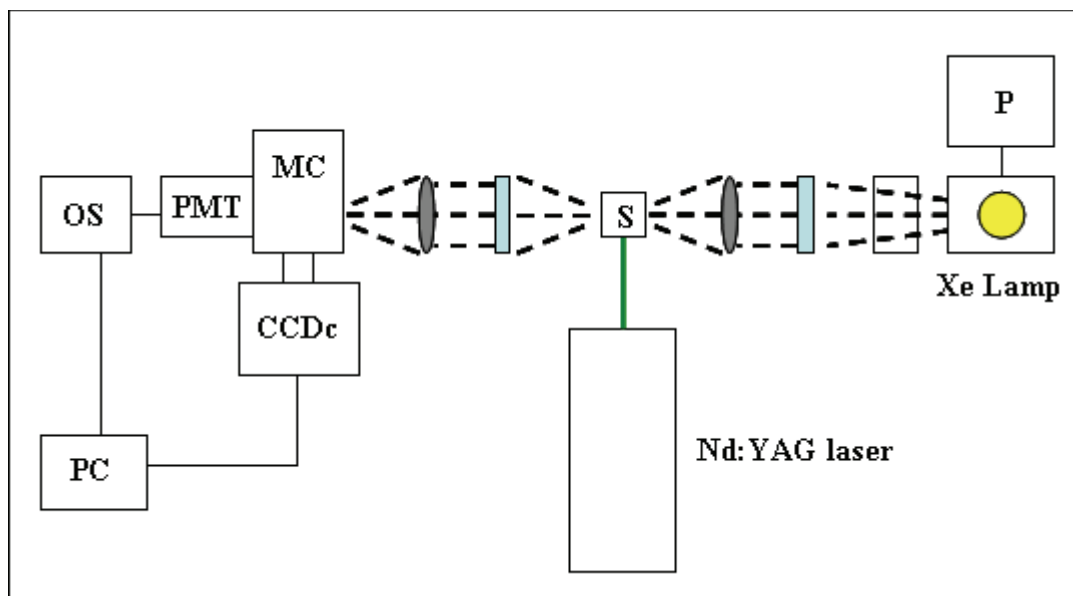

Figure 5. Nanosecond Laser flash photolysis setup. Green line, excitation light; black dashed line, analysis light; P, pulser; S, sample; MC, monochromator; CCDc, CCD camera; PMT, photomultiplier tube; OS, oscilloscope.

2.3 UV-Vis Spectroelectrochemistry

Spectroelectrochemistry is a technique that combines UV-Vis absorption spectroscopy with electrochemistry in order to measure the absorption spectra of oxidized or reduced forms of an electroactive species. Generating the oxidized or reduced species by the application of an electrical potential gives some advantages over the generation with chemical reagents: control over the working electrode potential allows selectivity of the redox process and there's no possible interference due to absorption spectra of reagents.

In our setup the experiment is performed in a 1 mm optical path OTTLE (Optically Transparent Thin Layer Electrochemical Cell), employing a Pt minigrid as the working electrode, an Ag wire quasi-reference electrode and a Pt wire counter electrode. Electrodes

are connected to a Amel 552 potentiostat and the cell placed in a Jasco V-570 UV/Vis/NIR spectrophotometer.

Chapter 3

Self-Assembling Triads for Photoinduced Charge Separation.

A Proof of Concept.[δ]
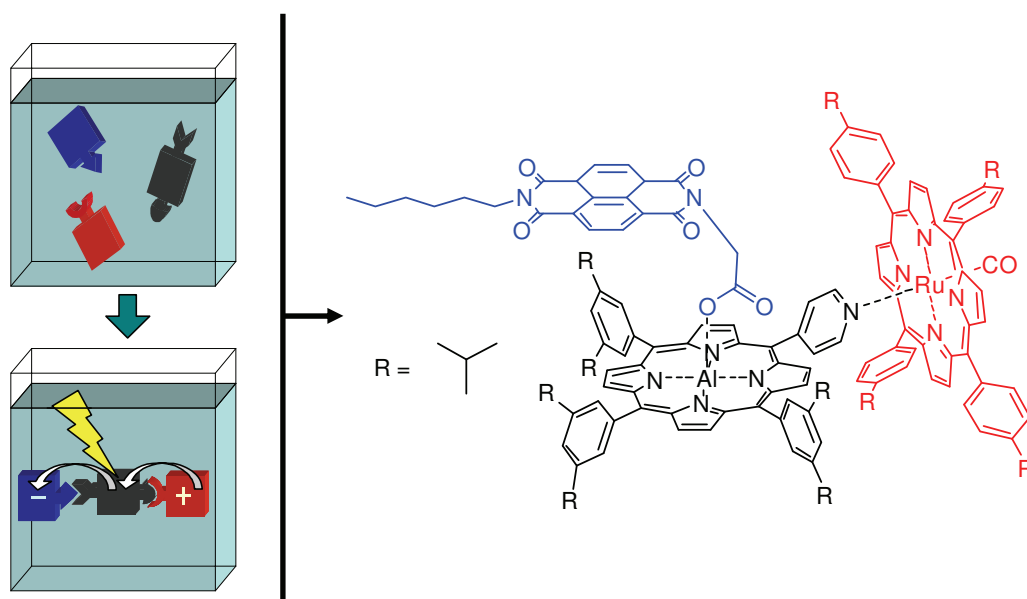
A triad for charge-separation is obtained by self-assembling of a Ru-porphyrin electron donor, an Al-porphyrin as the photoexcitable chromophore and a naphtalenebisimide electron acceptor.

[δ] E. Iengo, D. G. Pantoş, J. K. M. Sanders, M. Orlandi, C. Chiorboli, S. Fracasso, F. Scandola. *Manuscript in preparation.*

The work described in this chapter is the result of a collaboration between the Photochemistry Group at the Department of Chemistry of University of Ferrara (Ferrara, Italy), where i have done my Ph.D., the Inorganic Chemistry Group at University of Trieste (Trieste, Italy) and the Sanders Group at University of Cambridge (Cambridge, UK).

3.1 Introduction

In the last decades, classical organic chemistry has been the instrument of choice for the construction of functional units for artificial photosynthesis, including charge-separating reaction centers[1,2,3,4,5]. Despite its advantages from the viewpoint of robustness and structural definition, this covalent approach is demanding both in terms of synthesis and of molecular design. Perhaps at the expenses of some structural rigidity, softer, non-covalent strategies are advantageous in terms of mild reaction conditions, combinatorial flexibility, repair capabilities. Among these, considerable interest has been given to the use of metal coordination for assembling molecular components into appropriate functional structures ("metal-mediated" approach).[6] In this approach, depending on the type of metal used and of ligand function present on the molecular component, the assembling process may run under kinetic control (chemical synthesis, relatively mild conditions) or under thermodynamic control (true self-assembling).

The metal-mediated self-assembling strategies developed so far are ideally suited to the construction of symmetric multichromophoric systems. It must be pointed out, however, that triads and more complex systems for photoinduced charge separation, are intrinsically asymmetric. Implementation of metal-mediated self-assembling to the construction of triad systems is much less obvious, as it requires molecular recognition between the subunits to be assembled. This can only be achieved if highly selective metal-ligand interactions are used, and different types of such interactions are simultaneously implemented. The work described here is a first attempt [a,7,8] towards the challenging objective of a self-assembling triad.

The molecular components chosen are: (i) an aluminium porphyrin as the central photoexcitable chromophore (ii) a naphthalenebisimide as electron acceptor unit (iii) a

---

[a] A number of triads assembled by metal coordination have been described. They are, however, either symmetric systems (i.e., pseudo-diads)[7] or triads in which two out of three molecular components are covalently linked.[8]

ruthenium porphyrin as electron donor unit. The selective affinity of the two different metallo-porphyrins towards nitrogen or oxygen ligands is crucial for the efficient self-sorting of the desired three-component products. In particular, Al(III)-porphyrins can axially bind a carboxylic group (and with a much weaker affinity a nitrogen based moiety),[9] whereas Ru(II)(CO)-porphyrins can axially bind a pyridyl group. Thus, efficient assembling is implemented by introduction of a carboxylic function on the naphthalenebisimide unit and of a pyridyl appended ligand on the aluminium porphyrin. As it will be shown in the following sections, a single three-component adduct, **NDI-AlMPyP-RuP**, quantitatively self-assemble from a 1:1:1 mixture of the three starting units (Scheme 1).
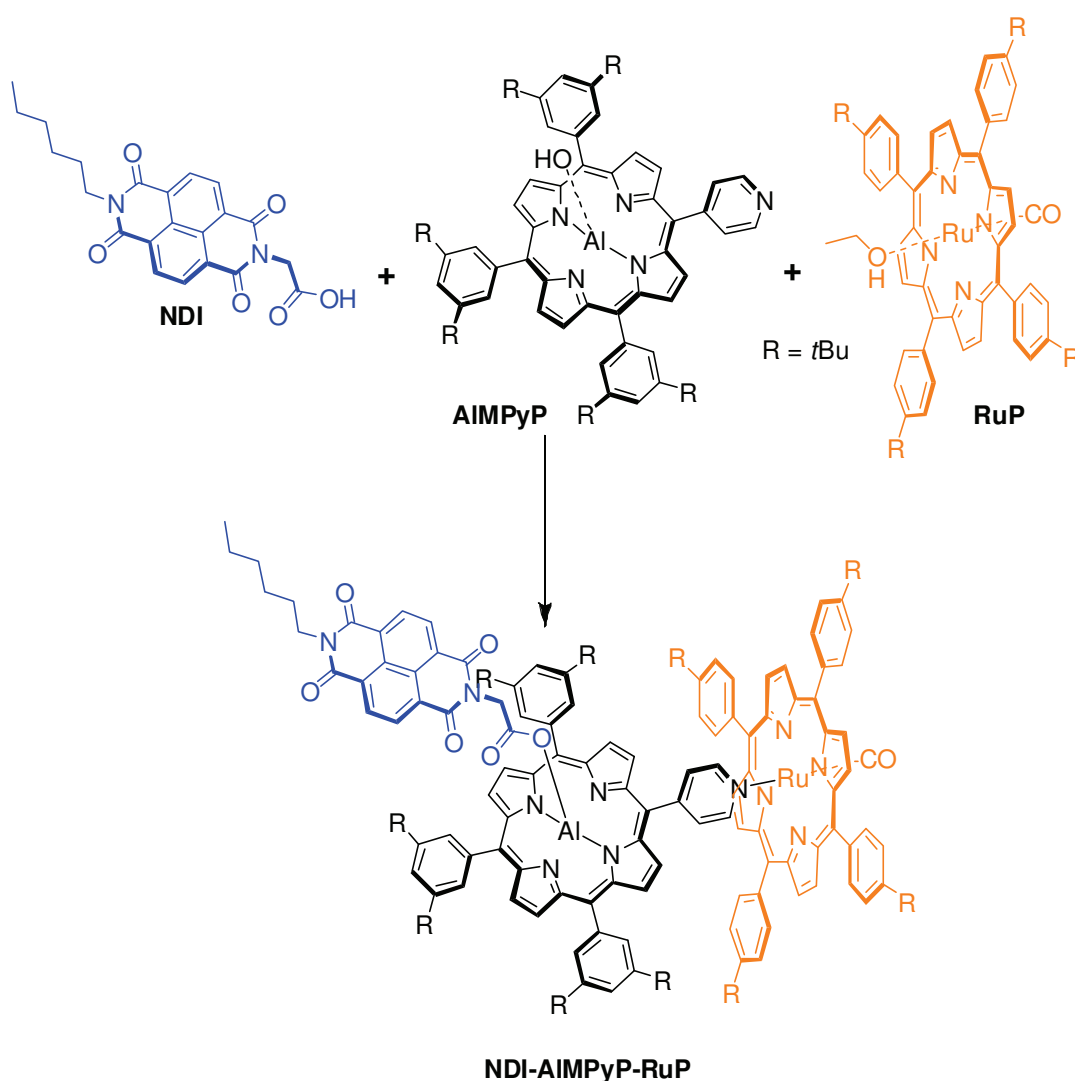
Scheme 1. Schematic representation of the self-assembling of the asymmetric triad **NDI-AlMPyP-RuP**.

Two related dyads, **NDI-AlP** and **RuP-NDI''-RuP**,[b] have also been designed for purposes of comparison (Chart 1).
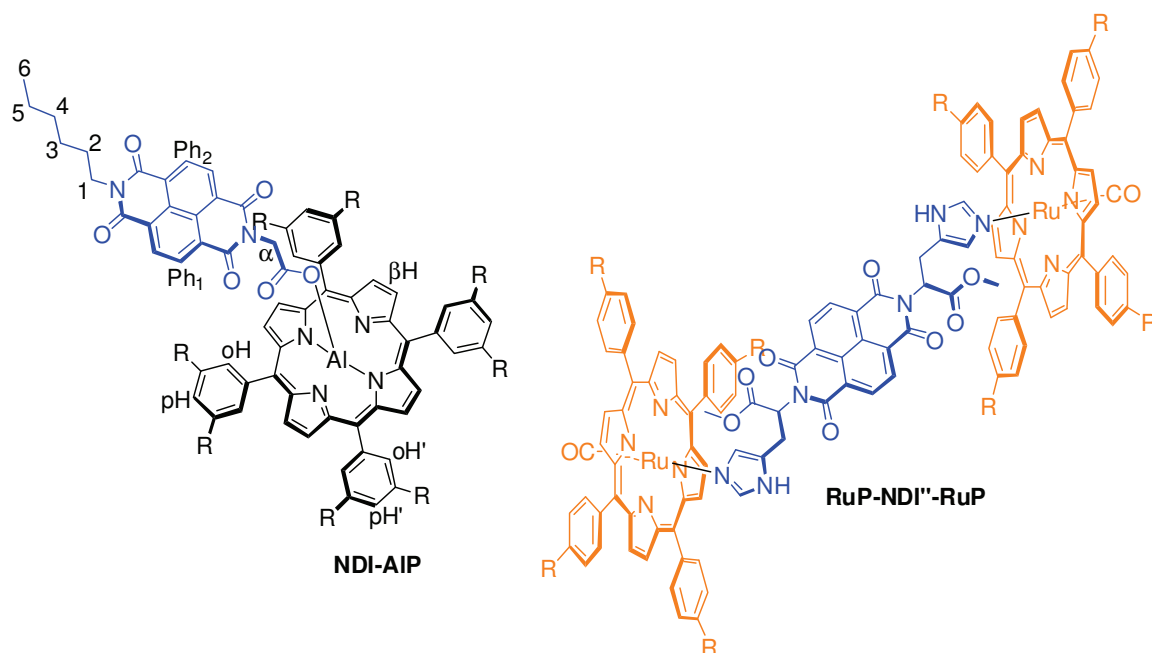

Chart 1. NDI-AlP and **RuP-NDI''-RuP** dyads.

The assembling and photophysical behavior of these systems has been investigated in solution and discussed by comparison with appropriate models of the individual molecular components (**NDI'**, **AlP(ba)**, **RuP(py)**, **AlMPyP(ba)**, and **AlMPyP-RuP** Chart 2).

The presence of *tert*-butyl groups on the phenyls on both the metallo-porphyrins is essential to give a wider range of solubility to the assembled systems. Moreover, the different positions of these alkyl substituents (in *meta* and in *para* for the aluminium porphyrins and for the ruthenium porphyrin, respectively) allows for a better resolution and easier attribution of the resonances in the aromatic region of the ^{1}H NMR (especially for **NDI-AlMPyP-RuP**, see below). It is worth mentioning that, to date, the use of Al(III)-porphyrins has mostly been limited to polymerisation reaction, activation of organic substrates, and halides sensing.[10] The efficient use of aluminium porphyrin as building units for the formation of multi-porphyrin arrays (either discrete or polymeric) has recently been reported.[9] To our knowledge there was only one previous example in which an Al(III)-porphyrin was employed in the synthesis of arrays via axial coordination with phenolate ligands.[11]

---

[b] **RuP-NDI''-RuP** is clearly a triad from a structural viewpoint. From the functional viewpoint, however, symmetric triads can be effectively considered as pseudo-dyads.

We have now inserted an aluminium center in a pyridyl porphyrin, and we demonstrate the versatility of such multi-site (both donor and bis-acceptor) equipped unit. For the first time such metallo-porphyrin is used as an active component for photophysical processes.
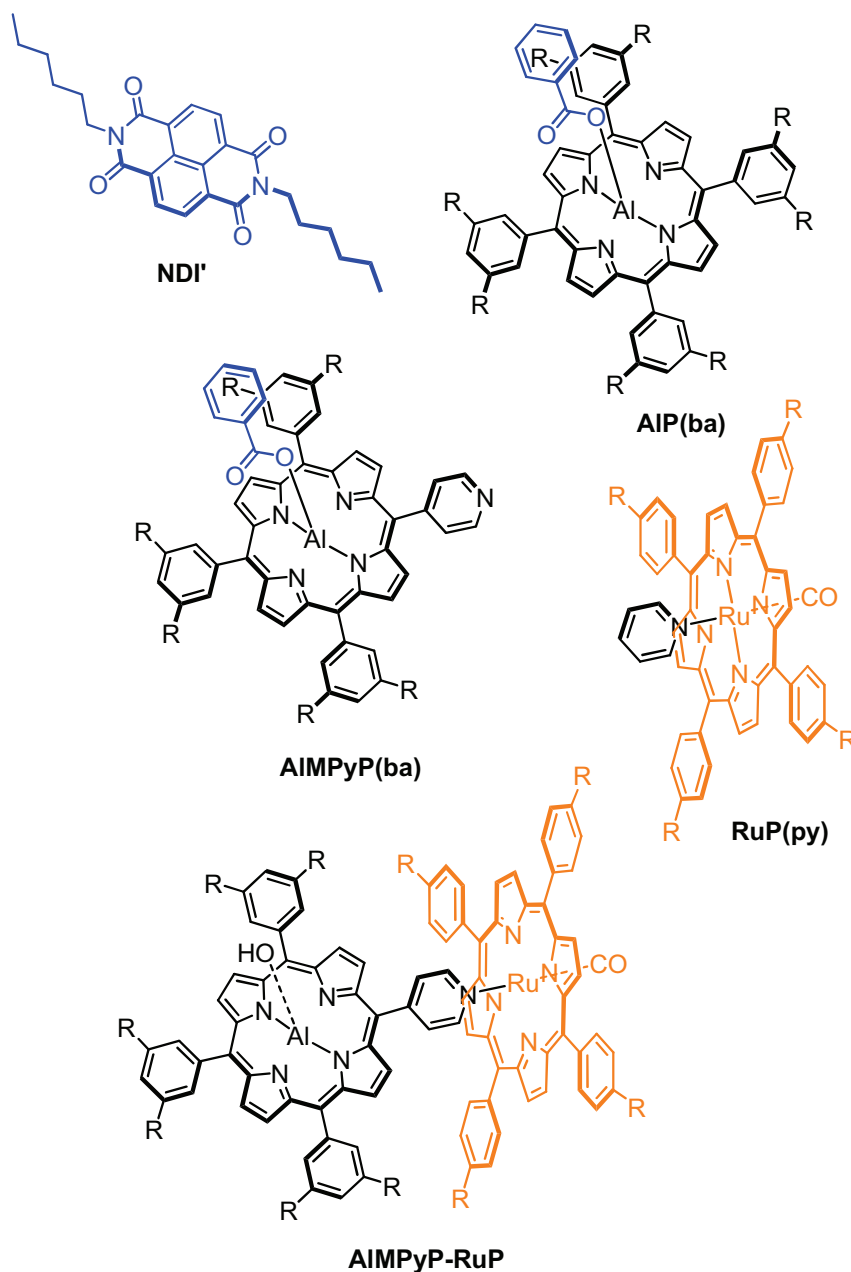

Chart 2. Model compounds.

3.2 Experimental section

The syntheses and characterization of the compounds discussed in this chapter were performed by Elisabetta Iengo in the research group of Prof. Enzo Alessio at University of Trieste (Trieste, Italy) and Dan G. Pantoş in the research group of Prof. Jeremy K. M. Sanders at University of Cambridge (Cambridge, UK). Details will be published in: E. Iengo, D. G. Pantoş, J. K. M. Sanders, M. Orlandi, C. Chiorboli, S. Fracasso, F. Scandola. *Manuscript in preparation.*

Reagents and spectroscopic-grade solvents were purchased and used as received, if not otherwise stated. See Chapter 2 for details on electrochemical and photophysical measurement apparatus and procedures.

3.3 Results and Discussion

Self-assembling.

All the systems reported have been characterized in solution by means of NMR conventional 1D and 2D experiments. Assembling of **NDI-AlP** and **RuP-NDI''-RuP** is straightforward. These dyads are obtained quantitatively by simple mixing of the components in chloroform solution at room temperature. In Figure 1 the ^{1}H NMR spectrum (CDCl$_3$) of **NDI-AlP**, compared to the spectrum (dmso-d_6) of free **NDI**, is reported.[c] Relative integration of the resonances of **NDI** and **AlP** confirms the formation of a 1:1 adduct; the signals of **NDI**, corresponding to the protons closer to the metal center, are remarkably upfield shifted as expected for an axially connected species. All the resonances are sharp indicating the formation of a stable adduct.

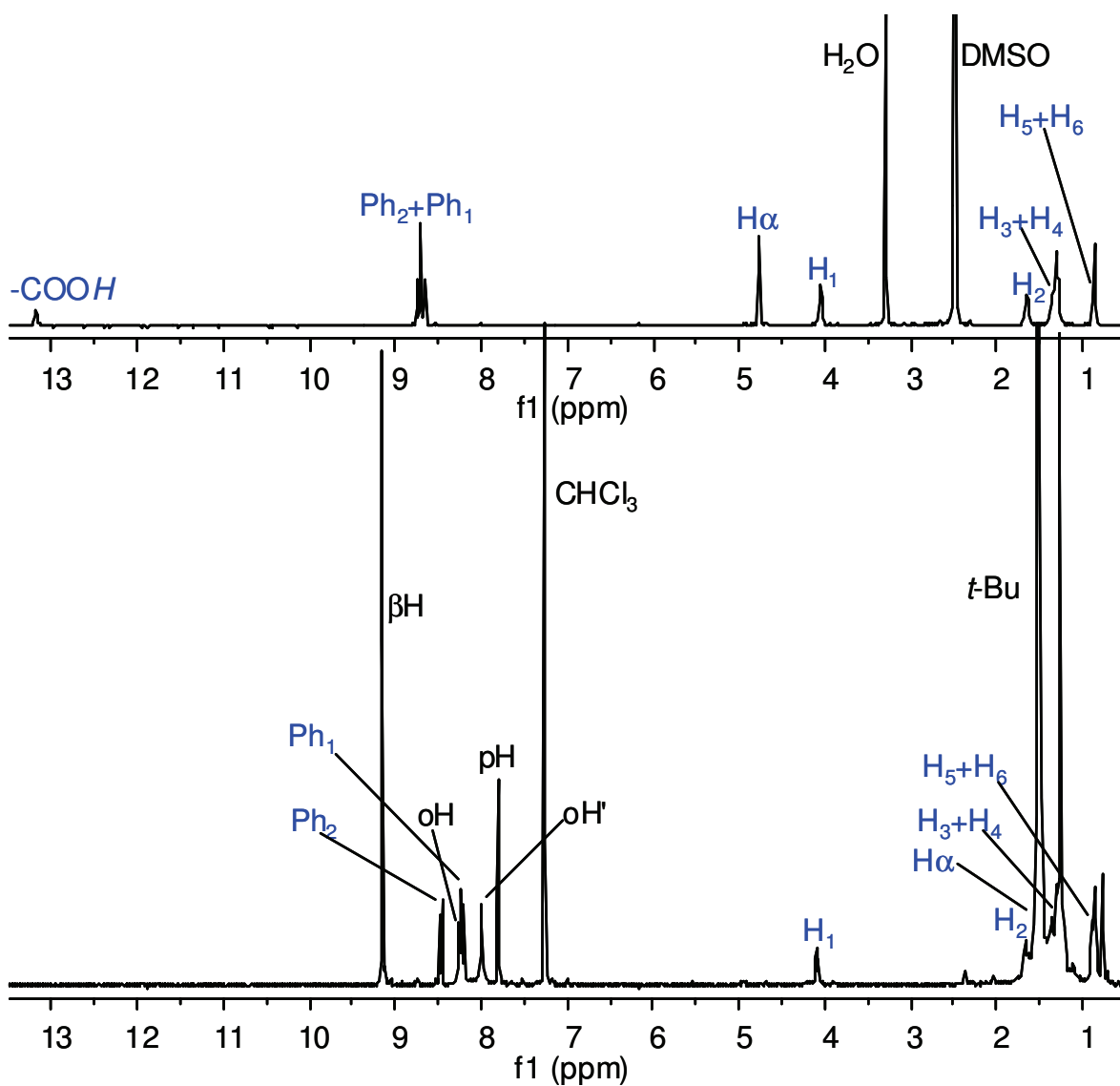[c] Free **NDI** is barely soluble in chlorinated solvents.

Figure 1. ^1H NMR (CDCl$_3$) of NDI-AlP (bottom), compared to the ^1H NMR (DMSO-d_6) of NDI (top). See Chart1 for proton labels.

The characterization of Al(OH)(3,5-di-*t*BuMPyP), **AlMPyP**, deserves a small discussion. Insertion of aluminium in the monopyridyl porphyrin core proceeds smoothly, as already reported for its tetraphenyl porphyrin analogue.[9a] Nevertheless, this species is present in chloroform solution as one or more self-assembled structures [**(AlMPyP)$_n$**], as the pyridyl groups of one molecule are axially bound to the aluminium of an other molecule (Scheme 2).
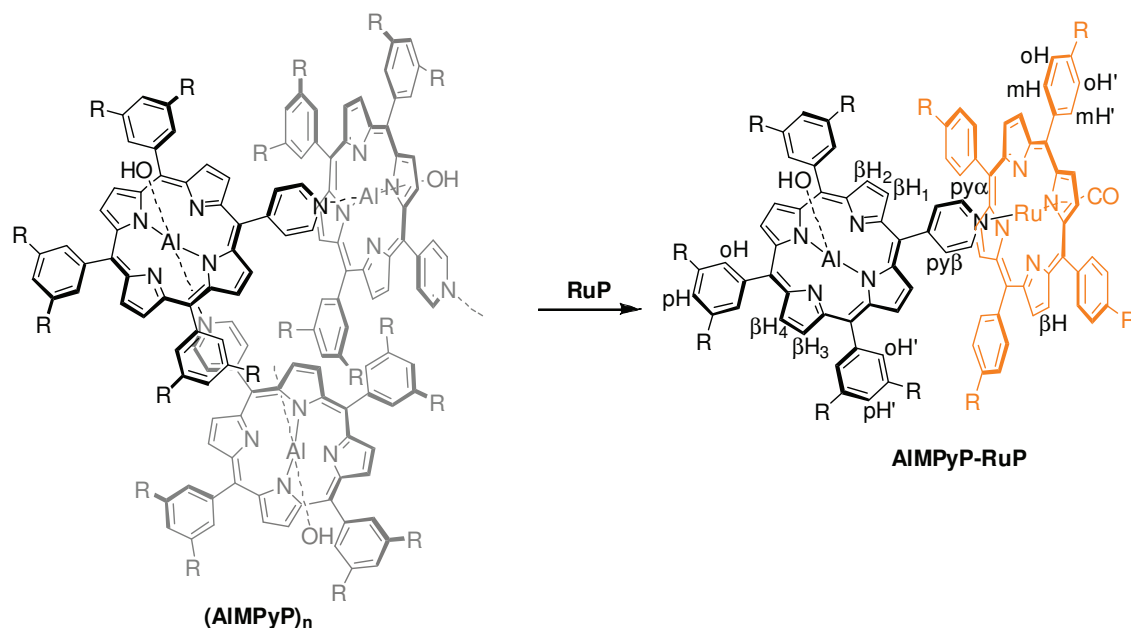
Scheme 2.

This type of interaction is not very strong (an association constant of ca. 3×10^{-3} M^{-1} was estimated for 4-*tert*-butylpyridine binding to an aluminium tetraphenyl porphyrin[9a]) probably leading to the presence of several assemblies in equilibrium. As a consequence the ^{1}H NMR spectrum (CDCl$_3$) of **AlMPyP** shows broad, concentration dependent, resonances (Figure 2).
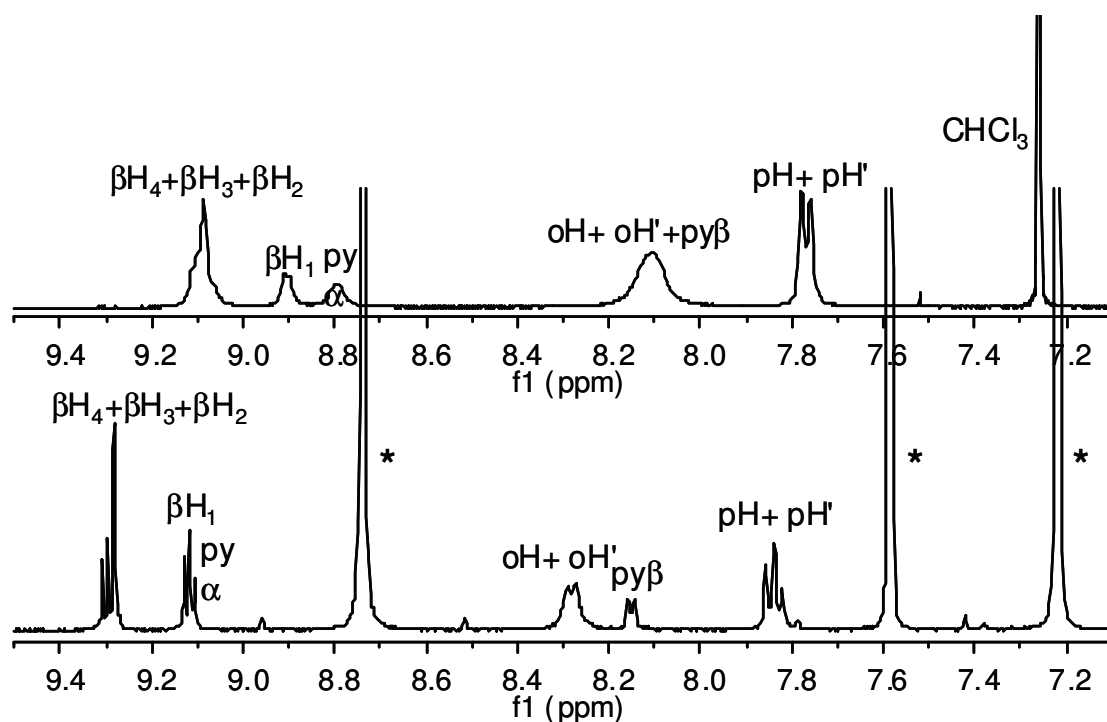
Figure 2. Aromatic region of the ^{1}H NMR of **AlMPyP** in CDCl$_3$, top, and pyridine-d_5, bottom. See AlMPyP part of Scheme 2 for proton labels. Peaks of residual non-deuterated pyridine are indicated with an asterisk.

In particular, broad upfield shifted signals are present, relating to the pyridyl, βH$_1$ and βH$_2$ protons as they fall under the shielding effect of the porphyrin ring current in these self-assembled species (Figure 2, top). Addition of an excess of competing pyridine-d_5 gives rise to a sharp well-resolved ^{1}H NMR spectrum (Figure 2, bottom). Analogously, addition of equimolar amounts of **RuP**, breaks the weak aluminium-pyridyl bond in favour of the more stable and inert ruthenium-pyridyl interaction, thus leading to the selective and quantitative formation of **AlMPyP-RuP**. This side-to-face bis metallo-porphyrin assembly, obtained at room temperature in a few minutes, shows only sharp resonances in the ^{1}H NMR spectrum (Figure 3), with the typical upfield shifts for the resonances of the side metallo-porphyrin **AlMPyP** (e.g., Δδ = -7.19, -2.13 and -1.63 for pyα, pyβ and βH$_1$ of **AlMPyP**, respectively). And in particular the ruthenium porphyrin act as a shifting reagent for the βH protons of **AlMPyP** which resonances are well resolved and spread over *ca.* 2 ppm. The phenyl protons of both the metallo-porphyrins are split into two resonances each, as for both units the two sides of the porphyrin planes are not equivalent. The rotation along the C$_{meso}$–C$_{ring}$ bond is slow on the NMR timescale at room temperature for **RuP** and intermediate-to-fast

for **AlMPyP**, resulting in distinct sharp resonances for the *ortho* and *meta* protons of **RuP** and distinct but broad resonances for the *ortho* protons of **AlMPyP**.

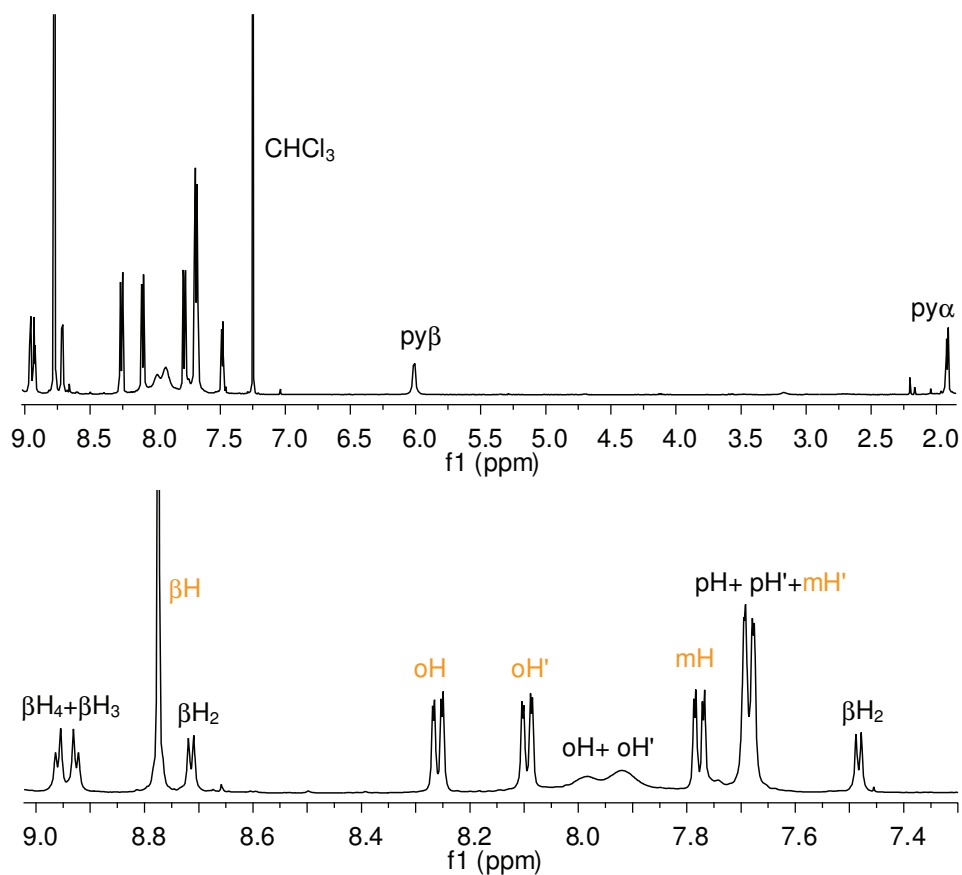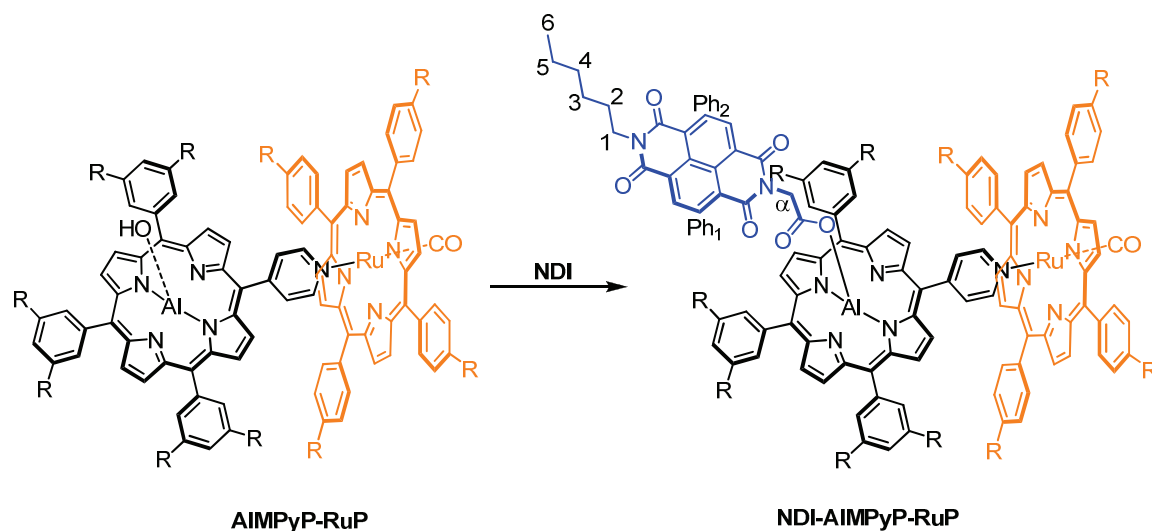**Figure 3.** ^{1}H NMR (CDCl$_3$) of **AlMPyP-RuP** (top, *tert*-butyl groups omitted for clarity) and its enlarged aromatic region (bottom). See Scheme 2 for proton labels.

The target triad, **NDI-AlMPyP-RuP**, can be easily obtained by subsequent addition of an equimolar amount of **NDI** to **AlMPyP-RuP** (Scheme 3).

Scheme 3.

The bisimide axially binds to the aluminium center (with elimination of water) via the carboxylic functionality. The reaction is selective, quantitative and takes place at room temperature (stirring is necessary to favour the dissolution of **NDI**, that is barely soluble in chloroform by itself). In Figure 4 the ^{1}H NMR spectrum (CDCl$_3$) of **NDI-AlMPyP-RuP** is shown. Most of the protons show well-resolved and sharp signals, the ones closer to the metallo-porphyrins being more affected by the shielding cones of the macrocycles, reflecting the stability and total absence of scrambling processes plus the axial coordination motif of the assembly. It has to be remarked here that the same final three-component assembly, **NDI-AlMPyP-RuP**, forms uniquely either by subsequent addition of the starting units in a different order or, more strikingly, by mixing the three units in stoichiometric ratio one-pot (Scheme 1). Therefore, the affinity of the metal centers, together with the metal coordination number and the appropriate functionalization of the modules, is fundamental for the success of the self-selection process and the obtainment of a single stable product.
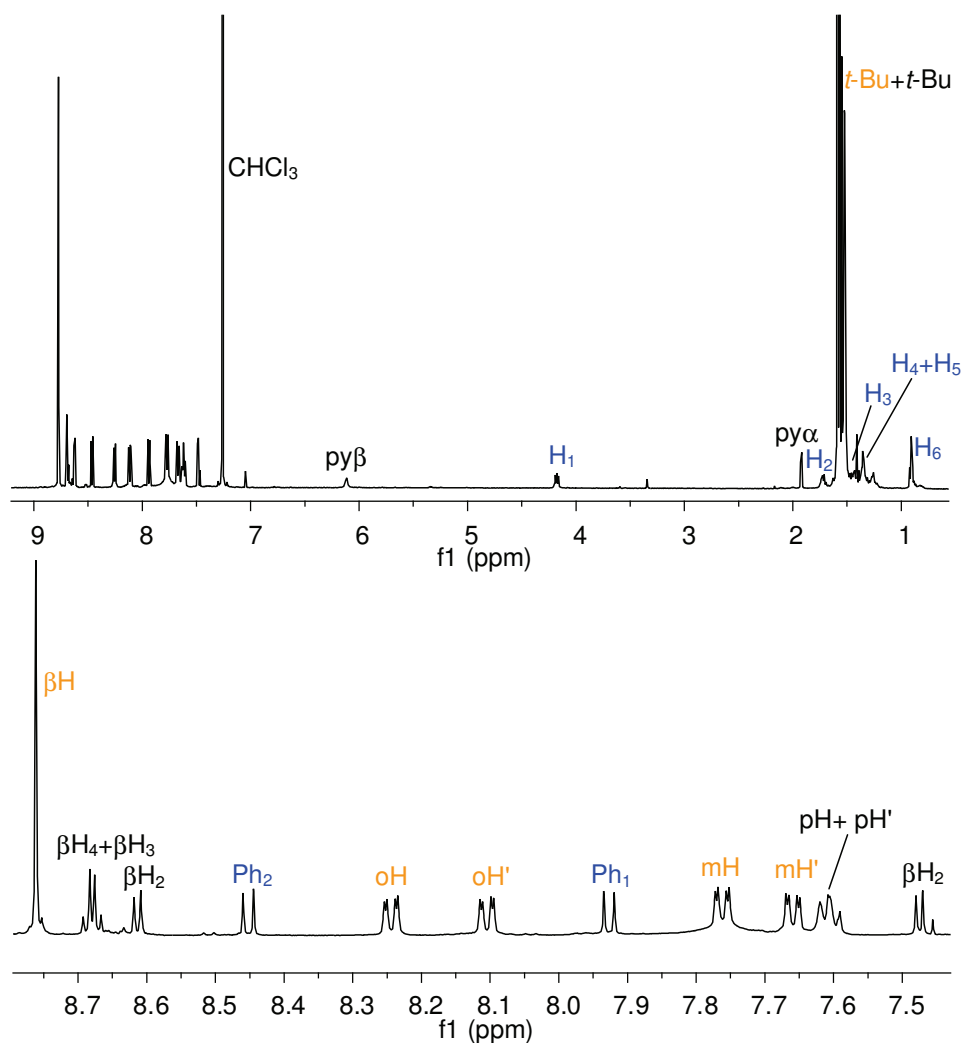
Figure 4. ^{1}H NMR (CDCl$_3$) of NDI-**AlMPyP-RuP** (top) and its enlarged aromatic region (bottom). See Scheme 2 and Scheme 3 proton labels.

Supramolecular nature of assemblies.

As already observed for related side-to-face and axially coordinated assemblies,[12,13] the dyad and triad systems studied are truly supramolecular in nature. For **NDI-AlP** and **NDI-AlMPyP-RuP** this is demonstrated by the appreciable additivity of the absorption spectra of the subunits (Figure 5).
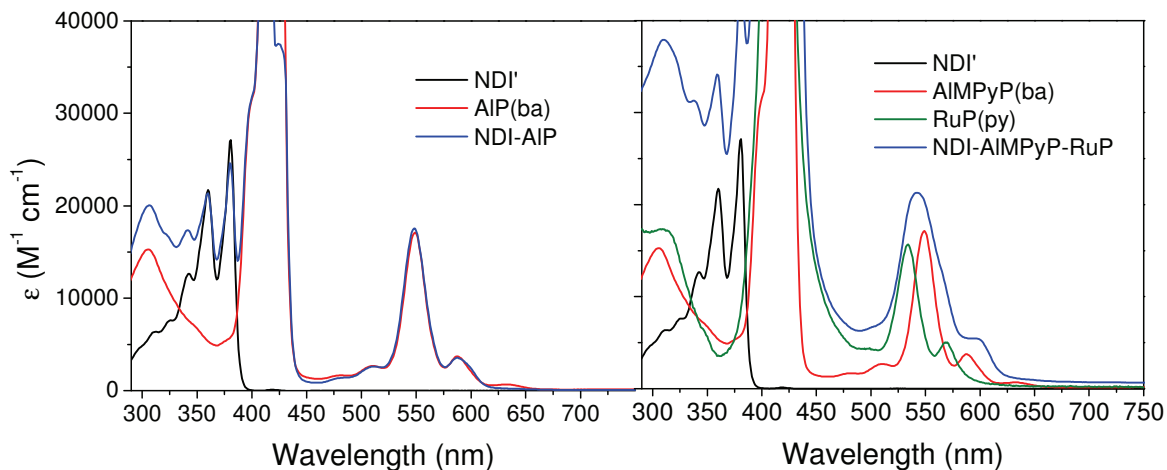
Figure 5. Absorption spectra of **NDI-AlP** (left) and **NDI-AlMPyP-RuP** (right) and of their model compounds.

The self-assembling of **AlMPyP(ba)** evidenced by ^{1}H-NMR is also observed in the absorption spectrum, as a broadening of the main Q band at 550 and a red shift (ca. 10 nm) of 590-nm band (Figure 6). However, the effect is concentration dependent and practically disappears for $< 5 \times 10^{-5}$ M solutions. No self-association takes place at the concentrations used in the spectroscopic investigations.
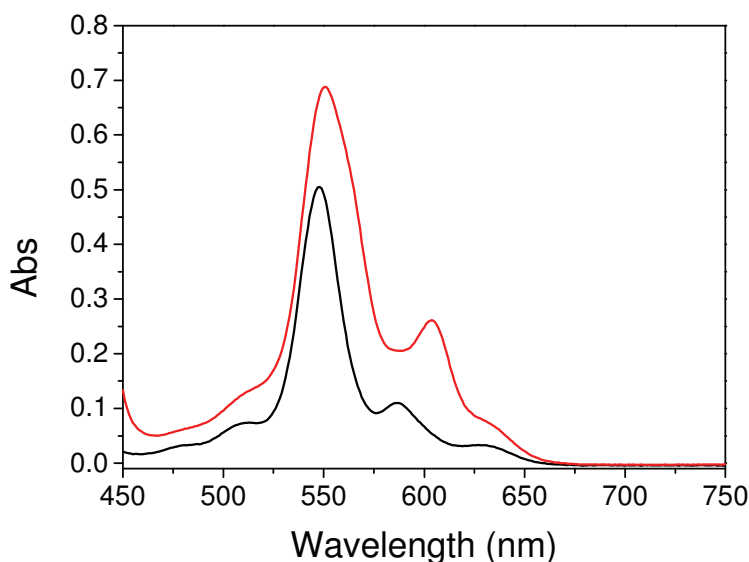
Figure 6. Absorption spectra of **AlMPyP(ba)** at different concentrations (black line, ca. 3×10^{-5}, 1cm cell; red line, ca. 4×10^{-4}, 1mm cell) in dichloromethane.

On close inspection, some minor differences between the spectrum of the **NDI-AlMPyP-RuP** triad and the sum of those of the molecular components can be noticed, in particular a red shift of the lowest energy aluminium porphyrin band at ca 600 nm. This shift, very similar to that observed when **AlMPyP(ba)** self-associates in concentrated solution, tends to disappear upon strong dilution ($<5 \times 10^{-5}$ M) of the solutions and can be taken as a marker of the coordination of the pyridyl group. These spectrophotometric dilution experiments (monitoring the stability of the AlMPyP-RuP linkage), together with spectrofluorimetric dilution experiments on the **NDI-AlP** dyad (vide infra, monitoring the stability of the NDI-AlP linkage), lead to the conclusion that the dyad and triad systems are stable in dichloromethane solution down to a concentration of 5×10^{-5} M.

The supramolecular nature is also apparent when the electrochemistry of these systems is compared to that of the component subunits (Table 1). For example, in the **NDI-AlMPyP-RuP** triad the reduction of the aluminium porphyrin, the two reductions of the NDI unit, the oxidation of the ruthenium porphyrin and the oxidation of the aluminium porphyrin can be easily assigned, as their potentials are coincident within experimental error with those of the constituent units.

	reduction			oxidation	
NDI-AlP	- 1.30	- 1.09	-0.69		0.83
NDI-AlMPyP-RuP	- 1.19	- 1.05	- 0.68	0.76	0.90
RuP(py)				0.78	
AlP(ba)	- 1.31				0.82
AlMPyP(ba) [b]	- 1.21				0.88
NDI'		- 1.06	- 0.65		
[a] In CH2Cl2 at 298 K, 0.1 M TBA(PF$_6$) as electrolyte, SCE as reference electrode, ferrocene (0.46 V vs. SCE[14]) as internal standard. [b] Concentration independent in the 1×10^{-4}-5×10^{-5} M range.[d]					

Table 1. Electrochemical data for **AlP-NDI** and **NDI-AlMPyP-RuP** and their molecular components.[a]

---

[d] This indicates that the self-association has little effect on the reduction potential of this species.

Photophysics and spectroelectrochemistry of molecular components.

The **NDI'** model exhibits in dichloromethane the weak structured fluorescence (λ_{max}, 380 nm; τ, ca. 15 ps) typical of this type of chromophore.[15]

In room-temperature dichloromethane solution, **AlP(ba)** shows a typical metal porphyrin fluorescence, with prominent vibronic bands at 596 and 648 nm and a lifetime of 5.5 ns. At 77K, in addition to fluorescence, a weak phosphorescent emission can be observed at 782 nm. The spectroscopic signature of the singlet excited state, as obtained by femtosecond absorption spectroscopy (excitation at 550 nm), is shown in Figure 7a. It is characterized by Q-band bleach at 550 nm (partially covered by the excitation pulse) absorption at longer wavelengths, with superimposed stimulated emission (apparent bleach at ca 600 and 650 nm). The spectrum is appreciably constant in the 1-1000 ps time scale. The broad excited-state difference absorption spectrum of the triplet state (T_1), as obtained by nanosecond laser photolysis (excitation at 532 nm), is shown in Figure 7b. It decays with oxygen-dependent lifetime (ca. 8.0 µs in deaerated dichloromethane).

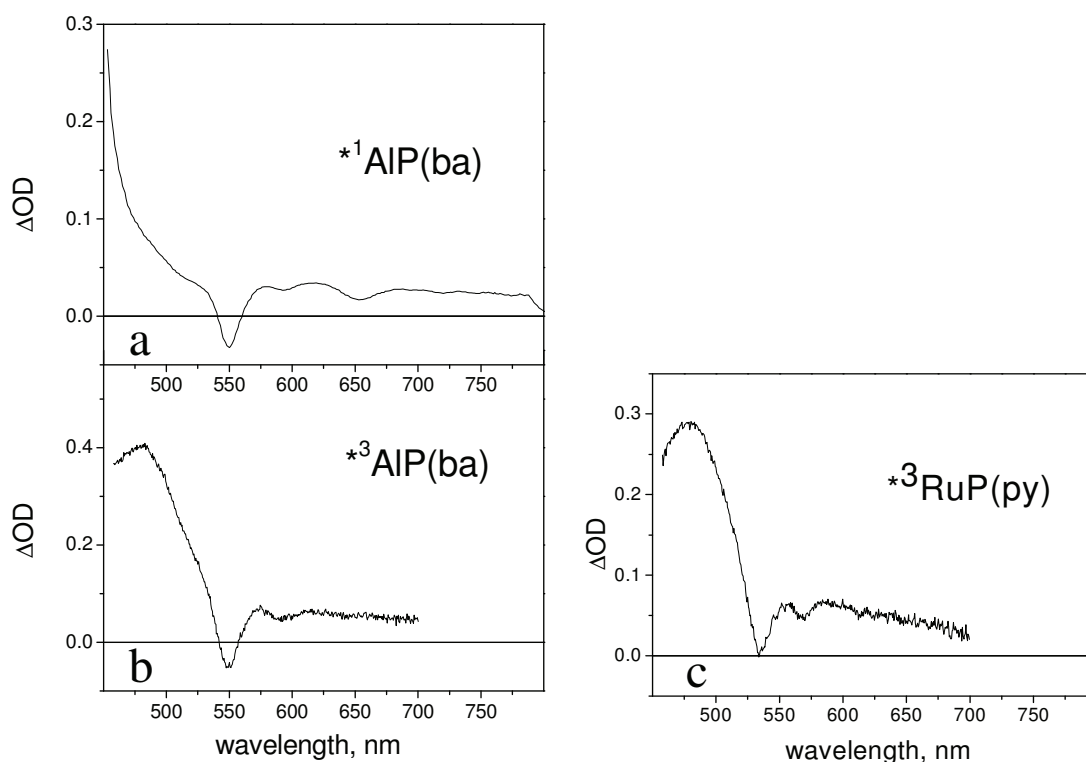**Figure 7.** (a) transient absorption spectrum of the singlet excited state of **AlP(ba)**, obtained by femtosecond spectroscopy (for details, see text); (b) transient absorption spectrum of the triplet excited state of **AlP(ba)**, obtained by nanosecond laser photolysis (for details, see text); (c) transient absorption spectrum of the triplet excited state of **RuP(py)**, obtained by nanosecond laser photolysis (for details, see text).

As it is usual for ruthenium porphyrins,[12] the S_1 state of the **RuP(py)** model does not fluoresce but rather undergoes very fast intersystem crossing. The T_1 state can be detected at 77K by a weak phosphorescence (λ_{max} = 726 nm) or at room temperature by nanosecond transient absorption measurements (spectrum in Figure 7c, lifetime ca. 30 µs in deaerated dichloromethane). Femtosecond spectroscopy shows that triplet formation is complete in a sub-picosecond time scale.

The difference spectra obtained in spectroelectrochemistry for one-electron reduction of **NDI'** and oxidation of **AlP(ba)** and **RuP(py)**[e] are shown in Figure 8. The main spectrocopic signatures for NDI$^-$ are two sharp maxima at 475 and 510 nm. For the AlP(ba)$^+$ and RuP(py)$^+$ radical cations, the most distinctive features are the bleaches of the main Q band, at 550 and 530 nm, respectively. Sum spectra are also shown in Figure 8, to simulate the spectral behavior expected for charge-separated states that may be formed in the dyad and triad systems.
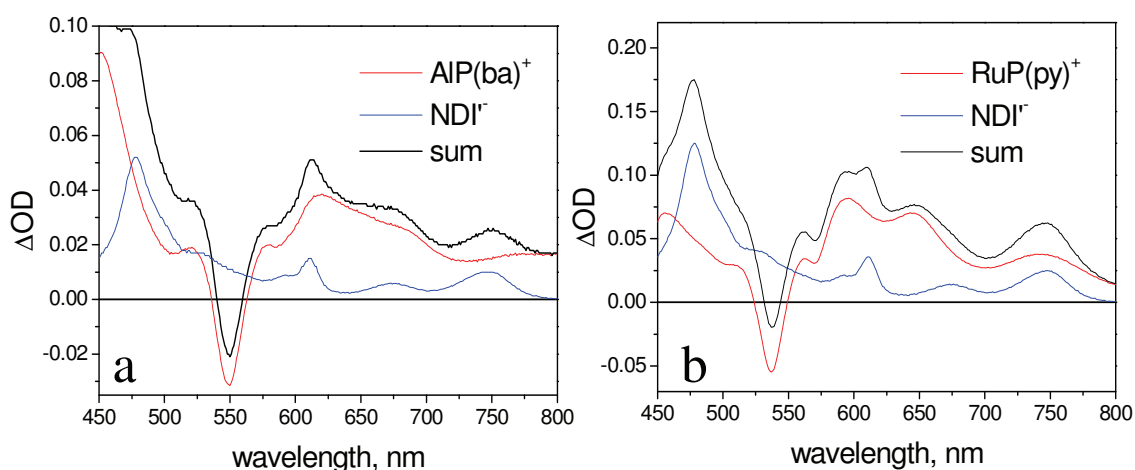

Figure 8. Sum spectra of the one-electron reduced form of **NDI'** and the one-electron oxidized forms of **AlP(ba)** (a) and **RuP(py)** (b). (for details, see text).

---

[e] Relative intensities of the component radical ion spectra from spectroelectrochemical experiments on equal concentration solutions of the **AlP(ba)**, **NDI'** and **RuP(py)** models.

Photophysics of the NDI-AlP Dyad.

A simplified energy level diagram for the **NDI-AlP** dyad in dichloromethane (high-lying excited states of the NDI unit, omitted for clarity) is shown in Figure 9a. It is inferred from the spectroscopic and electrochemical data of Table 1, with inclusion of the appropriate electrostatic work terms[f,16] in the calculation of the energy of the charge separated state. A strongly exergonic electron transfer pathway is clearly available for deactivation of the singlet state of the metal porphyrin unit.
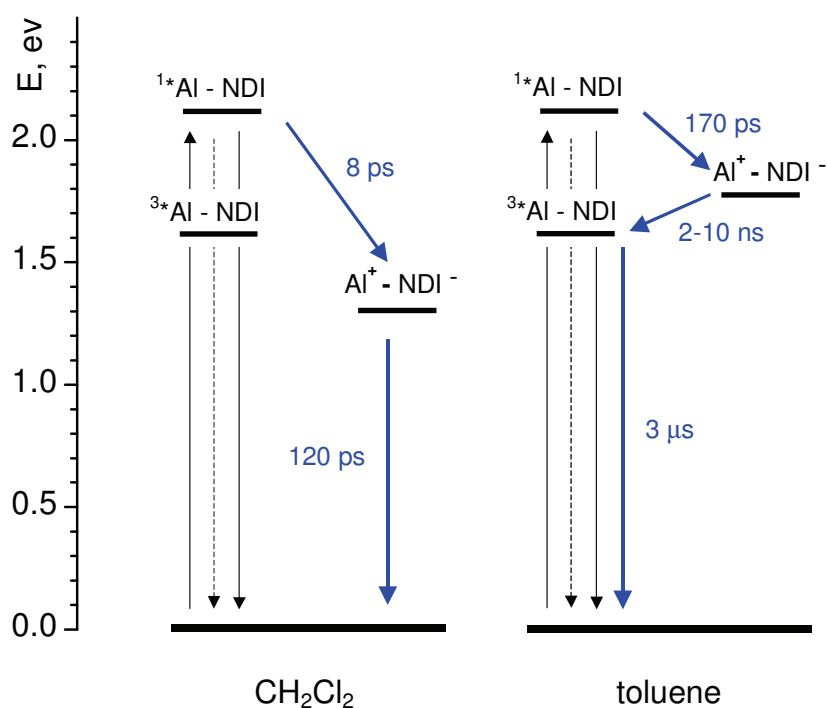
Figure 9 Energy level diagrams and photophysical mechanisms for the **NDI-AlP** dyad in dichloromethane (a) and toluene (b). Shorthand notation: AlP = Al.

---

[f] For the **NDI-AlP** dyad, a center-to-center distance of 8.5 Å, as obtained from the DFT-optimized structure, has been used. For the **NDI-AlMPyP-RuP** triad, in which the conformational freedom allows for a range of center-to-center distances, an average value of 12 Å has been assumed. Effective radii of 4 and 5 Å were assumed, respectively, for the NDI and porphyrin molecular fragments.

As a matter of fact, in dichloromethane the naphthalene bisimide and aluminium porphyrin fluorescent emissions are, respectively, completely (>99%) and strongly (ca 90%) quenched in **NDI-AlP** relative to those of the model compounds. Single-photon counting experiments demonstrate that the residual emission (lifetime, ca. 5 ns) arises from impurities of unquenched aluminium porphyrin species[g] whereas the fluorescence lifetime of the **NDI-AlP** dyad lies below the instrumental time resolution (<250 ps). The transient spectral changes observed by ultrafast spectroscopy, Figure 10 (λ_{exc} = 590 nm, 100% AlP excitation), provide insight into the quenching mechanism. The initial spectrum is that of the excited singlet state of the aluminium porphyrin unit (see, for comparison Figure 7a). The transient spectral changes are clearly biphasic, with a fast increase in optical density in the 580-720 range (the 570-610 nm region, hidden in Figure 10 by the excitation pulse, can be monitored by using 550 nm as excitation wavelength), and decrease at λ > 720 nm (Figure 10a), followed by a decay of the whole spectrum towards the baseline with isosbestic points at ΔOD = 0 (Figure 10b). The kinetics analysis (Figure 10c) yields time constants of 8.1 and 120 ps for the two processes. No long-lived transient can be observed in the nanosecond laser photolysis of **NDI-AlP** in dichloromethane.

---

[g] The unquenched emission indicates the presence of aluminium porphyrin lacking the NDI coordinated group. In principle, this could arise from (i) an equilibrium between coordinated and uncoordinated species or (ii) an excess of free aluminum porphyrin from the synthesis. The fact that the proportion of unquenched emission is constant as a function of concentration (in the 5×10^{-6}-6×10^{-5} M range) rules out hypothesis (i). On the other hand, hypothesis (ii) is consistent with a quantitative analysis of the absorption spectra of Figure 5, which reveals a small (ca. 10% excess) of porphyrin over NDI spectral features.
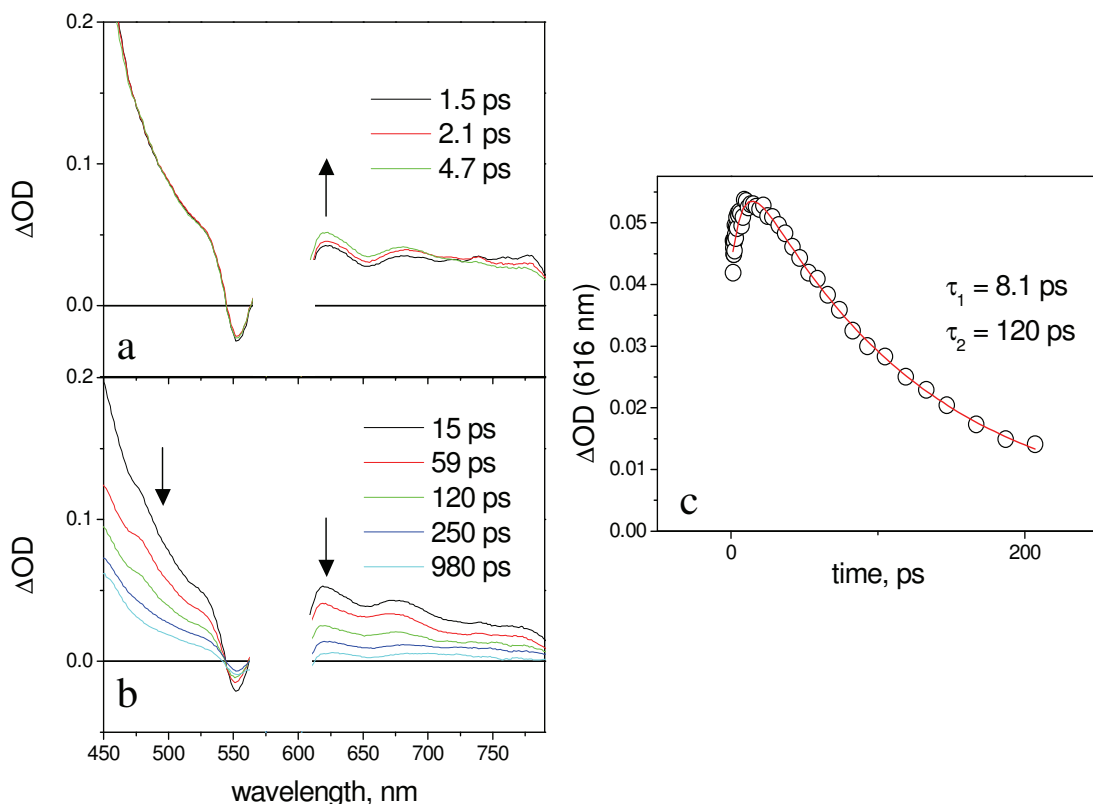
Figure 10. Transient absorption spectra (a, b) and kinetics (c) obtained in the femtosecond spectroscopy of **NDI-AlP** in dichloromethane (for details, see text).

These spectral changes are consistent with an electron transfer quenching mechanism. The early spectral changes with time constant 8.1 ps can be assigned to charge separation, and the subsequent ones with time constant 120 ps to charge recombination. The spectral changes for the forward reaction are relatively small, as the spectrum of the AlP excited state (Figure 7a) and that expected for a charge separated product (Figure 8a) are not very different. However, some features of the NDI$^-$ radical anion can be recognized in the spectrum of the transient, e.g. the sharp maximum at 610 nm and the shoulder at 475 nm. The broad absorption in the 600-700 nm range, as well as the Q-band bleach at 550 nm, are signatures of the aluminium porphyrin radical cation. The photophysical behavior of the dyad in dichloromethane is summarized in Figure 9a.

When the solvent is changed to chloroform, the qualitative behavior (Figure 11) remains the same as in dichloromethane, albeit with somewhat slower kinetics: 9 and 300 ps for the first and second processes, respectively.

Figure 11. Transient absorption spectra obtained in the femtosecond spectroscopy of **NDI-AlP** in chloroform. Excitation wavelength = 550 nm.

In toluene, on the other hand, only the first process (increase in optical density in the 580-710 range, time constant of 170 ps) is observed in the time window (0-1 ns) of the ultrafast experiment, implying that further decay takes place in a longer ns time scale (Figure 12).
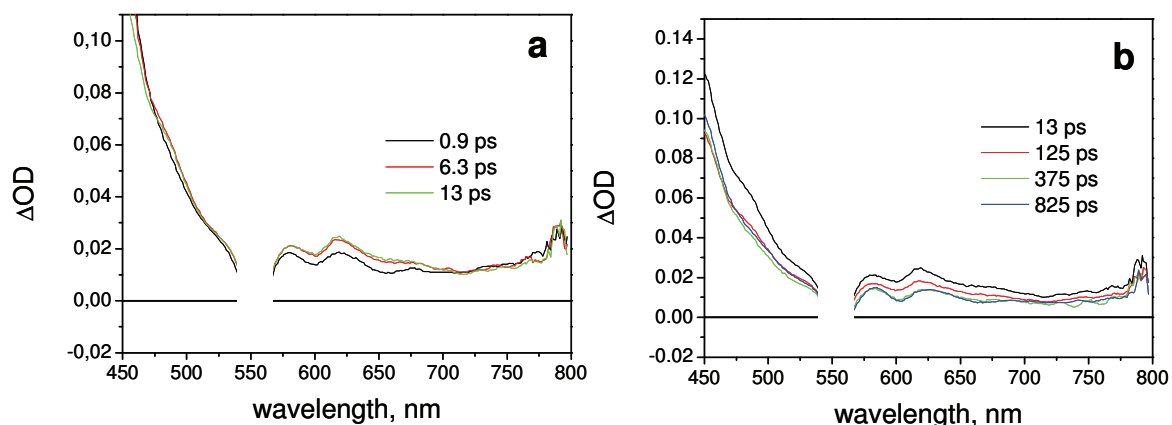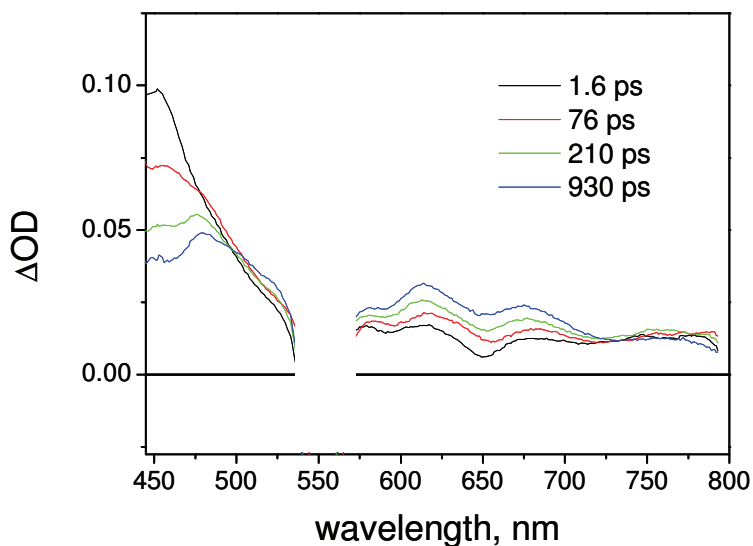

Figure 12. Transient absorption spectra obtained in the femtosecond spectroscopy of **NDI-AlP** in toluene. Excitation wavelength = 550 nm.

The solvent effect on the observed kinetics is as expected for an electron transfer quenching mechanism. A decrease in solvent polarity brings about (i) a raise in energy of the charge-separated state and (ii) the decrease in reorganizational energy. For charge recombination, lying in the Marcus inverted region, both factors cooperate to slow down the rates (120 ps in dichloromethane, 320 ps in chloroform, > 2 ns in toluene). For charge separation, in the less exergonic regime, the effect on rates is more complex: almost constant in dichloromethane and chloroform (8 and 9 ps), because of partial compensation between the two effects; definitely slower in toluene (170 ps), because of the prevailing effect of small driving force. The fate of the long-lived (> 2 ns) charge separated state in toluene can be inferred from nanosecond laser photolysis results (Figure 13). The observed transient, that decays with oxygen-dependent kinetics (lifetime, 560 ns and ca. 6 µs in aerated and deaerated solution, respectively), matches exactly the triplet state of the **AlP(ba)** model (Figure 7b).
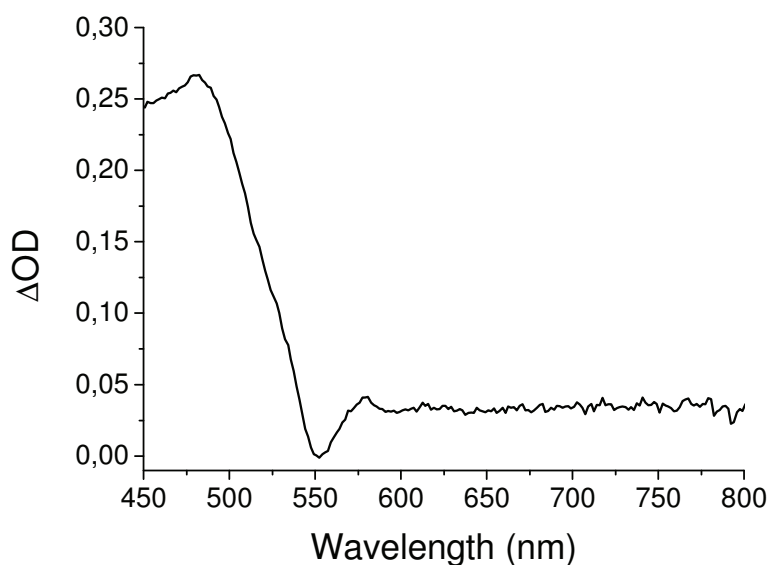
Figure 13. Transient absorption spectrum obtained in the nanosecond laser flash photolysis of **NDI-AlP** in toluene. Excitation wavelength = 532 nm, delay time 50 ns.

The photophysical mechanism in toluene can be schematized in the energy-level diagram of Figure 9b (where an approximate energy of the charge separated state is obtained from the experimental redox potentials in dichloromethane, by accounting[16] for the ion solvation energy differences between the two solvents). The charge-separated state is initially formed by photoinduced electron transfer in a singlet spin state. Whereas in dichloromethane charge recombination to the ground state is rapid and 100% efficient, in

toluene such a process is slowed down sufficiently by inverted-region effects to allow spin inversion[17] to occur in the charge-separated state. Thus, charge recombination yields the triplet state of the aluminium porphyrin unit rather than the ground state.

Photophysics of the NDI-AlMPyP-RuP triad.

A simplified energy level diagram for the **NDI-AlMPyP-RuP** triad (high-lying excited states of the NDI unit, omitted again for clarity), as inferred from the spectroscopic and electrochemical data of Table 1, is shown in Figure 14. It can be seen that a variety of quenching pathways is available following excitation of both AlP and RuP chromophoric units.
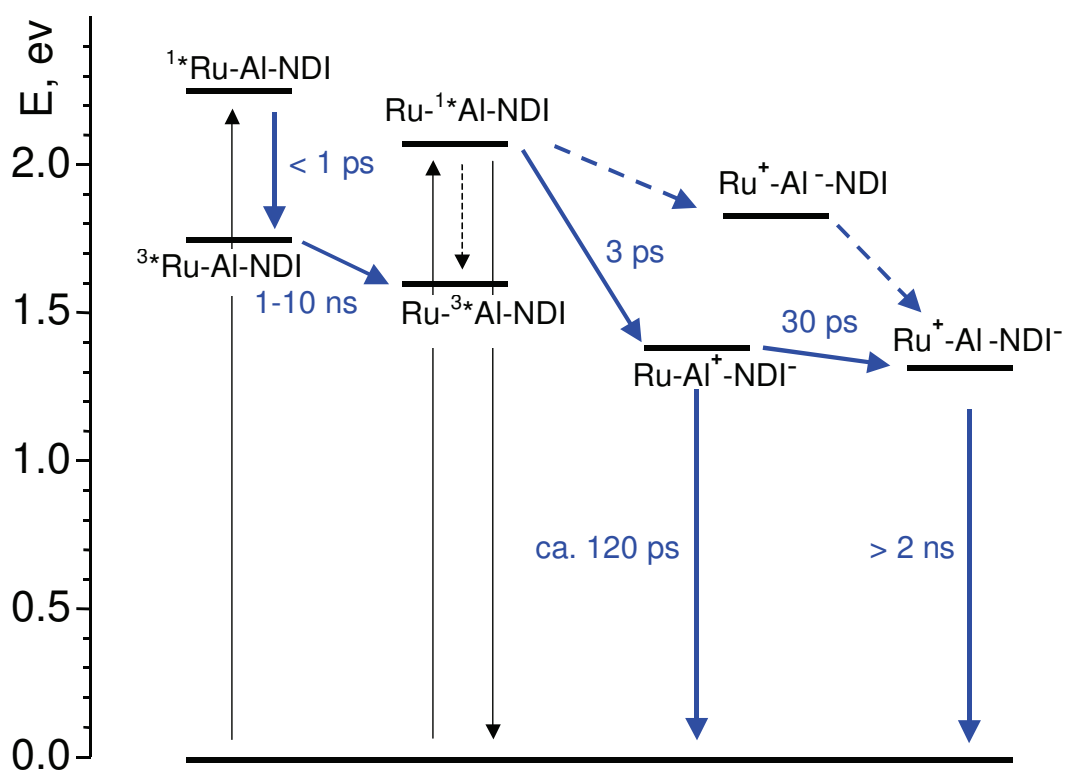
Figure 14. Energy level diagram and photophysical mechanisms for the **NDI-AlMPyP-RuP** triad in dichloromethane. Shorthand notation: AlMPyP = Al, RuP = Ru.

In the **NDI-AlMPyP-RuP** triad in dichloromethane, the naphthalene bisimide and aluminium porphyrin fluorescent emissions are completely quenched relative to those of the model compounds. The transient spectral changes observed in dichloromethane by ultrafast spectroscopy (λ_{exc} = 590 nm, 95% AlP excitation) are shown in Figure 15. The initial

spectrum is that of the excited singlet state of the aluminium porphyrin unit (see, for comparison Figure 7a). The transient spectral changes are clearly biphasic.
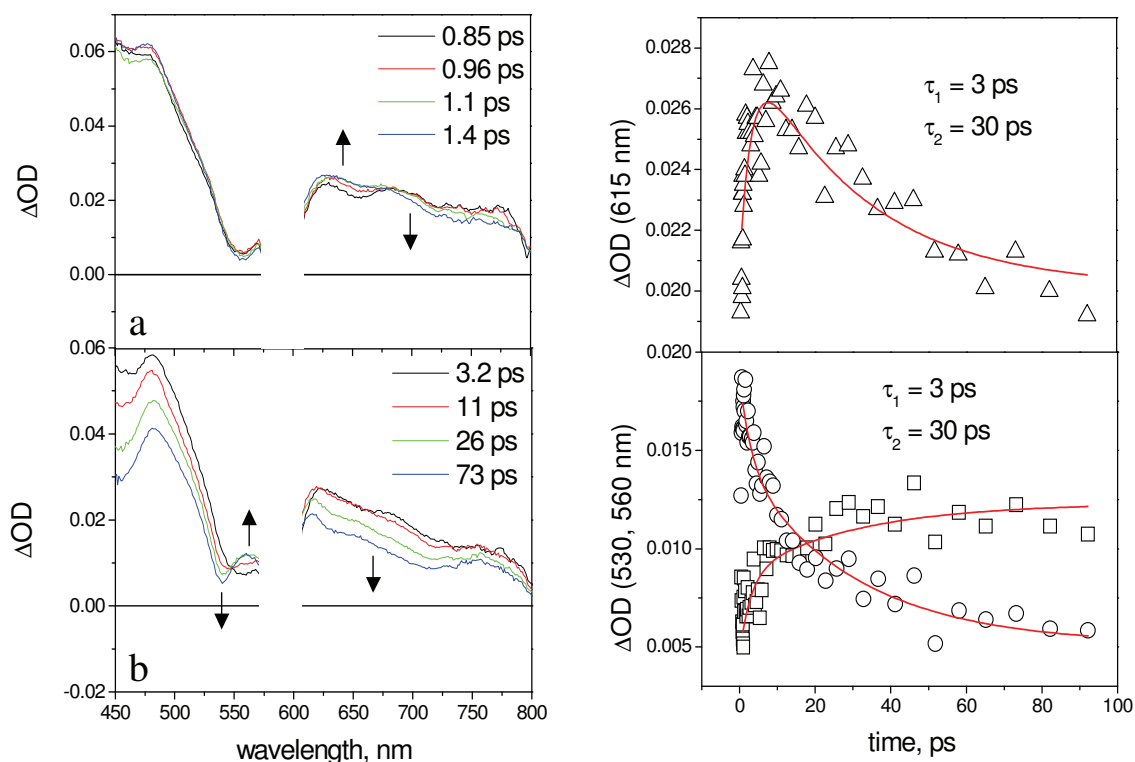
Figure 15. Femtosecond spectroscopy of **NDI-AlMPyP-RuP** in dichloromethane (for details, see text). Left: transient absorption spectra. Right: kinetics measured at 530 nm (dots), 560 nm (squares), and 615 nm (triangles).

The relatively small, early spectral changes (time constant, 3 ps, increase in optical density in the 580-690-nm range and decrease at $\lambda > 690$ nm) resemble closely those observed for the **NDI-AlP** dyad (Figure 10) and can be assigned to the same type of photoinduced electron transfer, i.e. to **Ru-^{1}*Al-NDI $\rightarrow$ Ru-Al$^+$-NDI$^-$** primary charge separation (Figure 14). In the subsequent time scale, however, the behavior of the **NDI-AlMPyP-RuP** triad differs sharply from that of the **NDI-AlP** dyad. Instead of a uniform decay towards the baseline, complex spectral changes with a time constant of 30 ps are observed: aside from a moderate decrease in absorbance in the 610-800 nm range, the most evident feature is a displacement of the sharp bleach originally present at 550 nm towards 530 nm. As these wavelenghts are typical of the Q-bands of the AlP and RuP units (Figures 8a and 8b), the bleach displacement can be easily assigned to hole shift from the AlP to the RuP unit, i.e. to **Ru-Al$^+$-NDI$^-$ $\rightarrow$ Ru$^+$-Al-NDI$^-$** secondary charge separation (Figure 14). As

a matter of fact, the final spectrum of Figure 15 (constant in the 200-1000 ps time range, is very similar to that calculated for a charge separated state where the NDI unit is reduced and the RuP unit is oxidized (Figure 8b) and to that experimentally observed following photoinduced charge separation in the **RuP-NDI''-RuP** symmetric triad (Figure 16).
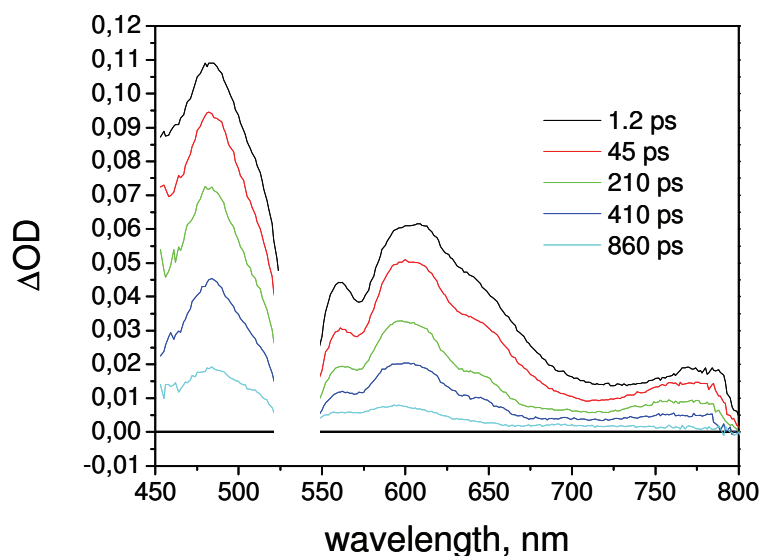
Figure 16. Transient absorption spectra obtained in the femtosecond spectroscopy of **RuP-NDI''-RuP** in dichloromethane. Excitation wavelength = 530 nm.

The process assigned to charge shift (30 ps) is sufficiently fast to compete favorably with primary charge recombination, expected to take place in ca. 120 ps, as measured in the **NDI-AlP** dyad. Considering its constancy in the time window of the ultrafast experiment, the long-range charge separated state has a lifetime longer than 2 ns. In flash photolysis experiments carried out by excitation with 590-nm, 10-ns pulses, the spectral profile of the charge separated state can be observed, although its decay could not be deconvoluted from that of the excitation pulse. Therefore, the lifetime of the long-range charge separated state lies in the few nanosecond range.

It should be remarked that an alternative electron transfer pathway is energetically available in the triad for obtaining the fully charge separated state following AlP excitation, i.e., photoinduced hole transfer from the AlP to the RuP unit, followed by electron shift from AlP to NDI (Figure 14, dashed arrows). In this hypothesis, neglecting the early 3-ps spectral changes, the 30-ps spectral shift of the bleach (Figure 15) could be attributed to photoinduced hole transfer, **Ru-^{1}*Al-NDI $\rightarrow$ Ru$^+$-Al-NDI$^-$** (Figure 14). In fact, the sharp maximum at 470 nm characteristic of the NDI radical anion seems to develop, rather than

disappear, in the 30-ps process. Therefore, although the alternative route cannot be definitely ruled out, the most likely electron transfer pathway for deactivation of the AlP excited state is that indicated by full arrows in Figure 14.

When the excitation wavelength is changed to 530 nm, so as to achieve substantial (ca. 80%) excitation of the RuP unit, ultrafast spectroscopy of the **NDI-AlMPyP-RuP** triad in dichloromethane yields the spectrum shown in Figure 17 (delay 1.5 ps). This spectrum is clearly that of the triplet state
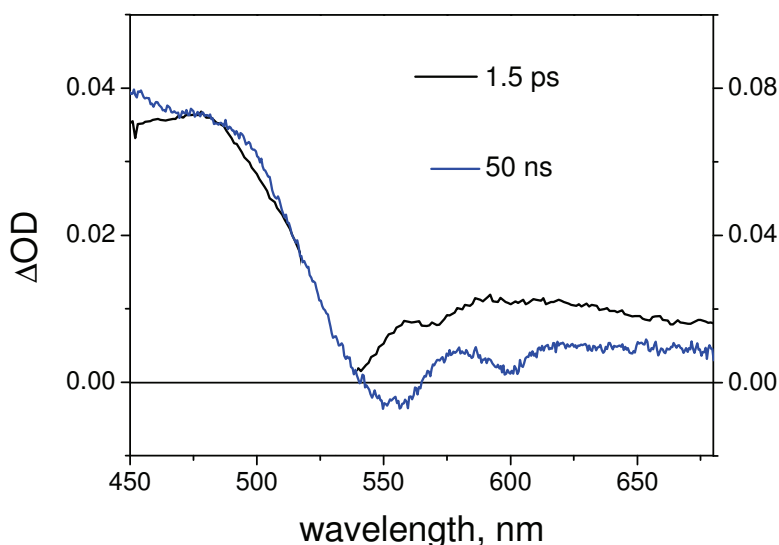
Figure 17. Transient absorption spectra obtained in femtosecond (black, 530-nm excitation) and nanosecond (blue, excitation at 532 nm) time-resolved spectroscopy of **NDI-AlMPyP-RuP** in dichloromethane (for details, see text).

of the RuP(py) unit (Figure 7c). This state is formed by prompt (< 1 ps) intersystem crossing and remains constant over the 1-1000 ps time scale. On the other hand, nanosecond flash photolysis (532-nm excitation) yields a clearly different spectrum (Figure 17, delay 50 ns). Since this spectrum matches well that of the triplet state of the AlP(ba) unit (Figure 7b), the obvious conclusion is that efficient triplet energy transfer from the RuP to the AlP unit, **^{3}*Ru-Al-NDI → Ru-^{3}*Al-NDI**, must occur in the "blind" time window between the two experiments (1-10 ns). The photophysical mechanism following excitation of the ruthenium porphyrin is also indicated in Figure 14.

3.4 Conclusions

The possibility to obtain triads for photoinduced charge separation by self-assembling of appropriate subunits has been explored using a metal-mediated strategy. An aluminium porphyrin, a ruthenium porphyrin and a naphthalenbisimide unit have been used as photosensitizer, donor, and acceptor units, respectively. The key problem, i.e., how to introduce the required asymmetry into the self-assembling process, has been tackled by choosing appropriate ligand functions on the various units (carboxylate on naphthalene bisimide, pyridyl on aluminium porphyrin) and exploiting hard/soft discrimination to achieve preferential coordination (carboxylate with aluminium, pyridyl with ruthenium).

The actual photophysical behavior of the **NDI-AlMPyP-RuP** triad has been investigated, by comparison with the **NDI-AlP** dyad and the individual molecular components, using time resolved spectroscopy in the fs-ps and ns time domains. The results in dichloromethane provide clear evidence for the occurrence of stepwise electron/hole transfer, leading to a charge separated state with reduced naphthalene bisimide acceptor and oxidized ruthenium porphyrin donor, with lifetime in the few nanosecond range. Thus, the triad behaves indeed as intended by molecular design, not only with respect to self-assembling but also in terms of light-induced function, providing an unprecedented example of a charge-separating functional unit obtained by self-assembly of molecular components via coordinative bonds. The performance of the triad is clearly not exceptional in absolute terms, particularly with regard to charge separation lifetime. In fact, the system is far from being ideal in several respects (e.g., uneven energy gradients in primary and secondary electron transfer steps, conformational flexibility in the axial linkage between aluminium porphyrin and the acceptor, relatively short charge separation distance). With this type of assembling strategy, however, improvements in the performance of the triad can be simply sought by appropriate chemical modification of the individual molecular components. In fact, the system described here can be seen as a case of a more general procedure, whereby the key bi-functional aluminium pyridyl-porphyrin unit can be reacted with a wide library of molecular components bearing complementary reactive sites. The self-sorting ability of the library members is indeed very powerful, as the assembling process occurs in few minutes, in mild conditions, and leads to the desired final adduct in quantitative yield.

In perspective, this strategy should easily open the access to a broad choice of triad systems, confining the synthetic effort to the single components. This is where self-

assembling promises to be superior, in terms of ease and flexibility, to conventional covalent synthetic strategies.

3.5 References

[1] (a) M. R. Wasielewski, *Chem. Rev*. **1992**, *92*, 435; (b) B. Rybtchinski, L. E Sinks, M. R. Wasielewski, *J. Am. Chem. Soc* **2004**, *126*, 12268; (c) M. R. Wasielewski, *J. Org. Chem.* **2006**, *71*, 5051.

[2] (a) D. Gust, T. A. Moore, A. L. Moore, *Acc. Chem. Res.* **1993**, *26*, 198. (b) D. Gust, T. A. Moore, A. L. Moore in *Electron Transfer in Chemistry*; V. Balzani, Ed.; Wiley-VCH: Weinheim, Germany, **2001**; Vol. III, Part 2, Chapter 2, pp 273-336; (c) I.M. Bennett, H. M. Vanegas Farfano, F. Bogani, A. Primak, P. A. Lidell, L. Otero, L. Sereno, J.J. Silber, A. L. Moore, T. A. Moore, D. Gust, *Nature* **2002**, *420*, 398; (d) M. Di Valentin, A. Bisol, G. Agostini, P. A. Liddell, G. Kodis, A. L. Moore, T. A. Moore; D. Gust, D. Carbonera, *J. Phys. Chem. B,* **2005**, *109*, 14401.

[3] (a) A. Harriman, J.-P. Sauvage, *Chem. Soc. Rev.* **1996**, *25*, 41; (b) E. Baranoff, J.-P. Collin, L. Flamigni, J.-P. Sauvage, *Chem. Soc. Rev.*,**2004**, *33*, 147.

[4] E. Danielson, C. M Elliott, J. W. Merkert, T. J. Meyer *J. Am. Chem. Soc.*, **1987**, *109*, 2519. (b) S. L. Larson, C. M. Elliott, D. F.Kelley, *J. Phys. Chem.*, **1995**, *99*, 6530. (c) J. M. Weber, M. T. Rawls, V. J. MacKenzie, B. R. Limoges, C. M. Elliott *J. Am. Chem. Soc.* **2007**, *129*, 313.

[5] D. M. Guldi, *Pure Appl. Chem.* **2003**, *75*,1069; (b) D. M. Guldi, H. Imahori, K. Tamaki, Y. Kashiwagi, H. Yamada, Y. Sakata, S. Fukuzumi *J. Phys. Chem. A* **2004,** *108,* 541.

[6] (a) C-C. You, R. Dobrawa, C. R. Saha-Möller, F. Würthner *Top. Curr. Chem.* **2005**, *258*, 39. (b) E. Iengo, E. Zangrando, E. Alessio, *Acc. Chem. Res.* **2006**, *39*, 841. (c) F. Scandola, C. Chiorboli, A. Prodi, E. Iengo, E. Alessio, *Coord. Chem. Rev.* **2006**, *250*, 1471. (d) E. Iengo, F. Scandola, E. Alessio, *Struct. Bonding (Berlin)* **2006**, *121*, 105. (e) J. T. Hupp *Struct. Bonding (Berlin)* **2006**, *121*, 145.

[7] (a) R. Dobrawa, F. Würthner, *Chem. Commun.* **2002**, 1878. (b) A. Harriman, J. Rostron, M. Cesario, G. Ulrich, R. Ziessel *J. Phys. Chem. A* **2006,** *110,* 7994. (c) Y. Terazono, G. Kodis, P. A. Liddell, V. Garg, M. Gervaldo, A. L. Moore, T. A. Moore, D. Gust, *Photochem. Photobiol.* **2007**, *83*, 464.

[8] (a) F. D'Souza, P. M. Smith, M. E, Zandler, A. L. McCarty, M. Itou, Y. Araki, O. Ito *J. Am. Chem. Soc.*, **2004**, *126*, 7898. (b) F. D'Souza, M. E. El-Khouly, S. Gadde, M. Zandler, A. L. McCarty, Y. Araki, O. Ito *Tetrahedron* **2006**, *62*, 1967.

[9] (a) G. J. E. Davidson, L. H. Tong, P. R. Raithby, J. K. M. Sanders, *Chem. Commun.* **2006**, 3087; (b) G. A. Metselaar, J. K. M. Sanders, J. de Mendoza, *Dalton Trans.* **2008**, 588. (c) G.

J. E. Davidson, L. A. Lane, P. R. Raithby, J. E. Warren, C. V. Robinson, J. K. M Sanders *Inorg. Chem.* **2008**, *47*, 8721.

[10] (a) H. Sugimoto, T. Kimura, S. Inoue *J. Am. Chem. Soc.* **1999**, *121*, 2325. (b) J. M. Rowley, E. B. Lobkovsky, G. W. Coates, *J. Am. Chem. Soc.* **2007**, *129*, 4948. (c) T. Aida, H. Sugimoto, M. Kuroki, S. Inoue *J. Phys. Chem.* **1995**, *8*, 249. (d) I. H. A. Badr, M. E. Meyerhoff *Anal. Chem.* **2005**, *77*, 6719.

[11] P. P. Kumar, B. G. Maiya *New. J. Chem.* **2003**, *27*, 619.

[12] A. Prodi, M. T. Indelli, C. J. Kleverlaan, F. Scandola, E. Alessio, T. Gianferrara, L. G. Marzilli *Chem. Eur. J.* **1999**, *5*, 2668.

[13] M. T. Indelli, C. Chiorboli, M. Ghirotti, M. Orlandi, F. Scandola, H. J. Kim, H.-J. Kim *J. Phys. Chem. B*, **2010**, *114*, 0000.

[14] N. G. Connelly, W. E. Geiger, *Chem. Rev.* 1996, *96*, 877.

[15] S. Alp, U. Erten, C. Karapire, B. Köz, A. O. Doroshenko, S. Içli, *J. Photochem. Photobiol. A* **2000**, *135*, 103.

[16] D. Rehm, A. Weller, *Ber. Bunsen-Ges. Phys. Chem.* **1969**, *73*, 834.; A. Weller, *Z. Phys. Chem.* **1982**, *133*, 93.

[17] T. van der Boom, R. T. Hayes, Y. Zhao, P. J. Bushard, E. A. Weiss, M. R. Wasielewski, *J. Am. Chem. Soc.* **2002**, *124*, 9582.

Chapter 4

Photoinduced Electron Transfer in Ruthenium(II)/Tin(IV) Multiporphyrin Arrays.[γ]
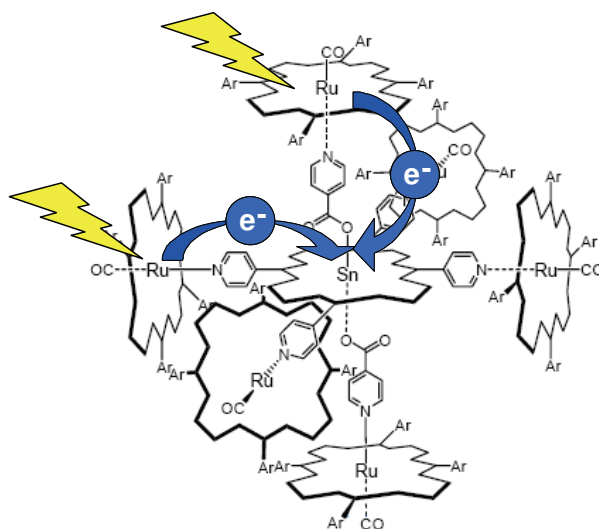
A Sn-porphyrin and a Ru-porphyrin are combined in a series of supramolecular arrays which exhibit a number of intercomponent photoinduced electron-transfer processes leading to a common charge-separated state.

The work described in this chapter is the result of a collaboration between the Photochemistry Group at the Department of Chemistry of University of Ferrara (Ferrara, Italy) and the Group of Professor Kim at Kumoh National Institute of Technology (Gumi, Republic of Korea).

4.1 Introduction

Porphyrins and metalloporphyrins have been extensively used in recent years as building blocks for the construction of supramolecular arrays, exploiting a variety of binding motifs (covalent linkages usually through the *meso* positions of the porphyrin ring[1] or coordinative bonds involving axial coordination of peripheral ligands to porphyrin metal ions[2]).

In particular, Sn(IV) porphyrins present some properties especially interesting for the design of charge-separating systems: while being comparable in terms of photophysical properties, it is a definitely much easier to reduce unit than typical porphyrins (e.g., free-base or Zn porphyrins).[3] Therefore its inclusion in supramolecular porphyrin arrays is expected to introduce facile electron transfer pathways. Furthermore, the tendency to form two strong axial bonds with oxygen donor ligands can be exploited for the construction of arrays of higher complexity. For these attractive features, Sn(IV) porphyrin units have been included as photoexcitable and/or electron-acceptor molecular components in a number of interesting supramolecular systems.[3,4,5,6,7,8, 9,10,11,12]

The work described in this chapter consists of the investigation of the photophysical and redox behavior of a series of supramolecular arrays (Chart 1) and related model compounds (Chart 2). In these arrays, a central Sn(IV) porphyrin is attached to two (**SnRu₂**), four (**SnRu₄**) or six (**SnRu₆**) ruthenium porphyrin units.

Chart 1. Structural formulas of the arrays studied.

Chart 2. Structural formulas of the monomeric model compounds **Sn** and **Ru.**

4.2 Experimental Section

The syntheses and characterization of the compounds discussed in this chapter were performed by Hyun Jung Kim and Hee-Joon Kim at Kumoh National Institute of Technology (Gumi, Republic of Korea).

Reagents and spectroscopic-grade solvents were purchased and used as received, if not otherwise stated. See Chapter 2 for details on electrochemical and photophysical measurement apparatus and procedures.

4.3 Results

Stability in Solution

Given the moderate strength of the Ru(II)-N(py) coordination bond,[13] the stability in solution of the arrays is a critical experimental question. All the photophysical experiments refer to freshly prepared solutions at concentration higher than 2×10^{-5} M. In these conditions all the arrays studied were found to be stable as checked by concentration dependent spectrophotometric and spectrofluorimetric measurements.

In the time resolved absorption experiments, dichloromethane solutions saturated with potassium carbonate were used to remove traces of acidity that were found to promote photodecomposition under prolonged laser irradiation. Photodecomposition was always negligible, as checked spectrophotometrically before and after each experiment.

Redox Behavior

The electrochemical behavior of **SnRu$_2$** and **SnRu$_4$** arrays was studied in CH_2Cl_2 solution. **Sn** model was also studied in the same experimental conditions for comparison. The potential values for the first oxidation and reduction processes are summarized in Table 1. As we can see from Table 1, the redox behavior of the arrays is a reasonable superposition of those of the model compounds. For both arrays, the first oxidation process that occurs at the same potential of the ruthenium porphyrin model can be easily assigned to the ruthenium porphyrin unit whereas the reduction process takes place at the tin porphyrin central unit. It is important to note that in **SnRu$_4$** the presence of four pyridyl groups attached to the central porphyrin ring causes a significant anodic shift in the reduction

potential of the tin porphyrin unit. A similar effect was observed in a previous work for a related pentameric multiporphyrin array.[13]

Table 1. Electrochemical data for the arrays and for the model compounds.[a]

Compound	$E_{1/2 \text{ (red)}}$,[b] V	$E_{1/2 \text{ (ox)}}$,[b] V
Sn	- 0.90	+ 1.4
Ru[c]	- 1.76	+ 0.79
SnRu$_2$	- 0.90	+ 0.80
SnRu$_4$	- 0.62	+ 0.83

[a] In CH_2Cl_2 at 298 K (0.1M TBA(PF$_6$) as electrolyte, scan rate 200 mV/s, SCE as reference electrode, and glassy carbon as working electrode). [b] Halfwave potential in cyclic voltammetry ($\Delta E_p = 60 - 80$ mV). [c] Ref. 5.

Photophysical Behavior

Monomeric systems. The photophysical properties of the ruthenium porphyrin model system (**Ru**) were described previously.[13,14] Excitation is followed by ultrafast (< 1ps) intersystem crossing leading to quantitative population of the triplet state. The triplet state, which can be detected at room temperature by laser flash photolysis ($\lambda_{max} = 470$ nm), or by phosphorescence emission ($\lambda_{max} = 726$ nm), decays with a lifetime of 30 μs (deaerated solution).

The absorption spectrum (Figure 1) of the tin chromophoric model (**Sn**) shows the typical pattern of regular metal porphyrins with two Q-bands in addition to the Soret band. The emission (Figure 2) is fluorescence from the lowest singlet $\pi-\pi^*$ state, with the 0-0 and 0-1 transition at 600 and 660 nm. The lifetime in CH_2Cl_2 solution is of 1.1 ns. Based on values measured for Zn(TTP), the fluorescence quantum yield is about 0.03. The ^{3*}Sn triplet state is non emissive at room temperature, although a distinct phosphorescent emission is observed at 77 K (Figure 2).
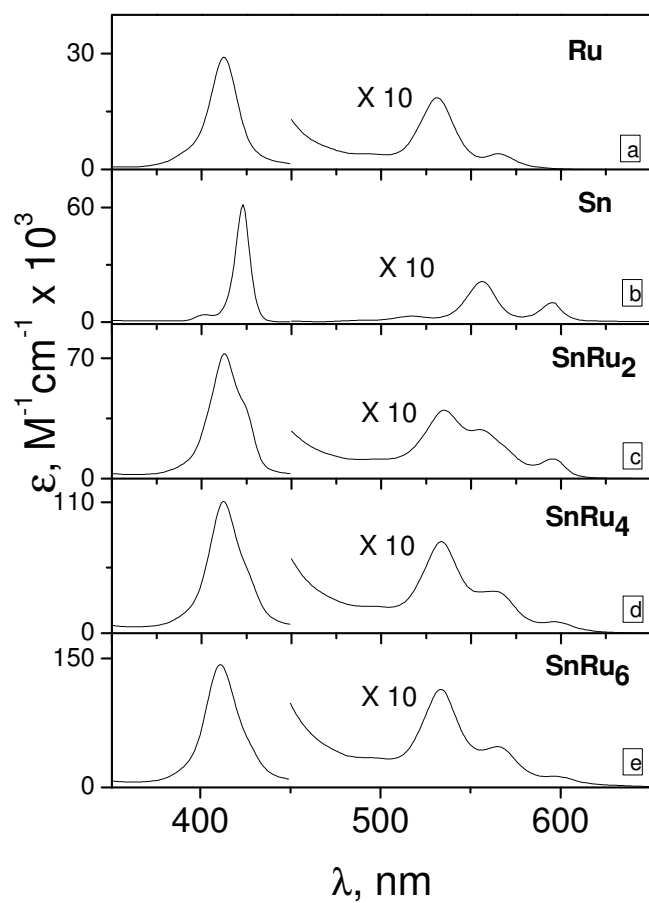
Figure 1. Absorption spectra of model compounds and of the arrays in CH_2Cl_2. **Ru** (a) and **Sn** (b), **SnRu$_2$** (c), **SnRu$_4$** (d), **SnRu$_6$** (e).
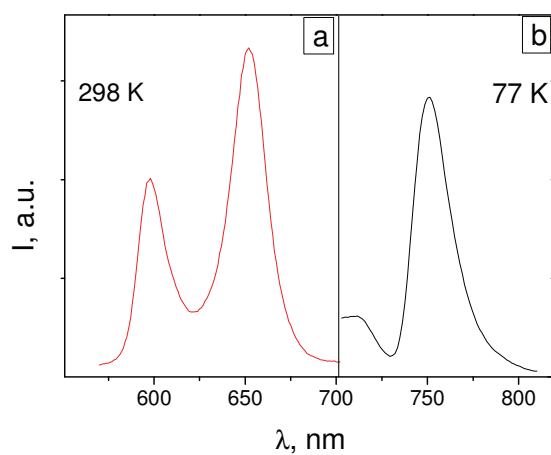
Figure 2. Emission spectra for **Sn**; (a) room-temperature in CH_2Cl_2 and (b) low-temperature in EtOH/MeOH 4/1 matrix.

[3*]Sn can be conveniently monitored by transient absorption in nanosecond laser flash photolysis (λ_{max} = 480 nm, Figure 3). The quantum yield of triplet formation is about 0.9. At low laser power, the triplet absorption decays following an appreciably first order kinetics with a lifetime of 20 µs in deaerated CH_2Cl_2 solutions. The lifetime in aerated solution is of 1.3 µs.
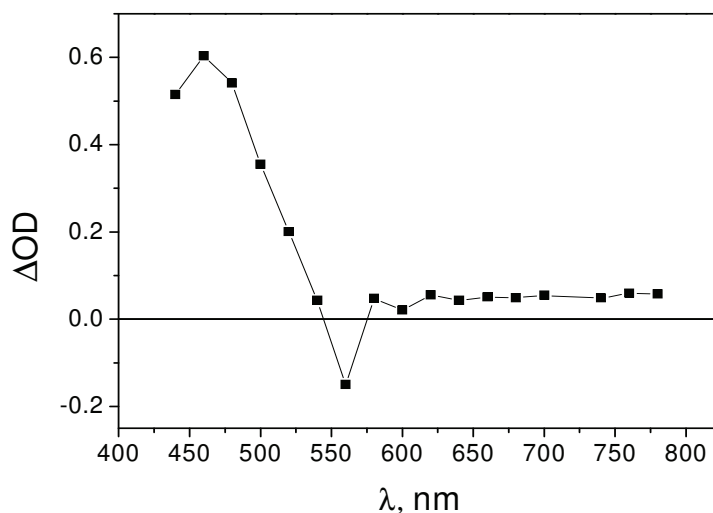
Figure 3. Triplet difference absorption spectrum obtained in the laser flash photolysis (λ_{xc} = 532 nm) of **Sn** in CH_2Cl_2.

The Sn porphyrin complex was also investigated by ultrafast transient spectroscopy. The differential absorption spectrum obtained using 555 nm excitation pulses in CH_2Cl_2 is reported in Figure 4 and corresponds to the spectrum of the [1*]S singlet state. This spectrum shows as distinctive features a broad featureless positive absorption throughout the visible region, with superimposed the bleaching of the ground state Q-band at 600 nm and additional apparent bleaching corresponding to stimulated fluorescent emission at 630 < λ < 680 nm. This transient spectrum is formed in less than 1 ps and is practically constant in the 1-1000 ps time window.
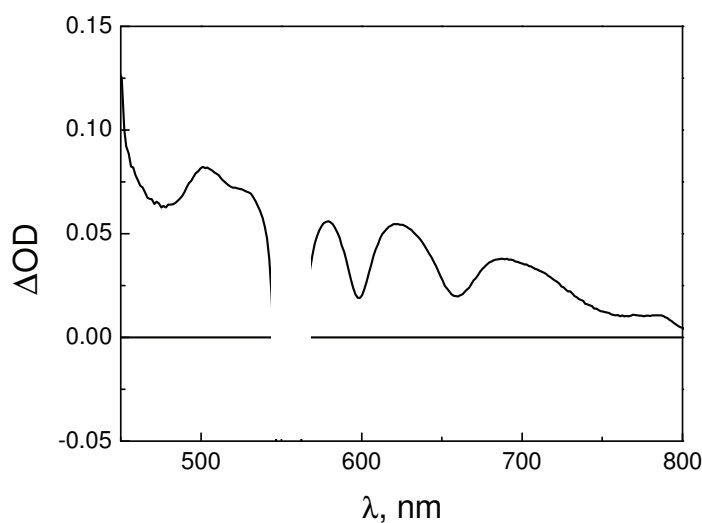
Figure 4. Transient absorption spectrum obtained for **Sn** in ultrafast spectroscopy (CH_2Cl_2, λ_{xc} = 555 nm, 1 ps delay).

Arrays. The absorption spectra of **SnRu$_2$**, **SnRu$_4$** and **SnRu$_6$** are shown in Figure 1. In the visible region, the spectra of the arrays can always be reproduced by a superposition of the spectra of the molecular models. As we can see from the figure, in going from **SnRu$_2$** to **SnRu$_4$** and **SnRu$_6$** the Q-band region is dominated by the ruthenium porphyrin absorption features with an increase of the 534-nm band proportional to the number of ruthenium units.

All the arrays examined were found to have very similar emission behavior in stationary experiments. They exhibit an exceedingly weak emission both in aerated and deaerated solution. It is clearly seen that this weak emission is fluorescence from the tin chromophore, strongly quenched with respect to that of the **Sn** model. For all the arrays a quenching ratio >>10 has been estimated from optically matched solutions of the array and tin model (excitation wavelength, 595 nm, corresponding to 100% excitation, of the tin porphyrin unit). The excitation spectra of this residual fluorescence (Figure 5) show the complete lack of ruthenium porphyrin absorption features and the close correspondence to the absorption spectrum of the tin porphyrin model. No transient emission has been observed with a single-photon lifetime apparatus that has 300 ps as lower detection limit.

Following excitation of the Ru-based unit the typical phosphorescence from ruthenium porphyrin chromophore is completely quenched also in deaerated solution.
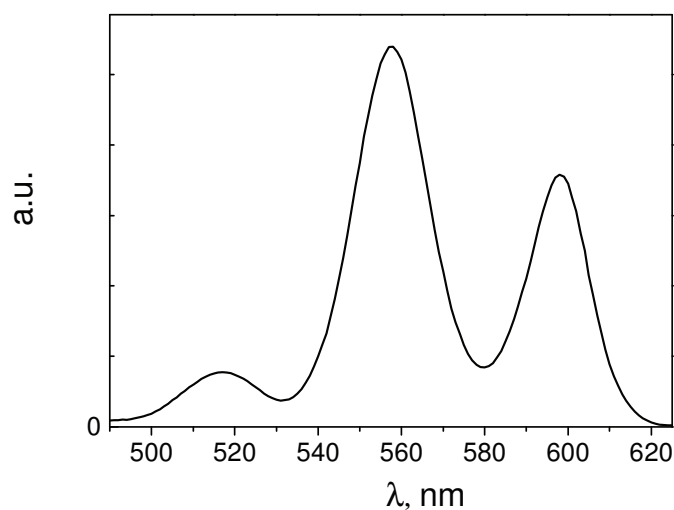
Figure 5. Excitation spectrum of **SnRu$_2$** in CH$_2$Cl$_2$.

Time-resolved spectroscopy of SnRu$_2$. An appropriate choice of excitation wavelength allows the selective excitation of the two chromophores. In practice, for **SnRu$_2$** 555 nm is a convenient wavelength for efficient excitation (70%) of the tin chromophore while selective (> 90%) absorption by the ruthenium porphyrin unit can be obtained at 530 nm.

The transient spectral changes obtained in ultrafast spectroscopy by 555-nm excitation of **SnRu$_2$** in dichloromethane are shown in Figure 6. The differential absorption spectrum, taken immediately after the laser pulse (0.9 ps), is identical to that exhibited by free **Sn** model (see Figure 4). In the early time scale (< 50 ps) a fast evolution from this initial spectrum to a new spectrum is observed. In the spectral changes clear features are: i) the decrease of the ground-state bleaching at 600 nm and the complete disappearance of the stimulated emission at $630 < \lambda < 680$ nm, ii) the rise of a positive absorption at $\lambda > 550$ nm (broad absorption in the 600-650 nm range and a band with a maximum at ca.725 nm). Kinetic analysis of the absorption rise at 725 nm yields a time constant of ca. 25 ps. (Figure 6, inset). This absorption remains constant in the whole kinetic range of the ultrafast experiment (ca. 1 ns).
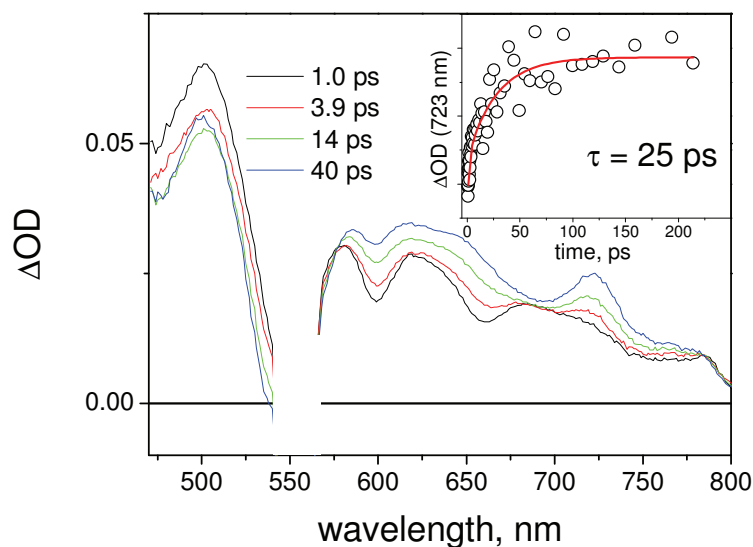
Figure 6. Ultrafast spectroscopy of **SnRu$_2$** in CH$_2$Cl$_2$ (excitation at 555 nm). Inset: Kinetic analysis at 725 nm.

The transient behavior upon selective excitation of the ruthenium porphyrin unit ($\lambda = 530$ nm) has been also investigated. The spectral variations are depicted in Figure 7. The initial spectrum (1 ps) is very similar to that exhibited by the Ru(TPP)(CO) model, showing a positive absorption with a maximum at 460 nm. A clear evolution from this spectrum to a final spectrum with features practically identical to those found upon 555 nm excitation (broad absorption at $\lambda > 560$ nm with a maximum at 730 nm) is observed in the 1-500 ps time scale. The time for formation of this transient is by far slower than that observed for excitation at 550 nm. Kinetic analysis of spectral changes at 650 nm yields a time constant of 200 ps (inset of Figure 7). As in the case of tin unit excitation, these spectral changes remain constant over the time window of the experiment.
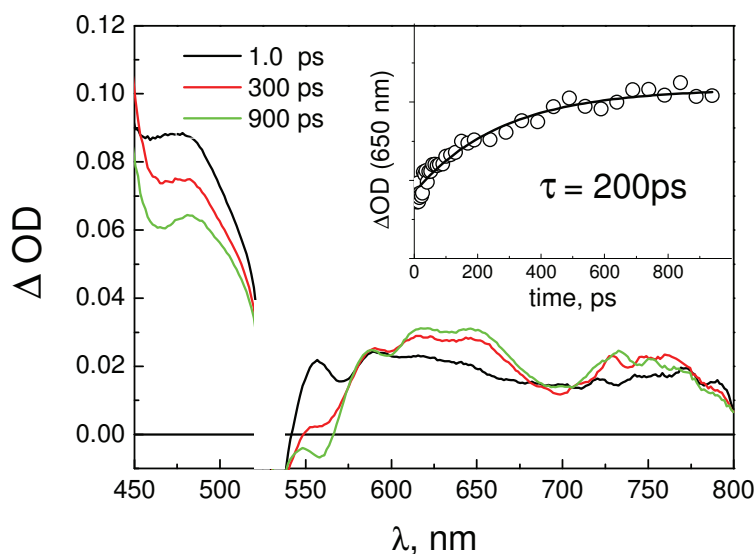
Figure 7. Ultrafast spectroscopy of **SnRu$_2$** in CH$_2$Cl$_2$ (excitation at 530 nm). Inset: Kinetic analysis at 650 nm.

Nanosecond laser flash photolysis (excitation wavelength 532 nm) has been used to investigate the fate of the long-lived (> 1 ns) transient observed by femtosecond spectroscopy. The transient spectrum (Figure 8a) recorded right at the maximum of the excitation pulse showing a pronounced absorption peaking at 460 nm followed by a broad absorption in the 500-800 region, is superimposable to the final spectrum of the ultrafast experiment. This transient decays back to the ground state in the same time scale as the excitation pulse, with apparent lifetime of 8 ns.

In order to investigate the effect of solvent polarity on the photophysics of **SnRu$_2$**, experiments were carried out also in toluene and compared with those obtained in CH$_2$Cl$_2$. The stationary experiments showed that, as in CH$_2$Cl$_2$, the phosphorescence from Ru-porphyrin is completely quenched. In contrast, the results of nanosecond transient absorption obtained in toluene differ strongly from those observed in CH$_2$Cl$_2$. Following excitation at 532 nm, a long-lived transient was observed exhibiting the characteristics features (spectrum and lifetime) of the triplet state of tin component (Figure 8b).
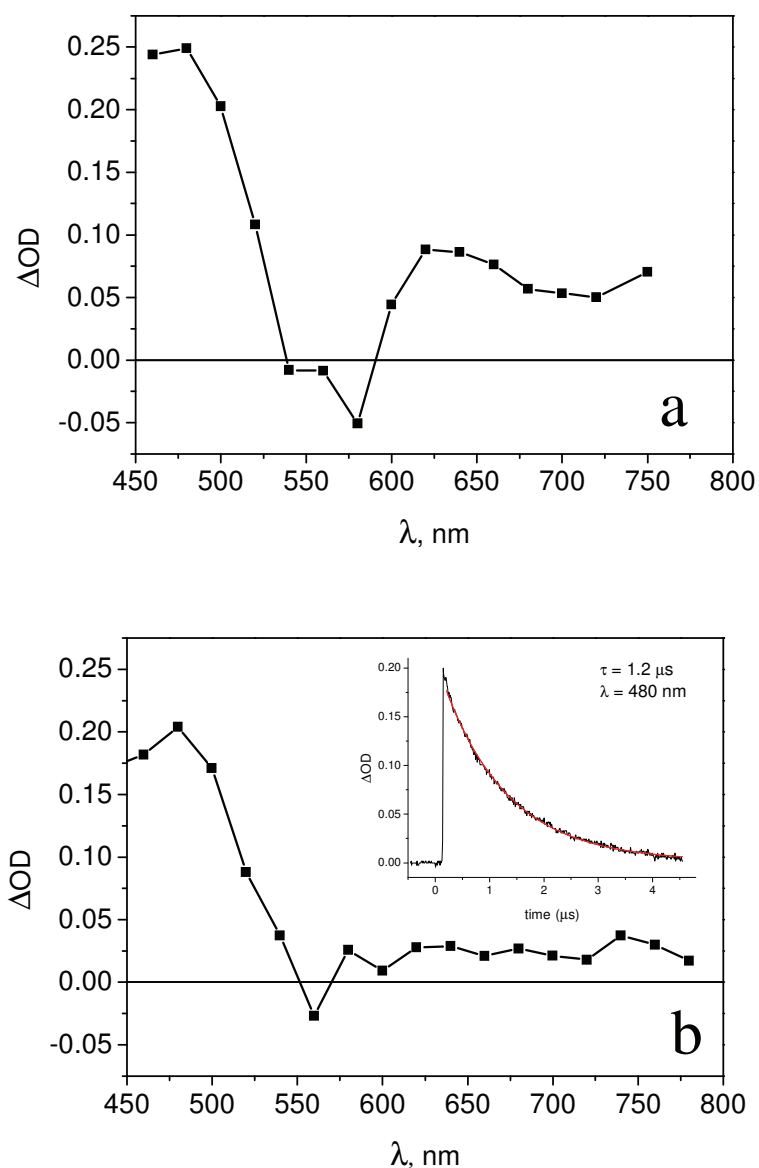
Figure 8. Nanosecond laser flash photolysis of **SnRu$_2$**, λ_{xc} = 532 nm. (a) CH$_2$Cl$_2$, differential absorption spectrum recorded at the maximum of the excitation pulse. (b) Toluene, differential absorption spectrum recorded at 50 ns delay time; inset, kinetic analysis at 480 nm.

Ultrafast spectroscopy (Figure 9) clearly shows the formation of the triplet state of tin component from the ruthenium-porphyrin triplet (time constant, ca 1.5 ns).
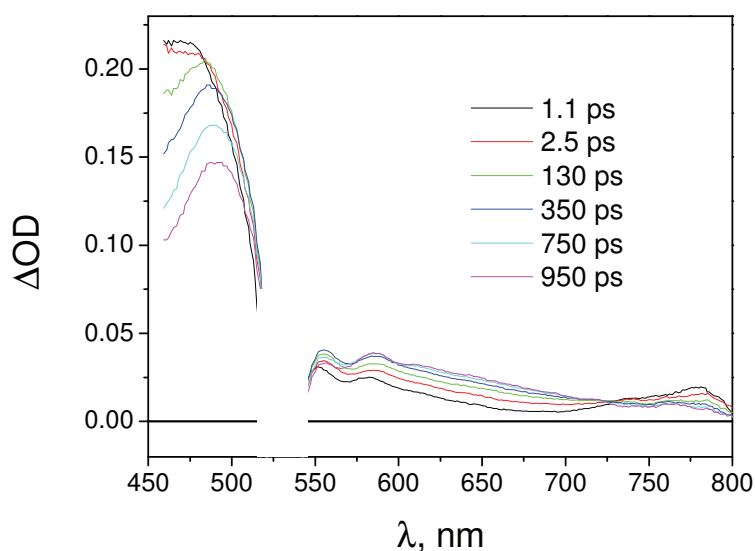
Figure 9. Ultrafast spectroscopy of **SnRu$_2$** in toluene (excitation at 530 nm).

Time-resolved spectroscopy of SnRu$_4$. For **SnRu$_4$**, selective excitation of the tin porphyrin unit is obtained by exciting at 595 nm. The transient spectral changes obtained by ultrafast spectroscopy in CH$_2$Cl$_2$ are shown in Figure 10. The behavior is clearly biphasic. In the shorter time scale (1-16 ps, Figure 10a), the spectral changes (formation of a positive broad absorption at $\lambda > 550$

Figure 10. Ultrafast spectroscopy of **SnRu$_4$** in CH$_2$Cl$_2$ (excitation at 595 nm): (a) t = 1-16 ps; (b) t = 16 - 930 ps.
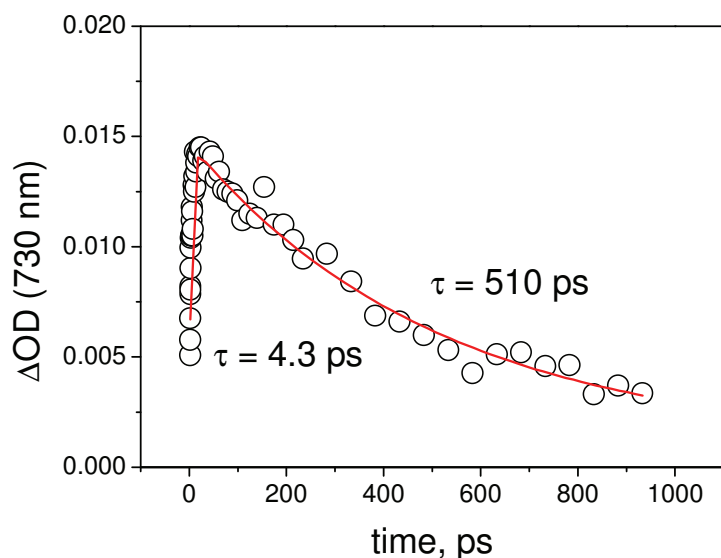
Figure 11. Kinetic analysis at 730 nm for **SnRu$_4$** upon 595 nm excitation in CH$_2$Cl$_2$.

peaking at 730 nm) are very similar to those observed for **SnRu$_2$** under the same experimental conditions (see Figure 6). Contrary to what happened for **SnRu$_2$**, however, this spectrum decays in the time window of the ultrafast experiment (Figure 10b). The time constants for the two processes are 4.3 and of 510 ps, respectively (Figure 11).

Upon excitation of **SnRu$_4$** at 530 nm, where the excitation light is 100% absorbed by the Ru porphyrin unit, the spectral changes (Figure 12a) in the initial time scale are qualitatively the same as observed for **SnRu$_2$** in the same experimental conditions (Figure 7). In contrast the kinetic behaviour was found to be quite different. The initial spectrum, taken immediately after the excitation pulse (Figure 12a), evolves in the early timescale (< 20 ps) to a new spectrum featuring broad absorption at λ > 560 nm with a maximum at 730 nm. The formation of this transient is much faster than in the case of **SnRu$_2$**. A time constant of 8 ps is obtained from the kinetic analysis at 730 nm (Figure 13). On a longer time scale this transient (Figure 12b) decays to ground state uniformly at all wavelengths with a time constant of 560 ps, while in the case of **SnRu$_2$** the transient spectral changes remain constant over the time window of the experiment (Figure 7).
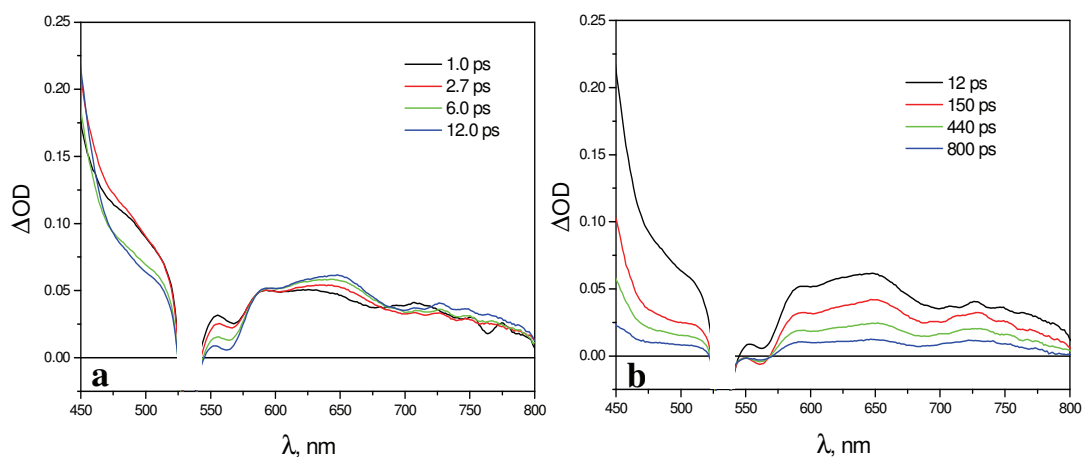
Figure 12. Ultrafast spectroscopy of **SnRu₄** in CH_2Cl_2 (excitation at 530 nm): (a) t = 1-12 ps; (b) t = 12 -800 ps.
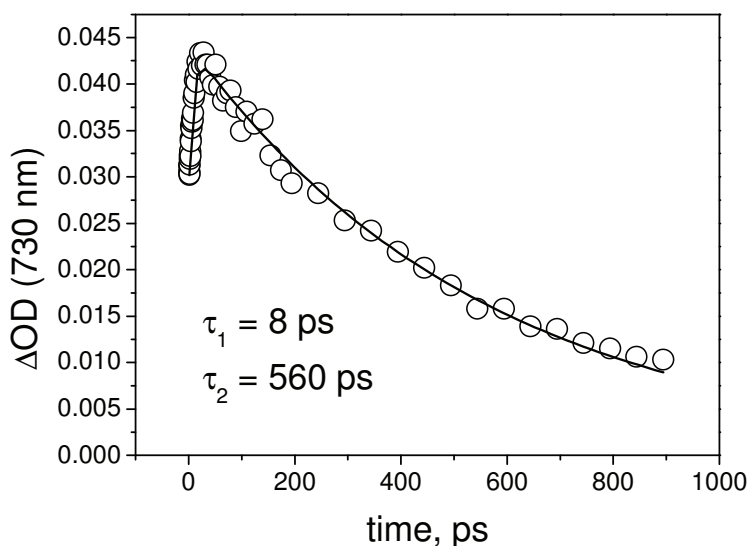
Figure 13. Kinetic analysis at 730 nm for **SnRu₄** upon 530 nm excitation in CH_2Cl_2.

Time-resolved spectroscopy of SnRu₆. For this array, the presence of six ruthenium porphyrin chromophores makes selective excitation of the tin porphyrin unit difficult to achieve at any practical wavelength. Selective excitation of the ruthenium porphyrin chromophores is easy, on the other hand, at 530 nm. The transient changes observed upon 530-nm excitation were very similar (spectral shape and time scale) to those detected for **SnRu₄** in the same experimental conditions. A transient spectrum featuring broad absorption at $\lambda > 560$ nm with maxima at 650 nm and 730 nm (Figure 14) is formed in 7 ps and decays to ground state in 650 ps (Figure 15).
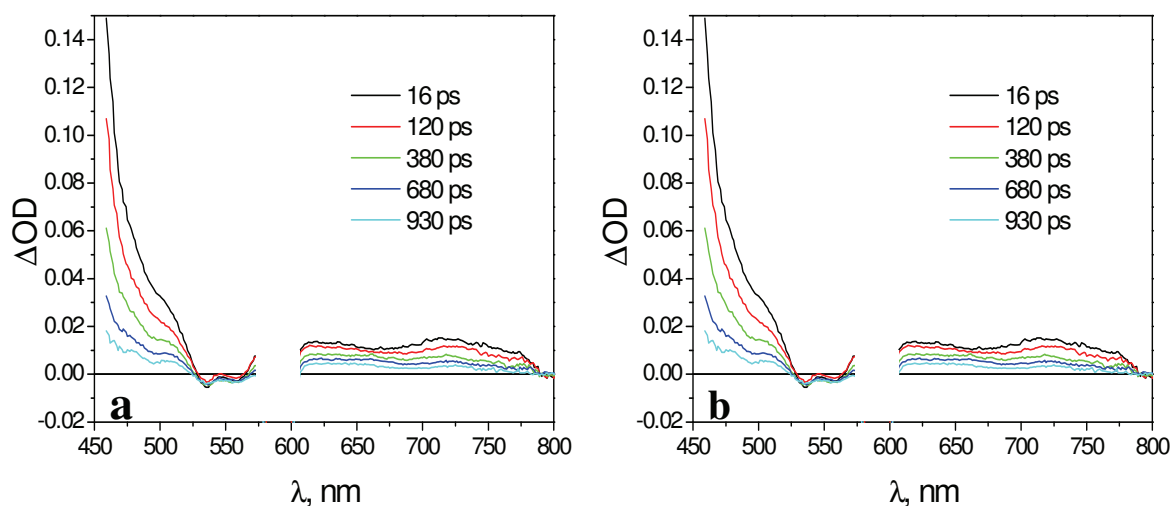
71
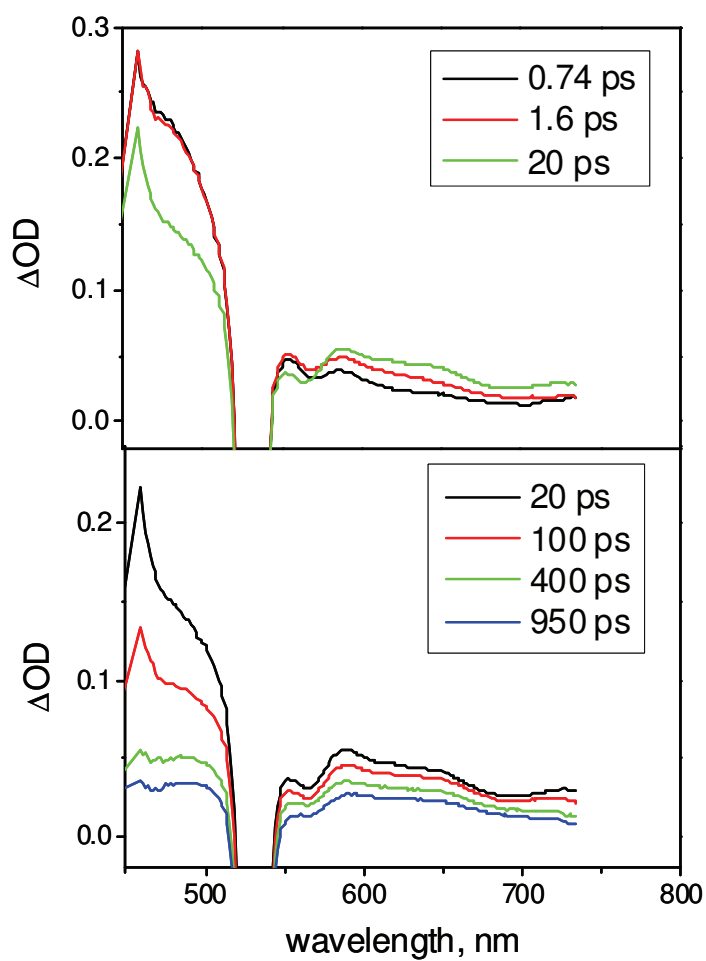
Figure 14. Ultrafast spectroscopy of **SnRu$_6$** in CH$_2$Cl$_2$ (excitation at 530 nm).
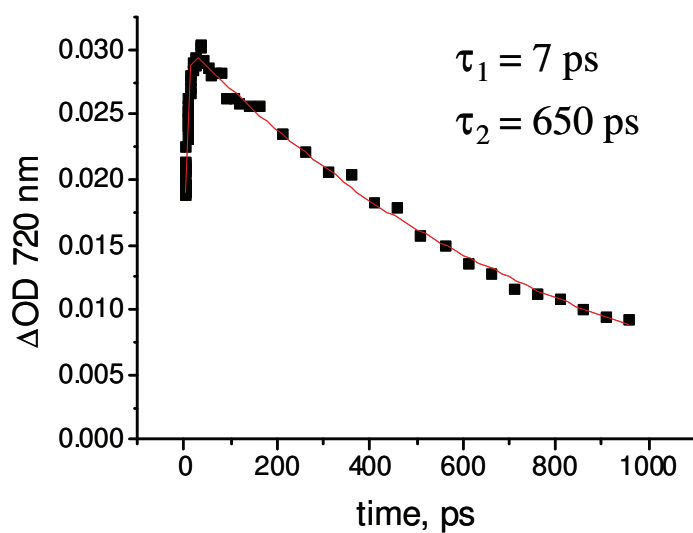
Figure 15. Ultrafast spectroscopy of **SnRu$_6$** in CH$_2$Cl$_2$ (excitation at 530 nm). Kinetic analysis at 720 nm.

4.4 Discussion

Energy Levels of the Arrays.

The photophysical behaviour of the arrays will be discussed by comparison with that of the molecular component units, taking Ru(TPP)(CO)py (**Ru**) and Sn(TPP)(4COO-py)$_2$) (**Sn**) as model compounds. The photophysical properties of **Ru** have been fully characterized in previous works[13,14] and are summarized in the energy level diagram of Figure 16. The energy level diagram of **Sn** (Figure 16) is constructed on the basis of the photophysical results obtained in this work. In particular, the energies of the singlet (E(^{1}*S) = 2.05 eV) and triplet (E(^{3}*T) = 1.65eV) states are taken from the fluorescence and phosphorescence spectrum, respectively (Figure 2).
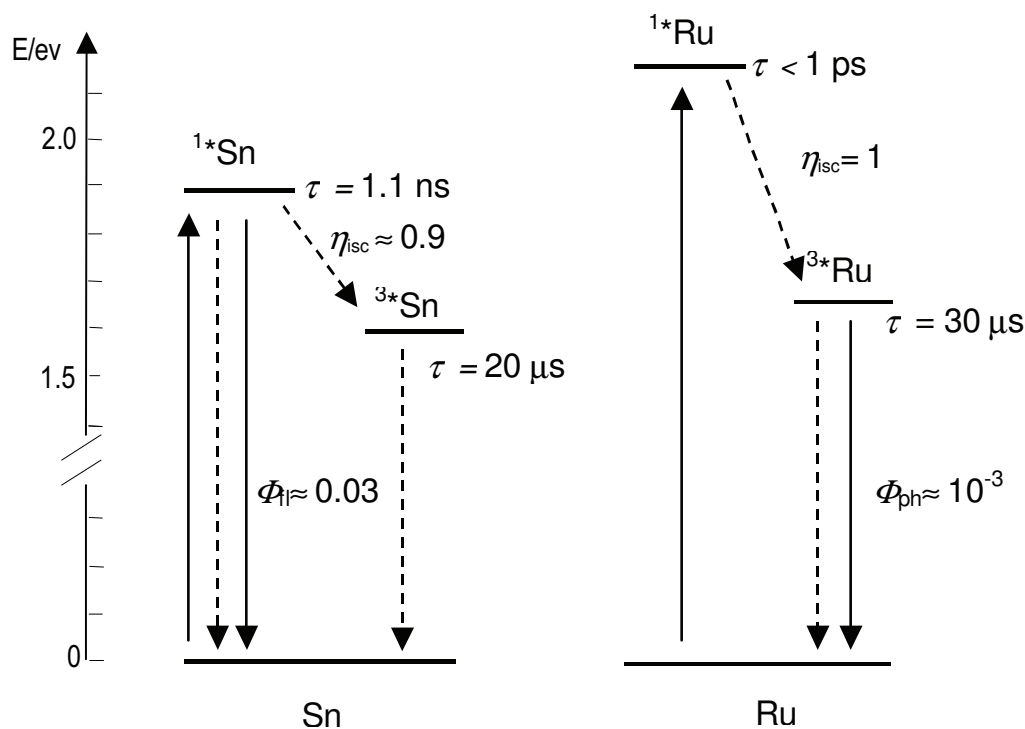
Figure 16. Energy level diagrams for **Sn** and **Ru** (arrow code: continuous = radiative processes, dashed = radiationless processes).

The supramolecular nature of the systems studied (as demonstrated by the additive nature of the spectroscopic and electrochemical properties of the molecular components, Figure 1 and Table 1), allows us to construct the energy level diagram of the arrays as a superposition of those of the component units. In addition, the energy level diagram of all the arrays must include an intercomponent charge transfer state, Sn$^-$-Ru$^+$, where a

ruthenium porphyrin is oxidized and the tin porphyrin is reduced. Actually, a variety of practically degenerate states of such origin is present, depending on (i) the singlet and triplet spin multiplicity of the radical ion pair and (ii) the number of the ruthenium porphyrin donors attached to the tin porphyrin acceptor. An estimate of the energy of these states can be obtained from experimental redox potentials of the arrays (Table 1) with appropriate correction for the electrostatic work term estimated according to standard procedures.[15] The electrostatic work term amounts to 0.16 eV at a center-center distance of 10 Å, a value suitable for both **SnRu₂** and **SnRu₄**.

Within the limits of this type of calculations, the charge-transfer state is estimated to lie at ca. 1.53 eV and at ca 1.25 eV for **SnRu₂** and **SnRu₄**, respectively. The diagram for **SnRu₂** is reported in Figure 17. Those for **SnRu₄** and **SnRu₆** are identical, except for a lower energy (ca 0.28 eV) of the charge-separated state.
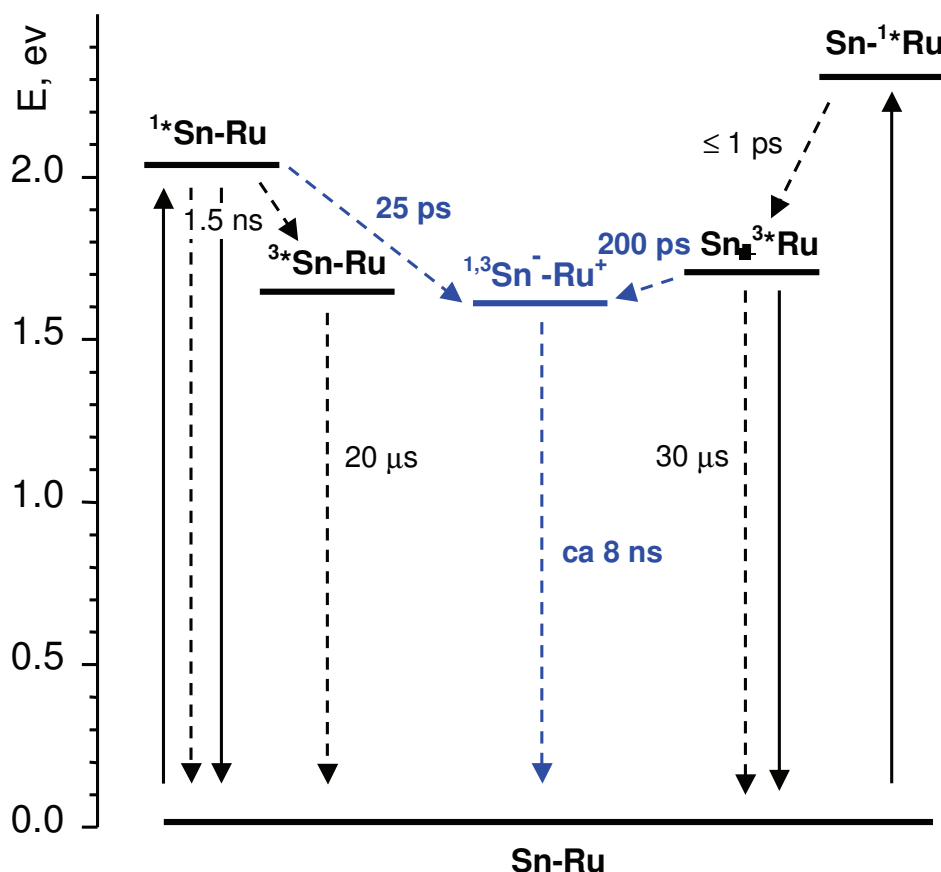
Figure 17. Energy level diagram and photophysical processes for **SnRu₂** (arrow code: continuous = radiative, dashed = radiationless, black = intra-component, blue = inter-component processes)

Figure 17 indicates that a variety of intercomponent processes (eq.1-4) are energetically allowed in the arrays:

$$Sn\text{-}^{1*}Ru \rightarrow {}^{1*}Sn\text{-}Ru \qquad \text{singlet energy transfer} \qquad (1)$$

$$Sn\text{-}^{3*}Ru \rightarrow {}^{3*}Sn\text{-}Ru \qquad \text{triplet energy transfer} \qquad (2)$$

$$^{1*}Sn\text{-}Ru \rightarrow {}^{1}Sn^{(-)}\text{-}Ru^{(+)} \qquad \text{singlet charge separation} \qquad (3)$$

$$Sn\text{-}^{3*}Ru \rightarrow {}^{3}Sn^{(-)}\text{-}Ru^{(+)} \qquad \text{triplet charge separation} \qquad (4)$$

$$^{1,3}Sn^{(-)}\text{-}Ru^{(+)} \rightarrow Sn\text{-}Ru \qquad \text{charge recombination} \qquad (5)$$
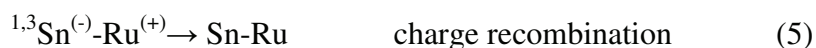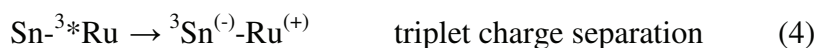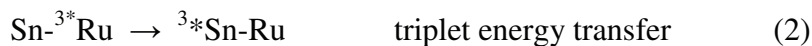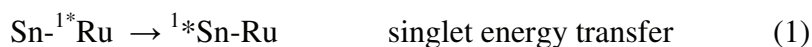
The occurrence of these processes can be checked by examining the photophysical behavior observed following selective excitation of the two types of molecular components.

Excitation of the Sn porphyrin chromophore

Upon excitation of the tin porphyrin chromophore, the very small intensity and short lifetime (<< 300 ps) of its typical fluorescence clearly indicate that the singlet excited state of this unit (^{1*}Sn-Ru) is strongly quenched in the arrays relative to the monomeric compound. From the energy level diagram of Figure 17, the only available pathway for the effective quenching is photoinduced electron transfer leading to a charge separated product in a singlet spin state (eq. 3) where the tin porphyrin unit is reduced and the ruthenium porphyrin unit is oxidized. Experimental proof and kinetic characterization of this process is provided by ultrafast time-resolved spectroscopy. The results obtained for **SnRu$_2$** (Figure 6) show that, as expected on the basis of selective excitation, the initial transient absorption spectrum of Figure 6 is that of the singlet excited state of the tin unit (^{1*}Sn-Ru). In the early time scale, the singlet state disappears, as shown by the decrease in stimulated emission, and converts to a transient with the spectroscopic signatures of the charge transfer product (rise of positive absorption around 630 nm characteristic of the Ru(TPP)(CO)-based radical cation[16] and positive absorption with a maximum at ca. 730 nm typical of the radical anion of tin porphyrin[17]). The kinetic analysis of the spectral changes yields a time constant of 25 ps for the formation of the charge-separated state. The observation that the charge-separated product does not decay appreciably in the 100-1000 ps time window of the ultrafast experiment indicates clearly that charge recombination is much slower (> 2 ns) than charge separation.

In the case of **SnRu$_4$** (Figure 10) the behavior is qualitatively similar, but with faster kinetics: the singlet excited state of the tin unit (^{1*}Sn-Ru) converts to a charge separated

product $^1Sn^{(-)}\text{-}Ru^{(+)}$ in 8 ps and decays back to ground state in 560 ps. The reasons for these kinetic differences are discussed below.

Excitation of the Ru porphyrin chromophore

The excitation spectrum of the residual tin porphyrin fluorescence lacks the ruthenium porphyrin absorption features. This finding thus clearly indicates that the singlet energy transfer from the excited ruthenium units (eq. 1) to Sn central porphyrin does not take place. This behavior, also observed in related systems,[13] is as expected on the basis of the exceedingly short lifetime of the ruthenium porphyrin singlet (< 1 ps). Thus, excitation of the ruthenium-based unit in these arrays populates quantitatively ($\Phi_{isc} = 1$) by ultrafast intersystem crossing the triplet state Sn-$^{3*}Ru$. This triplet state, however, is strongly quenched in the arrays relative to the model compound, as demonstrated by the finding that the arrays do not phosphoresce in deaerated solution.

Given the energy level diagram of Figure 17, two mechanisms could be responsible, in principle, for this quenching process: (i) electron transfer from the excited Ru porphyrin to the Sn porphyrin chromophore to yield the charge-separated $^3Sn^{(-)}\text{-}Ru^{(+)}$ product in a triplet spin state (eq. 4), (ii) triplet energy transfer to the triplet state of the tin unit (eq.2). An experimental answer is provided by ultrafast time-resolved spectroscopy. The transient changes obtained in CH_2Cl_2 for **SnRu₂** species (Figure 7) are clearly diagnostic of electron transfer quenching (eq. 4): a temporal evolution from initial spectral changes assigned to the triplet state of Ru-based chromophore to spectral changes containing the characteristic features of the charge transfer product $Sn^{(-)}\text{-}Ru^{(+}$ (broad absorption in the 600-650 nm range characteristic of the Ru(TPP)(CO)-based radical cation and a band with a maximum at ca.725 nm typical of the radical anion of tin porphyrin) is observed. The $^3Sn^{(-)}\text{-}Ru^{(+)}$ is formed here with a lifetime of 200 ps (Figure 7, inset), i.e., in a much slower process than obtained by excitation of the tin porphyrin component at 555 nm. Again, once formed, the charge separated product remains practically constant within the time window of the experiment. Nanosecond flash photolysis confirms the electron transfer quenching mechanism. Upon laser excitation at 532 nm of **SnRu₂** in CH_2Cl_2 the spectrum of charge separated product $^3Sn^{(-)}\text{-}Ru^{(+)}$ can be clearly detected (Figure 8a), although it disappears in the same time scale as excitation pulse (8 ns). This clearly indicates that the charge separation process (eq. 4) is followed by charge recombination (eq. 5) to yield quantitatively the ground state of the system, with a time constant in CH_2Cl_2 ranging between 2 and 8 ns.

The effect of solvent polarity on the photophysical behavior of excited ruthenium porphyrin in **SnRu₂** has been checked by comparing the flash photolysis results in dichloromethane ($\varepsilon = 8.93$) with those of analogous experiments carried out in toluene ($\varepsilon = 2.38$). As we can see from figures 8b and 9, in toluene, following laser excitation of the Ru unit, the spectrum of the triplet state of the tin porphyrin unit is observed. This result indicates that in this solvent, after prompt intersystem crossing in the Ru porphyrin unit, intercomponent triplet energy transfer to the tin-based unit (eq. 2) takes place in 1.5 ns followed by slow decay of the tin porphyrin triplet state. This drastic change in quenching mechanism (from electron to energy transfer) in going from CH_2Cl_2 to toluene can be easily explained in terms of standard electron transfer theory.[18] In toluene, because of the low solvent polarity, the energy of the charge separated state is lifted and the thermodynamics of the electron transfer process changes from slightly exergonic to endergonic. As a consequence, electron transfer is replaced by energy transfer in the deactivation of the excited Ru triplet.

The ultrafast transient spectroscopy of the array of higher nuclearity **SnRu₄** in CH_2Cl_2 upon excitation of the ruthenium component at 530 nm (Figure 12) yields spectral changes very similar to those reported in Figure 7 for the trimeric **SnRu₂** array in the same solvent, indicating again the occurrence of fast electron transfer process leading to charge transfer $^3Ru^+$-Sn^- product. The time constant for this forward process is 10 ps. Contrary to what happens for the trimeric array, the charge separated product decays to ground state in the time window of the experiment. A value of 400 ps for the time constant of the back electron transfer reaction is obtained from kinetic fits (Figure 13). In conclusion these results demonstrate that for the pentameric system both forward and back electron transfer processes (eqs 4 and 5) are faster than the corresponding ones observed for **SnRu₂**. The reason for this different kinetic behavior will be discussed in the next paragraph.

Also in the ultrafast spectroscopy of **SnRu₆** the spectral changes are diagnostic of the electron transfer process taking place from the triplet state of the ruthenium porphyrin.

Electron-Transfer Kinetics

Several electron-transfer processes have been observed in the photophysical study of the **SnRu$_n$** (n= 2,4,6) arrays. In principle, the kinetics of these processes can be rationalized in terms of standard electron transfer theory.[18] In the limit of weak-interaction (non-adiabatic regime), the rate constant for an electron transfer process is given by equation 6:

$$k = \frac{2\pi}{\hbar} H_{DA}{}^2 \, FCWD \qquad\qquad \text{eq. 6}$$

where H_{DA} is the electronic coupling between donor and acceptor and $FCWD$ is the thermally averaged nuclear Franck-Condon factor that accounts for the combined effects of the reorganizational energies and driving force. For a homogeneous series of processes (where H_{DA} and reorganizational energies are appreciably constant) eq. 6 provides a correlation between the rate constants and the driving force of electron transfer. For **SnRu$_2$** in dichloromethane the rate constants for the four processes (photoinduced charge separation from Ru porphyrin excited chromophore, photoinduced charge separation from Sn porphyrin excited chromophore and the corresponding charge recombination processes, eqs 3-5) were measured. The time constant values and the corresponding driving forces (known with reasonable accuracy) are reported in Table 2.

Table 2. Free energy changes and electron transfer rate constants for **SnRu$_2$** and **SnRu$_4$** [a]

Array	process	ΔG_{el}, eV [b]	1/k, ps
SnRu$_2$	$^1{}^*\text{Sn-Ru} \rightarrow {}^1\text{Sn}^{(-)}\text{-Ru}^{(+)}$	-0.52	25
	$\text{Sn-}^3{}^*\text{Ru} \rightarrow {}^3\text{Sn}^{(-)}\text{-Ru}^{(+)}$	-0.18	200
	$^1\text{Sn}^{(-)}\text{-Ru}^{(+)} \rightarrow \text{Sn-Ru}$	-1.53	$2\text{-}8 \times 10^3$
	$^3\text{Sn}^{(-)}\text{-Ru}^{(+)} \rightarrow \text{Sn-Ru}$	-1.53	$2\text{-}8 \times 10^3$
SnRu$_4$	$^1{}^*\text{Sn-Ru} \rightarrow {}^1\text{Sn}^{(-)}\text{-Ru}^{(+)}$	-0.80	4.3
	$\text{Sn-}^3{}^*\text{Ru} \rightarrow {}^3\text{Sn}^{(-)}\text{-Ru}^{(+)}$	-0.46	8
	$^1\text{Sn}^{(-)}\text{-Ru}^{(+)} \rightarrow \text{Sn-Ru}$	-1.25	510
	$^3\text{Sn}^{(-)}\text{-Ru}^{(+)} \rightarrow \text{Sn-Ru}$	-1.25	560

[a]All measurements were made in dichloromethane solution at 298 K. [b] Free energy changes calculated on the basis of the photophysical data and electrochemical potentials (Table 1).

To the extent to which the four electron-transfer processes studied are homogeneous in terms of electronic couplings, the main factor determining differences in observed rates is the driving force (Table 2). The two photoinduced processes ($^1{}^*\text{Sn-Ru} \rightarrow {}^1\text{Sn}^{(-)}\text{-Ru}^{(+)}$ and $\text{Sn-}^3{}^*\text{Ru} \rightarrow {}^3\text{Sn}^{(-)}\text{-Ru}^{(+)}$) take place on very different time scale (25 ps and 200 ps). Both are likely to be in the Marcus "normal region", but the latter is only slightly exergonic whereas the former is much more so. In addition, the photoinduced process $^1{}^*\text{Sn-Ru} \rightarrow {}^1\text{Sn}^{(-)}\text{-Ru}^{(+)}$

is expected to be two times faster for statistical reasons, because of the presence of two ruthenium components. As to the back recombination processes, the rates are much slower than for charge separation, and that of the formally spin allowed process ($^{1}Sn^{(-)}$-$Ru^{(+)} \rightarrow$ Sn-Ru) and of the formally spin forbidden one ($^{3}Sn^{(-)}$-$Ru^{(+)} \rightarrow$ Sn-Ru) seem to be of the same order of magnitude. The relative slowness of the these processes (2-8 ns) is determined by their larger driving force, which places the processes in the Marcus "inverted region". The similarity of the rates for the formally spin allowed and spin forbidden processes is likely due to the strong spin-orbit coupling provided by heavy metal, that favors fast spin inversion.

As to the kinetic data observed for **SnRu$_4$** (Table 2), the same arguments can be made concerning the relative rates of forward and back electron transfer and singlet and triplet charge recombination. While comparing rates of analogous processes for the two arrays, on the other hand, one should keep in mind that the peripheral ruthenium units are differently connected to the central tin porphyrin (see Chart 1). In **SnRu$_2$** the two Ru units are coordinated to the Sn center via a bifunctional 4-carboxypyridine ligand (axial position), whereas in **SnRu$_4$** the peripheral Ru porphyrin units are coordinated to four pyridyl substituents of the central tin porphyrin ring (equatorial position). On the basis of this different connecting motif a better electronic factor would be expected for **SnRu$_4$**. Thus, the charge separation processes taking place from the singlet state of the tin porphyrin ($^{1}*$Sn-Ru $\rightarrow$ $^{1}Sn^{(-)}$-$Ru^{(+)}$) and from the triplet state of the ruthenium porphyrin (Sn-$^{3}*$Ru $\rightarrow$ $^{3}Sn^{(-)}$-$Ru^{(+)}$) are always faster in **SnRu$_4$** than in **SnRu$_2$** because of better driving force, better electronic factors, and (for the first type of process) better statistical factors. The comparison between the singlet charge separation process,$^{1}*$Sn-Ru $\rightarrow$ $^{1}Sn^{(-)}$-$Ru^{(+)}$ in **SnRu$_2$** and the triplet charge separation process, Sn-$^{3}*$Ru $\rightarrow$ $^{3}Sn^{(-)}$-$Ru^{(+)}$, in **SnRu$_4$** is instructive: the former process, despite a slightly better driving force (see Table 2) and a more favorable statistical factor, is slower because of a less favorable electronic factor. As to the comparison of the charge recombination kinetics for the two arrays, again, the processes are faster in **SnRu$_4$**. This is likely due to the combined effects of better electronic factors and smaller driving force (Table 2). In the Marcus inverted region, where the charge recombination processes belong, a decrease in exergonicity causes an increase in the rate constant.

As to the ultrafast spectroscopy results for **SnRu$_6$**, the kinetic behavior is found to be very similar to that of **SnRu$_4$**. In this heptameric array, where the ruthenium units are connected to central core by two different types of connections, the processes involving the chromophores in axial and in equatorial position cannot be kinetically resolved. In this case,

the difference in their relative rate constants, related only to electronic factors, is likely to be smaller with respect to that observed (see Table 2) between **SnRu$_2$** and **SnRu$_4$** arrays.

4.5 Conclusions

A detailed photophysical study has been carried out on a series of arrays of different nuclearity made of a central tin porphyrin unit connected to two or more ruthenium porphyrin units. With respect to analogous systems based on free-base or zinc porphyrin units,[19] the use of tin porphyrin offers the advantage of opening new intercomponent electron transfer deactivation pathways, leading to arrays with a richer and more intriguing photophysical behavior.

The main interesting features of this study include the following: i) using a combination of emission spectroscopy and femtosecond and nanosecond time-resolved absorption techniques, a very detailed picture of the photophysics of these systems has been obtained; ii) a common (except for spin multiplicity) charge-separated state, where the ruthenium porphyrin is oxidized and the tin porphyrin is reduced, is reached by intercomponent electron transfer following selective excitation of both chromophoric components; iii) changing the solvent polarity from dichloromethane to toluene has the effect of lifting the energy of the charge-separated state, and thus of switching electron transfer off and triplet energy transfer on following excitation of the Ru-based units; iv) the kinetics of the various intercomponent processes has been rationalized on the basis of standard electron transfer theory.

4.5 References

[1] a) A. K. Burrell, D. L. Officer, P. G. Plieger, D. C. W. Reid, *Chem. Rev.* **2001**, *101*, 2751. b) H.L. Anderson, *Chem. Commun.* **1999**, 2323. c) D. Gust, T. A. Moore, A. L. Moore in *Electron Transfer in Chemistry*; V. Balzani, Ed.; Wiley-VCH: Weinheim, Germany, **2001**; Vol. III, Part 2, Chapter 2, pp 273-336; d) D. Holten, D.F. Bocian, J. S. Lindsey *Acc. Chem. Res.* **2002**, *35,* 57. e) D. Kim, A. Osuka *Acc. Chem. Res.* **2004**, *37*, 735. f) T. Hori, X. Peng, N. Aratani, A. Takagi, T. Matsumoto, T. Kawai, Z. S. Yoon, M.-C. Yoon, J. Yang, D. Kim, A. Osuka, *Chem Eur. J.* **2008**, *14*, 582. g) H. Song, M. Taniguchi, M. Speckbacher, L. Yu, D. F. Bocian, J. S. Lindsey, D. Holten *J. Phys. Chem. B* **2009,** *113,* 8011.

[2] a) J.-C. Chambron, V. Heitz, J.-P. Sauvage in *The Porphyrin Handbook*; K. Kadish, K. M. Smith, R. Guillard, Eds.; Academic Press: San Diego, CA, **2000**; Volume 6, pp 1-42; b) T. Imamura, K. Fukushima *Coord. Chem. Rev.* **2000**, *198*, 133. c) L. Baldini, C. A. Hunter, *Adv. Inorg. Chem.* **2002**, *53*, 213. d) J. Wojaczyński, L. Latos-Grażyński, *Coord. Chem. Rev.* **2000**, *204*, 113. e) C-C. You, R. Dobrawa, C. R. Saha-Möller, F. Würthner, *Top Curr Chem* **2005**, *258*, 39. f) C. M. Drain, I. Goldberg, I. Sylvain, A. Falber, *Top. Curr. Chem.* **2005**, *245*, 55. g) D.M.P. Mingos Ed., E. Alessio, volume Ed. *Structure Bonding "Non-Covalent Multi-Porphyrin Assemblies"*; Springer-Verlag: Berlin, **2006** , Vol. 121; h) E. Iengo, F. Scandola, E. Alessio *Struct. Bond.*, **2006,** *121*, 105. i) E. Iengo, E. Zangrando, E. Alessio, *Acc. Chem. Res.* **2006**, *39*, 841. j) A. Oliva, B. Ventura, F. Wurthner, A. Camara-Campos, C.A. Hunter, P. Ballester, L. Flamigni, *Dalton Trans.* **2009**, 4023. k) M. Beyler, V. Heitz, J.-P. Sauvage, B. Ventura, L. Flamigni, K. Rissanen, *Inorg. Chem.* **2009**, *48*, 8263. l) N. Nagata, Y. Kuramochi, Y. Kobuke, *J. Am. Chem. Soc.* **2009**, *131*, 10.

[3] D. P. Arnold, J. Blok, *Coord. Chem Rev* **2004**, *248*, 299 and references therein.

[4] a) H.-J Kim, N. Bampos, J. K. M. Sanders, *J. Am. Chem. Soc.* **1999**, *121*, 8120. b) J. K. M. Sanders, N. Bampos, Z.-C. Watson, S. L. Darling, J. C. Hawley, H.-J. Kim, C. C. Mak, S. J. Webb in *The Porphyrin Handbook*, K. M. Kadish, K. M. Smith, R. Guilard, Eds.; Academic Press: New York, **2000**; Vol. *3*, pp. 1–48.

[5] B. G Maiya, N. Bampos, A. A. Kumar, N. Feeder, J. K. M. Sanders, *New J. Chem.* **2001**, *25*, 797.

[6] a) L. Giribabu, A. A. Kumar, V. Neeraja, B. G. Maiya, *Angew. Chem. Int. Ed.* **2001**, *40*, 3621. b) A.A. Kumar, L. Giribabu, D. R. Reddy, B.G. Maiya, *Inorg. Chem.* **2001**, 40, 6757.

[7] J. Y. Lee, S. J. Lee, H.J. Kim, H.-J. Kim. *J. Phys. Chem. B* **2006,** *110,* 5337.

[8] J. Fortage, E. Goransson, E. Blart, H.C. Becker, L. Hammarstrom, F. Odobel, *Chem Comm.* **2007,** 4629.

[9] H.J. Kim, W.S. Jeon, J.H. Lim, C.S. Hong, H.-J. Kim, *Polyhedron* **2007**, *26*, 2517.

[10] H.J. Joon, J. K. Hee, H.-J. Kim, H.K. Chul, T. Joo, W.C. Dae, M. Yoon, *Bulletin of the Korean Chemical Society* **2007**, *28*, 1967.

[11] P.K. Poddutoori**,** P. Poddutoori**,** B.G. Maiya, T.K. Prasad, Y.E. Kandrashkin, S. Vasil'ev**,** D. Bruce**,** A. van der Est, *Inorg. Chem* **2008**, *47*, 7512.

[12] H.J. Kim, H. Jang Choi, T. Lee, J. Ko, M. Yoon, H-J. Kim. *Inorg. Chem.* **2008**, *47*, 2411.

[13] a) A. Prodi, M. T. Indelli, C. J. Kleverlaan, F. Scandola, E. Alessio, T. Gianferrara, L. G. Marzilli, *Chem. Eur. J.* **1999**, *5*, 2668.

[14] A. Prodi, C. Chiorboli, F. Scandola, E. Iengo, E. Alessio, R. Dobrawa, F. Würthner, *J. Am. Chem. Soc*. **2005**, *127*, 1454.

[15] (a) D. Rehm, A. Weller, *Ber. Bunsen-Ges. Phys. Chem*. **1969**,*73*, 834. (b) A. Weller, *Z. Phys. Chem.* **1982**, *133*, 93.

[16] G. M. Brown, F. R. Hopf, J. A. Ferguson, T. J Meyer, D. Whitten, *J. Am Chem. Soc*. **1973,** *95*, 5939.

[17] K. M. Kadish, Q. Y. Y. Xu, G. B. Maiya, J. M. Barbe, R.Guilard, *J. Chem Soc. Dalton Trans*. **1989**, 1531.

[18] (a) J. Jortner, *J. Chem. Phys.* **1976**, *64*, 4860. (b) J. Ulstrup, *Charge Transfer Processes in Condensed Media*; Springer-Verlag: Berlin,1979. (c) R. A. Marcus, N. Sutin, *Biochim. Biophys. Acta* **1985**, *811*, 265. (d) J. R. Miller, J. V. Beitz, R. K. Huddlestone, *J. Am. Chem. Soc* **1984**, *106*, 5057. (e) M. D. Newton, *Chem. Rev*. **1991**, *91*, 767.

[19] F. Scandola, C. Chiorboli, A. Prodi, E. Iengo, E. Alessio, *Coord. Chem. Rev.* **2006**, *250*, 1471.

Chapter 5

High Turnover Photochemical Hydrogen Production Catalyzed by a Model Complex of the [FeFe] Hydrogenase Active Site.$^{\varphi}$
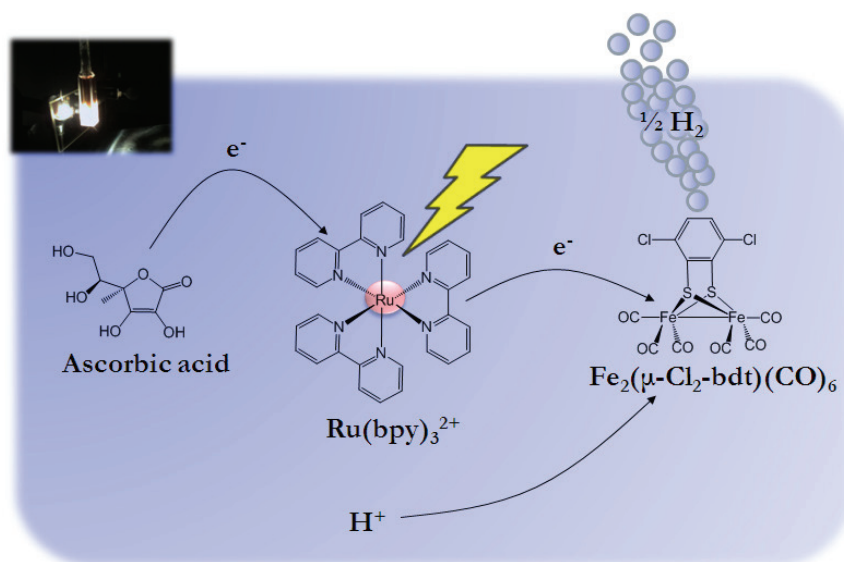
A model complex of the [FeFe] hydrogenase active site is tested as a proton reduction catalyst for photochemical hydrogen production, yielding high turnover numbers in a photocatalytic cycle with Ru(bpy)$_3^{2+}$ as photosensitizer and ascobic acid as sacrificial electron donor.

The work described in this chapter is the result of a collaboration between the Group of Prof. Leif Hammarstrom, where i spent a training period, and the Group of Prof. Sascha Ott at the Department of Photochemistry and Molecular Science of Uppsala University (Uppsala, Sweden).

5.1 Introduction

Colloidal platinum was presented as a heterogeneous catalyst for the reduction of protons to molecular hydrogen already 30 years ago,[1] and more recently molecular platinum- and palladium-based systems have been developed.[2,3] However, the chemical integrity of latter catalysts is a controversial point as Pd- or Pt-colloid formation has been detected during photochemical catalysis in some instances.[4,5] This not only precludes further improvement by synthetic manipulation, but has also led to the suggestion that the colloids rather than the molecular species are responsible for catalysis in these systems.[4,5] Moreover, neither platinum nor palladium exist in sufficient abundance as to qualify any catalyst based on these metals for large scale application. In this regard, cobalt complexes have been shown to be a viable alternative.[6,7] Likewise, active site models of the [FeFe] hydrogenases have received much attention, as the enzymes themselves catalyze the generation of hydrogen with high turnover rates close to the Nernstian potential.[8] Unlike the cobalt catalysts, however, these Fe_2 model complexes have so far almost exclusively been used for electrocatalytic reduction of protons, requiring significant overpotential and often strongly acidic conditions.[9] Many of the widely used $[(\mu\text{-}SCH_2XCH_2S)Fe_2(CO)_4(L)_2]$ (X = CH_2, NR; L = CO, CN^-, PR_3) complexes[10,11] exhibit reductive electrochemistry which is far from being reversible. Not surprisingly, the sparse attempts to utilize them for photochemical catalysis have hitherto been moderately successful if not poor, giving less than five equivalents of H_2 per catalyst.[12,13]

For a functional molecular photochemical system the catalyst needs to be structurally stable in the different redox states, or at least exhibits strictly reversible changes. Recently the $[(\mu\text{-}bdt)Fe_2(CO)_6]$ (bdt = benzene-1,2-dithiolate) complex was presented as the first Fe_2 model meeting these demands, exhibiting a reversible reductive electrochemistry and maintaining its structural integrity to a large extent also in the reduced state.[14] It was further shown that introduction of electron-withdrawing chloro-substituents shift the reduction potential to milder values as compared to the parent compound and that [(μ-

Cl$_2$bdt)Fe$_2$(CO)$_6$] (**1**; Scheme 1, Cl$_2$bdt = 3,6-dichlorobenzene-1,2-dithiolate) exhibits electro-catalytic activity at these milder potentials.[15] Complex **1** thus represents a class of Fe$_2$ model complexes combining unprecedented electrochemical reversibility with catalytic activity at mild potential.

In the work presented here complex **1** is for the first time employed as catalyst in a photochemical system. [Ru(bpy)$_3$]$^{2+}$ serves as photosensitizer and ascorbic acid as proton- and sacrificial electron donor for homogeneous photochemical proton reduction (Scheme 1).
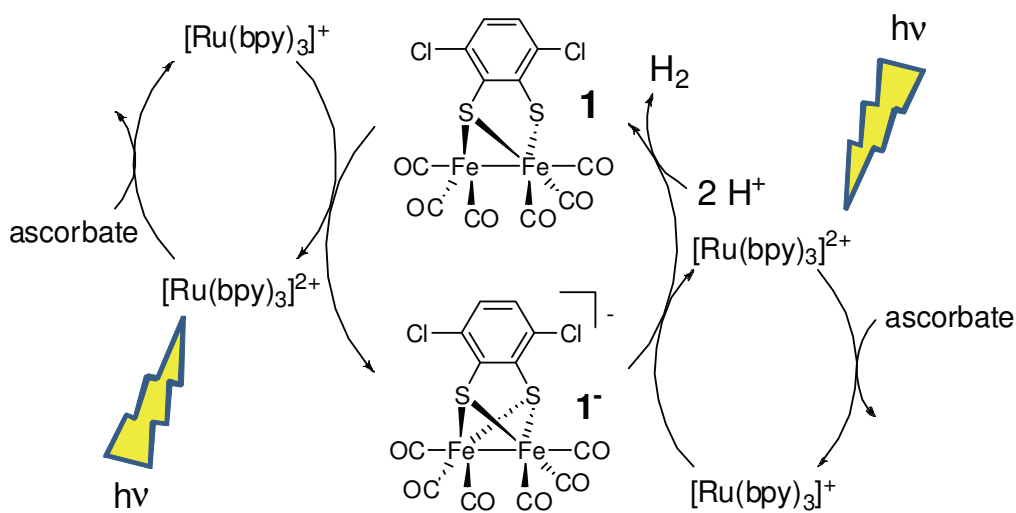
Scheme 1. Proposed catalytic cycle for the photochemical reduction of protons catalyzed by [(μ-Cl$_2$bdt)Fe$_2$(CO)$_6$] (Cl$_2$bdt = 3,6-dichlorobenzene-1,2-dithiolate) in H$_2$O/DMF (50/50).

5.2 Experimental section

Materials.

The syntheses and characterization of the compounds discussed in this chapter were performed by Lennart Schwartz et al. in the research group of Prof. Sascha Ott at the Department of Photochemistry and Molecular Science of Uppsala University (Uppsala, Sweden). Details can be found in Ref. 15. Other reagents and solvents were purchased and used as received, if not otherwise stated.

Apparatus.

All measurements were performed at the Department of Photochemistry and Molecular Science of Uppsala University with the instrumental setup described below.

Absorption spectra were acquired on a Cary5000 UV-Vis-NIR spectrophotometer (Varian).

For pH determination a Biotrode pH electrode (Metrohm) calibrated with aqueous pH 4 and 9 calibration buffers was employed.

Gaseous samples were analyzed with a CP4900 Micro Gas Chromatography setup (Varian) equipped with a 5 A Molsieve column operated with argon as carrier gas and directly attached to the measuring cell via a Swagelok connection. Temperature was maintained at 20 °C by using a thermostated sample holder.

Irradiation experiments were performed employing a KL2500 LCD light source (Schott) equipped with a commercial HLX 250 W halogen lamp (Osram) and a fiber glass beam guide. The light source was used at a color temperature of 3000 K without beam reduction. The unfiltered output from the beam guide corresponded to about 1 W. Prior to passing it through the sample the light was filtered with a BG21 NIR and GG455 long pass filter.

A Brilliant B laser (quantel) tuned to 470 nm by means of a *Magic*Prism™ OPO (quantel), and a pulsed 150 W Xenon Short Arc Display/Optic Lamp XBO (Osram) were employed as pump and probe light sources in an LKS60 laser flash photolysis setup (Applied Photophysics). For measurements in the millisecond range the probe lamp was run in unpulsed mode. Emission and transient absorption time traces were acquired as averages of 10 to 20 flashes for both baselines and actual measurements.

Hydrogen Evolution experiments.

All samples were prepared in a glove box under argon atmosphere. Stock solutions of ca. 140 µM $Ru(bpy)_3Cl_2$ in deoxygenated 1:1 DMF/H_2O were used for individual series of experiments (further referred to as **sensitizer stock**). Ascorbic acid (further referred to as **AAH**) was dissolved in undiluted sensitizer stock to a final concentration of 100 mM. The corresponding control without AAH contained 100 mM NaH_2PO_4 instead. Adjustment of the AAH containing samples to pH 5.5 was done by addition of 1 M NaOH in water. A corresponding amount of water was added in samples without pH adjustment. For latter the pH was found to be 3.5. The NaH_2PO_4 containing control was adjusted to pH 5.5 by addition of 1 M HCl. A fresh **catalyst stock** solution of approximately 200 µM **1** in neat

deoxygenated DMF was prepared for each individual experiment. The concentration was determined from the absorbance at 376 nm. The extinction coefficient had been determined to be 3970 ± 20 $M^{-1}cm^{-1}$ at this wavelength in neat DMF. To yield the final concentration of 14 µM, catalyst stock was diluted in sensitizer stock containing 100 mM AAH or NaH_2PO_4 at adjusted or unadjusted pH. 1.5 ml of sample solution were transferred with a syringe through a rubber septum into the argon purged measuring cell (14.48 ml volume). The gas composition in the cell prior to and during the experiment was monitored by gas chromatography. The photosensitizer concentration was determined from the absorbance at 453 nm assuming an extinction coefficient of 14700 $M^{-1}cm^{-1}$. Irradiation was performed in the way described above except that the light was filtered by passing it through a water-filled quartz cuvette (1 cm pathlength), a BG19 NIR filter and a GG455 long-pass filter thus limiting the spectral range of light passing through the sample to 455 – 850 nm. To preclude any impact of potential catalyst decomposition on the outcome of the experiment and thus on the interpretation of the data, care was taken to start irradiation of the sample always at exactly the same time after dissolving **1** in neat DMF. The headspace was sampled by GC in 3 min intervals and H_2, as well as O_2 and N_2 levels were monitored. The amount of hydrogen in the headspace was quantified from the integrated peak areas. Prior to each experiment a 7.5 % H_2 in argon gas mix was used for calibration and the amount of produced hydrogen calculated as:

H_2 [nmol] = (detected peak area) / (calibration peak area) * 0.075 * (headspace volume [ml]) / 24055.15 [ml / mol] * 10^9 [nmol / mol]

where 24055.15 ml / mol is the molar volume of an ideal gas at 293.15 K temperature and 101325 Pa pressure. Since the total amount of produced hydrogen never exceeded approx. 100 µl as compared to 12.98 ml total head space volume the corresponding overpressure was regarded as negligible.

Quantum Yield determination.

A methylviologen^{2+} / $[Ru(bpy)_3]^{2+}$ / EDTA actinometric system was used based on the system described in Mandal and Hoffman.[16] A 100 mM aqueous solution of EDTA at pH = 10.25 (adjusted with 5 M NaOH) was prepared (further referred to as **EDTA stock**). Further, two solutions of approx. 200 mM methylviologen^{2+} and 270 µM $Ru(bpy)_3Cl_2$ in the EDTA stock were prepared (the concentrations were determined from absorbances at 290

and 453 nm using extinction coefficients of 5330 and 14700 $M^{-1}cm^{-1}$ respectively). The three solutions were mixed in the dark prior to the experiment to yield a sample with 20 mM methylviologen^{2+}, 140 μM $[Ru(bpy)_3]^{2+}$ and 100 mM EDTA at pH $\approx$ 10.2. This pH corresponds to the pK$_a$ of the EDTA^{3-}/ EDTA^{4-} pair. Neglecting the singly and doubly charged fraction of EDTA molecules the ionic strength of this solution can be calculated to be approx. 0.8 M. 1.5 ml of sample were transferred to the hydrogen evolution measuring cell and deoxygenated by purging with argon for > 45 min at moderate gas flow to prevent solvent evaporation and thus concentration of the sample. The sample was exposed to irradiation under the same conditions as for the hydrogen evolution experiments with the exception of an additional OD = 1 or OD =2 filter between light source and sample to attenuate the velocity of methylviologen radical formation. The amount of latter was determined after different irradiation times from the absorbance at 605 nm using the reported[16] extinction coefficient of 13700 $M^{-1}cm^{-1}$). Using a quantum yield of 0.2 for the formation of methylviologen radical reported for the corresponding system[16] the number of absorbed photons was calculated taking the reduction in light intensity by the OD filter into account. These were plotted versus irradiation time. A fit to the linear initial phase of this plot yielded a photon absorption rate of 90±10 nmol photons per second. The maximum hydrogen evolution rate was determined from two runs under the best conditions. In a plot of nmol of produced hydrogen versus irradiation time the region between 10 and 60 min after irradiation start was fitted linearly. The average of the slopes yielded a maximum hydrogen production rate of 0.93±0.05 nmol H_2 per second. This gives an overall maximum quantum yield of 1 % H_2 per absorbed photon.

5.3 Results and discussion

In the proposed system the reaction free energy for electron transfer from photogenerated $[Ru(bpy)_3]^+$ to **1** can be estimated from the electrochemically determined $E_{1/2}$ to be $\Delta G^0 = -0.44$ eV. Considering the electrochemical stability and favourable thermodynamics it came as a surprise to see that complex **1** didn't produce more than 4 turnovers of H_2 initially (100 mM ascorbic acid in a 1:1 CH_3CN/H_2O mixture, $[Ru(bpy)_3]^{2+}$:**1** ratio of 1:10). However, at a $[Ru(bpy)_3]^{2+}$:**1** ratio of 10:1 more turnovers could be achieved suggesting that availability of reduction equivalents had been limiting catalysis.

Further investigation revealed that $[Ru(bpy)_3]^{2+}$ decomposes significantly over 1-2 hours when exposed to light ($\lambda > 455$ nm) in presence of 100 mM ascorbic acid. A change of solvents to a 1:1 DMF/H$_2$O mixture prevented the degradation, yielding a stable system for experiments with **1.**

At pH 3.5 and a 10:1 ratio of $[Ru(bpy)_3]^{2+}$:**1**, almost 40 turnovers of hydrogen per catalyst are obtained in 2.5 hours. A raise of pH to 5.5 leads to an increase in turnovers to >60 equivalents of hydrogen per complex **1** in the same time, even at a 1:1 $[Ru(bpy)_3]^{2+}$:**1** ratio. At the higher $[Ru(bpy)_3]^{2+}$:**1** ratio of 10:1 and pH = 5.5 the highest level of hydrogen production was obtained, reproducibly giving 200 turnovers at a maximum turnover frequency of 2.7 H$_2$ per catalyst per minute (Figure 1).
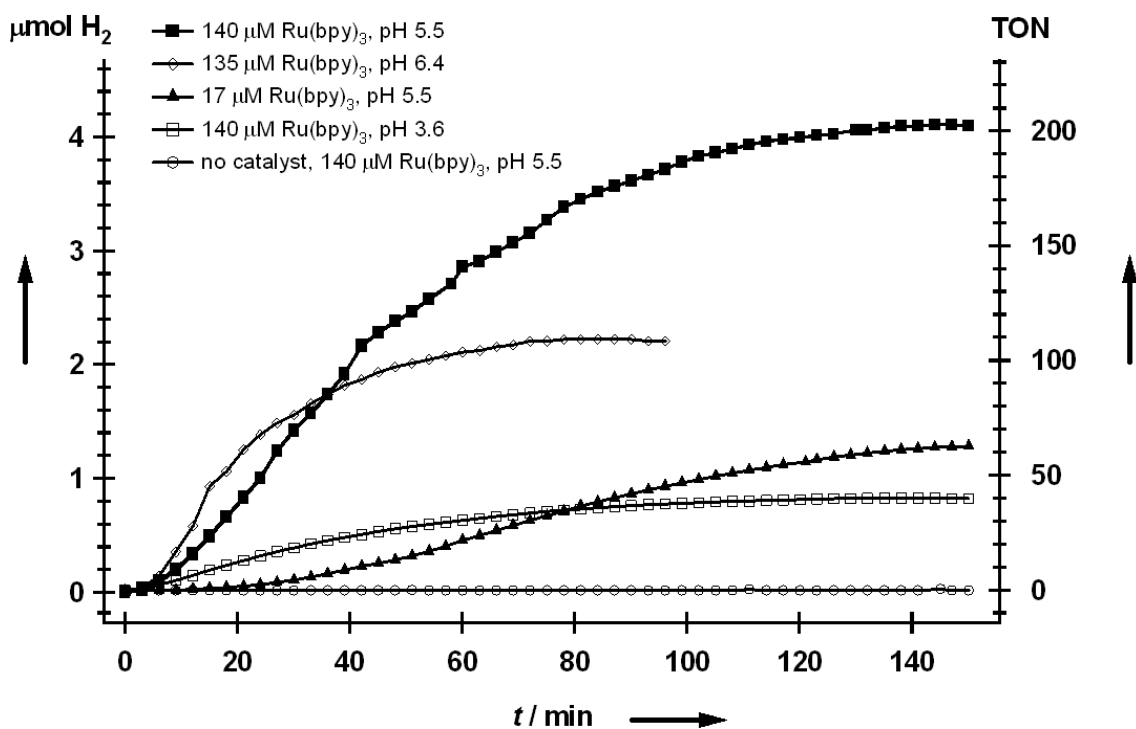
Figure 1. Light driven hydrogen production by 14 μM (21 nmol) **1** in presence of $[Ru(bpy)_3]^{2+}$ and 100 mM ascorbic acid in deoxygenated 1:1 DMF/H$_2$O at 20 °C. All samples were irradiated with light in the wavelength-range 455 – 850 nm. H$_2$ was detected by in situ gas chromatography.

Under these conditions the quantum yield for hydrogen formation was calculated from the absorbed photons (93.1 nmol photons/s) and the maximum hydrogen production rate (0.93 nmol/s) to be 1 %. The quantum yield and turnover frequency can reach even higher levels of 1.4 % and 3.7 turnovers per minute, respectively, at pH 6.4. At this pH,

however, catalysis stops earlier, yielding 100 turnovers of H_2. Control experiments in which either complex **1**, $[Ru(bpy)_3]^{2+}$, or ascorbic acid were separately omitted do not show significant hydrogen production. Catalysis stops after approximately 150 min under all experimental conditions described above. Since there are no substantial changes in the sample pH or in the UV-Vis absorption spectrum of the photosensitizer during the experiment, catalyst inactivation is the most likely cause for this observation.

Reductive quenching of $*[Ru(bpy)_3]^{2+}$ by ascorbic acid and subsequent re-oxidation of $[Ru(bpy)_3]^+$ by **1** as elementary reactions of the proposed catalytic cycle were verified and studied in more detail by transient emission and absorption spectroscopy (Figure 2 and Figure 3, respectively). The emission decay traces show that $*[Ru(bpy)_3]^{2+}$ excited state ($\tau_0 =$ 810 ns) is quenched with an efficiency of ca. 53 % (τ = 390 ns) by 100 mM ascorbic acid in 1:1 DMF/H_2O at pH 3.5.
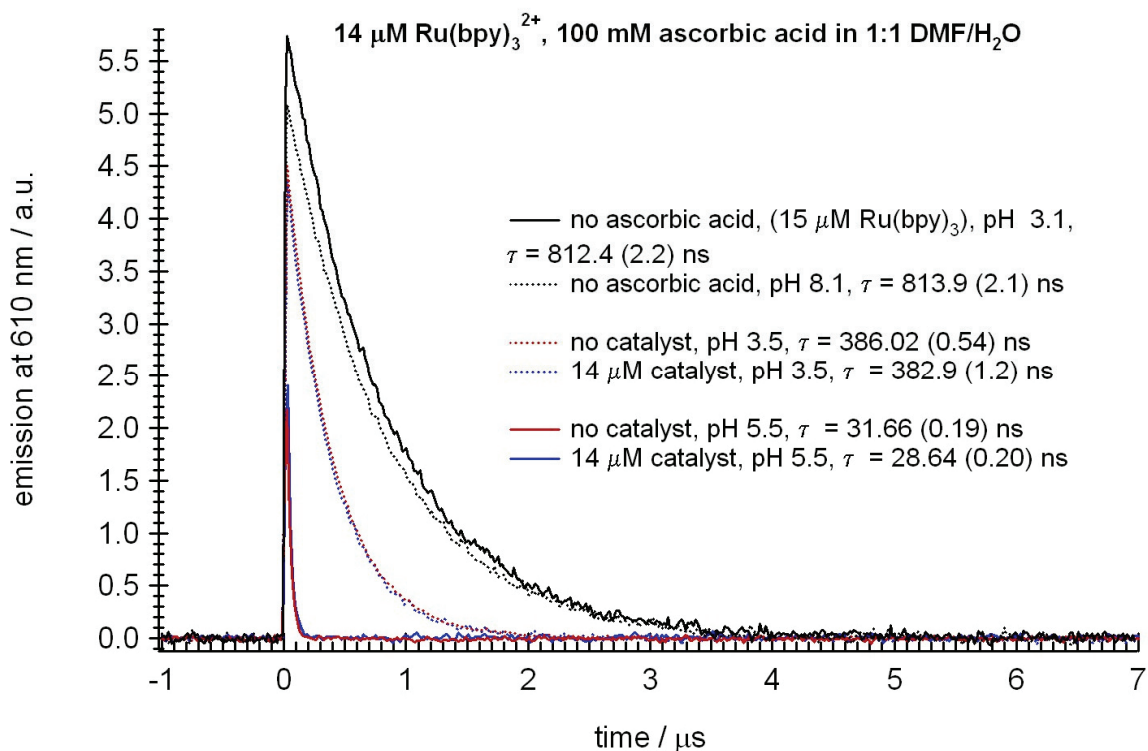
Figure 2. $*[Ru(bpy)_3]^{2+}$ emission decay traces at 610 nm. 13-15 µM $[Ru(bpy)_3]^{2+}$, 100 mM ascorbic acid, 1:1 DMF/H_2O, room temperature. Excitation at 470 nm.
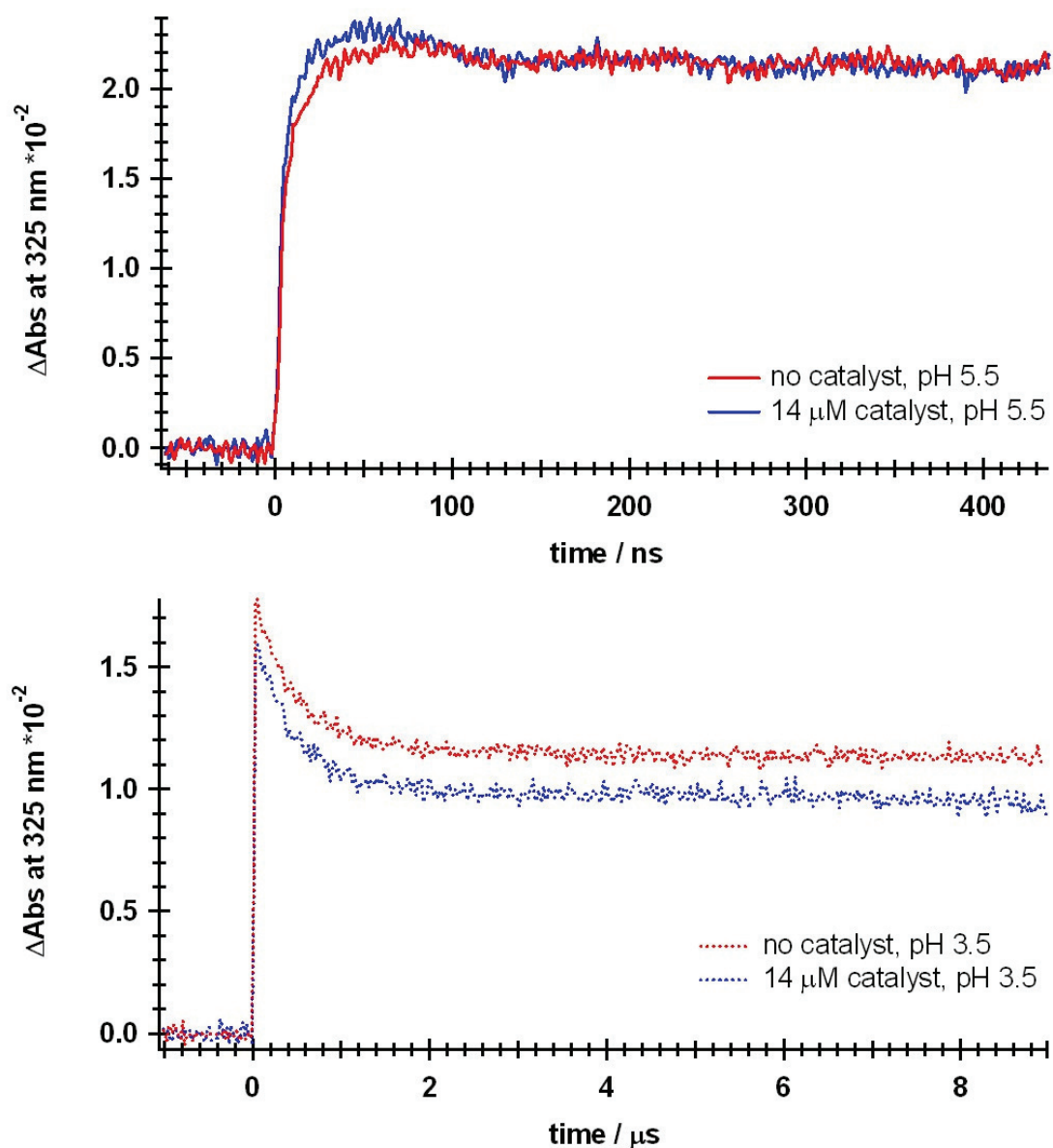
Figure 3. *[Ru(bpy)$_3$]$^{2+}$ transient absorption traces at 325 nm at high (top panel) and low pH (lower panel). 13-15 µM [Ru(bpy)$_3$]$^{2+}$, 100 mM ascorbic acid, 1:1 DMF/H$_2$O, room temperature. Excitation at 470 nm.

The quenching is unaffected by the presence of **1**, showing that the primary reaction occurs between the excited state and the electron donor. An increase of the ascorbate (pKa 4.1) fraction by raising the pH to 5.5 augments the reductive quenching efficiency to 96 % (τ = 30 ns). The quenching produces [Ru(bpy)$_3$]$^+$ in near-quantitative yield, as monitored by its transient absorption at 510 nm and the disappearance of the 455 nm bleach due to *[Ru(bpy)$_3$]$^{2+}$ (Figure 4, inset). The half-life of photo-generated [Ru(bpy)$_3$]$^+$ is reduced from

200 μs to 50 μs (Figure 4) in the presence of 14 μM **1**, irrespective of pH, implying that the primary reaction step of the catalytic sequence is reduction of complex **1** to **1⁻** by $[Ru(bpy)_3]^+$ Control experiments show that no $[Ru(bpy)_3]^+$ is produced in the absence of ascorbic acid (Figure 4).
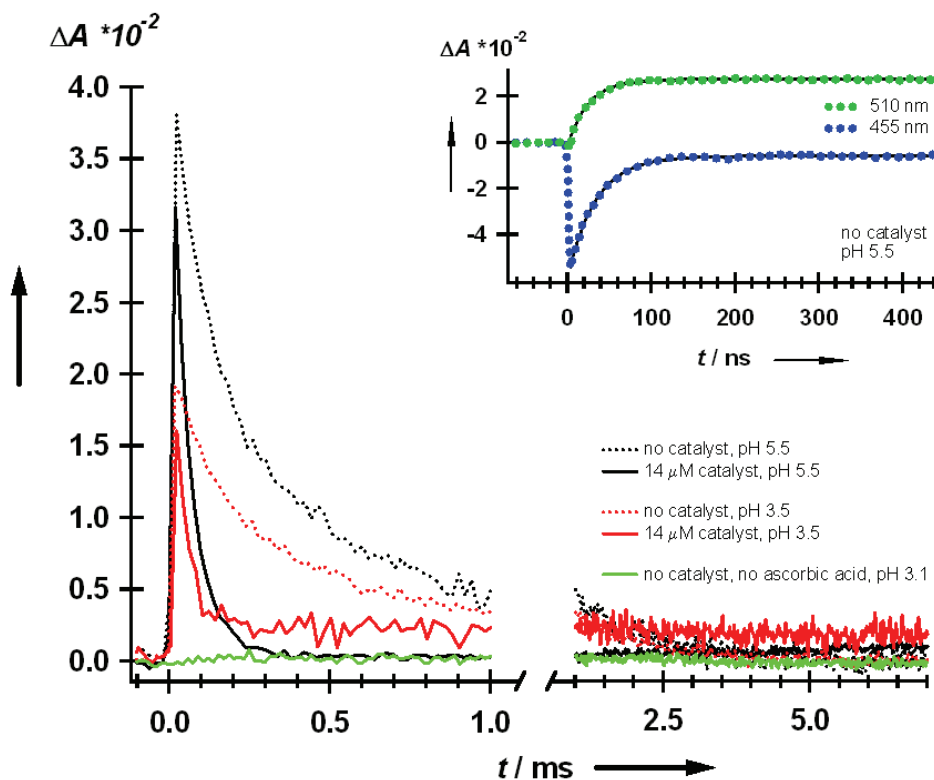
Figure 4. Effects of pH and the presence of catalyst **1** on the 510 nm transient absorption signal of $[Ru(bpy)_3]^+$ Conditions: 14 μM $[Ru(bpy)_3]^{2+}$, 0.1 M ascorbic acid in deoxygenated 1:1 DMF/H_2O at room temperature. Excitation wavelength: 470 nm. Inset: 510 and 455 nm transient absorption traces at pH = 5.5 on shorter timescales, with rise times of ca. 30 ns.

Radical anion **1⁻** is only attainable photochemically since its electrochemical reduction potential is more positive than that of neutral complex **1**. Due to the electrochemical inaccessibility of **1⁻**, the subsequent steps in the catalytic cycle have so far been elusive. Protonation, disproportionation or a second reduction are all plausible fates for **1⁻**. The experiments described above show that pH 6.4 is still sufficiently acidic to protonate the reduced state(s) of the catalyst (**1⁻**, **1²⁻**) to form a hydride intermediate, and to protonate this hydride to form hydrogen. None of the catalyst protonation steps seem to be rate limiting since the highest turnover rates are obtained at higher pH. Disproportionation or

bimolecular catalysis appear to be insignificant since the same turnover frequencies and numbers are obtained at 10 times lower absolute concentrations if the ratio of $[Ru(bpy)_3]^{2+}$:**1** is kept at 10:1 (data not shown). We therefore suggest that catalysis occurs intramolecularly and is rate limited by the transfer of the second electron to the catalyst (Scheme 1).

5.4 Conclusions

These results show that a new kind of [FeFe] hydrogenase active site model complex is an efficient catalyst for the photochemical production of hydrogen, in a mildly acidic 1:1 DMF/H_2O solution. $[(\mu\text{-}Cl_2bdt)Fe_2(CO)_6]$ achieves high turnover numbers that are competitive with those obtained from current state-of-the-art cobalt-based systems. Since synthetic model complexes may achieve the same high turnover numbers and frequencies that are reported for the enzymes themselves, [FeFe] hydrogenase active site mimics may well prove superior to other homogeneous catalysts in the future.

5.5 References

[1] J.-M. Lehn, J.-P. Sauvage, *Nouv. J. Chim.* **1977**, 1, 449.

[2] H. Ozawa, M. Haga and K. Sakai, *J. Am. Chem. Soc.* **2006**, 4926-.

[3] S. Rau, B. Schäfer, D. Gleich, E. Anders, M. Rudolph, M. Friedrich, H. Görls, W. Henry and J. G. Vos, *Angew. Chem.* **2006**, 118, 6361; *Angew. Chem. Int. Ed. Engl.* **2006**, 45, 6215.

[4] P. Du, J. Schneider, F. Li, W. Zhao, U. Patel, F. Castellano, R. Eisenberg *J. Am. Chem. Soc.* **2008**, 130, 5056.

[5] P. Lei, M. Hedlund, R. Lomoth, H. Rensmo, O. Johansson and L. Hammarström, *J. Am. Chem. Soc.* **2008**, 130, 26.

[6] A. Fihri, V. Artero, M. Razavet, C. Baffert, W. Leibl and M. Fontecave, *Angew. Chem.* **2008**, 120, 574; *Angew. Chem. Int. Ed. Engl.* **2008**, 47, 564.

[7] P. Du, K. Knowles and R. Eisenberg, *J. Am. Chem. Soc.* **2008**, 130, 12576.

[8] M. Frey, *ChemBioChem* **2002**, 3, 152.

[9] J.-F. Capon, F. Gloaguen, F.Y. Pétillon, P. Schollhammer and J. Talarmin, *Coord. Chem. Rev.* **2009**, 253, 1476.

[10] F. Gloaguen, J. D. Lawrence and T. B. Rauchfuss, *J. Am. Chem. Soc.* **2001**, 123, 9476.

[11] S. Ott, M. Kritikos, B. Åkermark, L. Sun and R. Lomoth, *Angew. Chem.* **2004**, 116, 1024; *Angew. Chem. Int. Ed. Engl.* **2004**, 43, 1006.

[12] Y. Na, M. Wang, J. Pan, P. Zhang, B. Åkermark and L. Sun, *Inorg. Chem.* **2008**, 47, 2805.

[13] A. M. Kluwer, R. Kapre, F. Hartl, M. Lutz, A. L. Spek, A. M. Brouwer, P. W. N. M. v. Leeuwen and J. N. H. Reek, *Proc. Natl. Acad. Sci.* **2009**, doi:10.1073/pnas.0809666106.

[14] G. A. N. Felton, A. K. Vannucci, J. Chen, L. T. Lockett, N. Okumura, B. J. Petro, U. I. Zakai, D. H. Evans, R. S. Glass and D. L. Lichtenberger *J. Am. Chem. Soc.*, **2007**, 129, 12521.

[15] L. Schwartz, P. S. Singh, L. Eriksson, R. Lomoth and S. Ott, *C. R. Chim.* **2008**, 11, 875.

[16] K. Mandal, M. Hoffman, *J. Phys. Chem.*, **1984**, 88, 5632.

Chapter 6

Ruthenium Polyoxometalate Water Splitting Catalyst: Very Fast Hole Scavenging from Photogenerated Oxidants.[ζ]
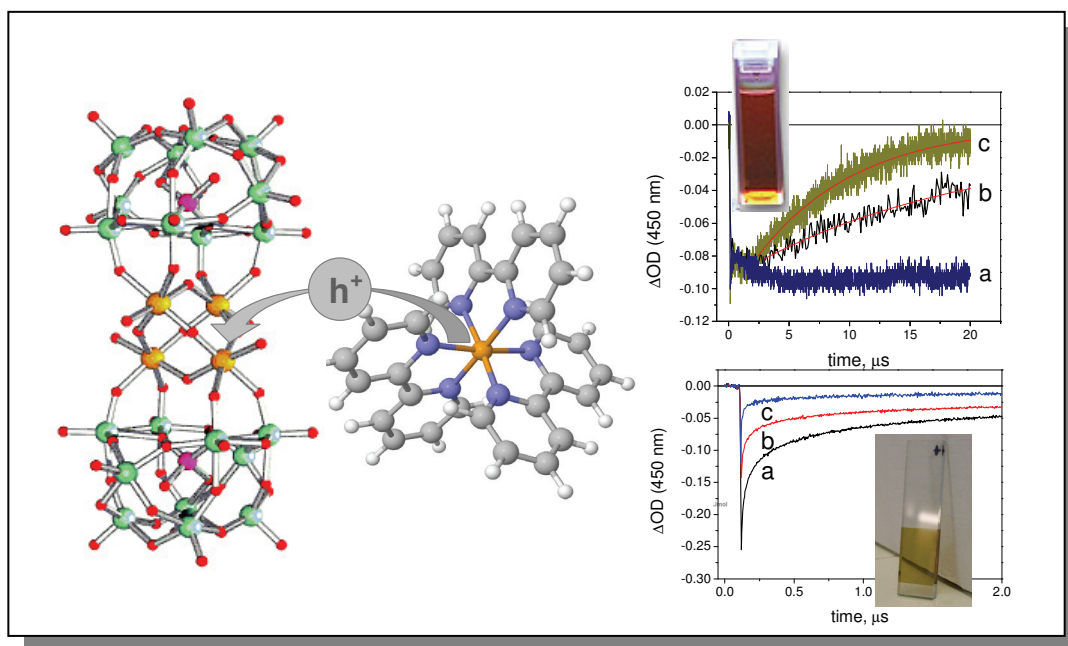
A tetraruthenium polyoxometalate water-oxidation catalyst performs very fast hole scavenging from photogenerated Ru(III) polypyridine oxidants, both in homogeneous solution and at a sensitized nanocrystalline TiO$_2$ surface.

The work described in this chapter is the result of a collaboration between the Photochemistry Group at the Department of Chemistry of University of Ferrara (Ferrara, Italy), where i have done my Ph.D., and the Group of Marcella Bonchio at ITM-CNR and the Department of Chemical Sciences at University of Padova (Padova, Italy).

6.1 Introduction

In most artificial photosyntetic schemes, water oxidation is considered to be the most demanding and difficult step.[1,2] Despite recent progress on water oxidation catalysts,[3] sufficiently stable and fast systems have not yet been developed. In a recent breakthrough in the field, $[Ru_4(\mu-O)_4(\mu-OH)_2(H_2O)_4(\gamma-SiW_{10}O_{36})_2]^{10-}$ (**1**) has emerged as a highly promising homogeneous catalysts for water oxidation.[4,5,6] In this totally inorganic, robust catalyst, the tetra-Ru(IV) μ-oxo core mimicks the oxygen-evolving complex of natural photosynthesis by undergoing four consecutive oxidation steps, followed by nucleophilic attack and water oxidation.[6] The remarkable performance of **1** as a water oxidation catalyst has been demonstrated in experiments making use of Ce(IV).[4] Efficient oxygen generation was also obtained with electrochemically generated $Ru(bpy)_3^{3+}$.[5]

Light-induced water oxidation catalyzed by **1** can be also obtained using photochemically generated $Ru(bpy)_3^{3+}$ as oxidant.[7] This well-established technique is based on the facile generation of $Ru(bpy)_3^{3+}$ by photoinduced electron transfer betweeen $Ru(bpy)_3^{2+}$ and an appropriate sacrificial electron acceptor (e.g., persulfate, Scheme 1, eq 1-4).[8] Besides providing a convenient way to evaluate the catalyst performance under continuous light irradiation, photocatalytic cycles can also yield, by the use of time-resolved fast techniques, relevant kinetic information.

$$[Ru_4(\mu\text{-}O)_4(\mu\text{-}OH)_2(H_2O)_4(\gamma\text{-}SiW_{10}O_{36})_2]^{10-} \quad (1)$$

$$Ru(bpy)_3^{2+} \xrightarrow{h\nu} {}^*Ru(bpy)_3^{2+} \qquad\qquad (1)$$

$$^*Ru(bpy)_3^{2+} + S_2O_8^{2-} \longrightarrow Ru(bpy)_3^{3+} + SO_4^{2-} + SO_4^{\cdot-} \qquad (2)$$

$$Ru(bpy)_3^{2+} + SO_4^{\cdot-} \longrightarrow Ru(bpy)_3^{3+} + SO_4^{2-} \qquad\qquad (3)$$

$$4Ru(bpy)_3^{3+} + 2H_2O \xrightarrow{\ 1\ } 4Ru(bpy)_3^{2+} + 4H^+ + O_2 \qquad (4)$$
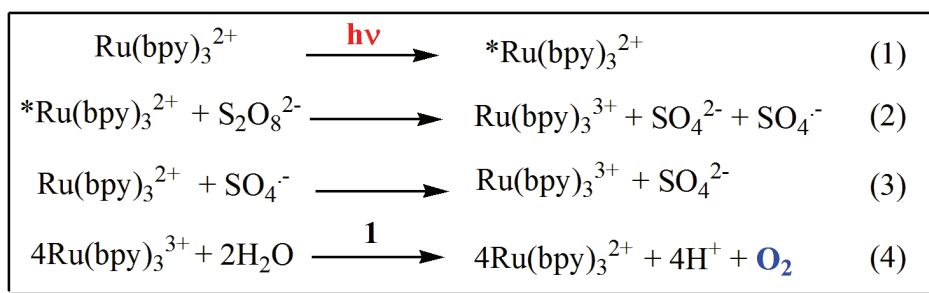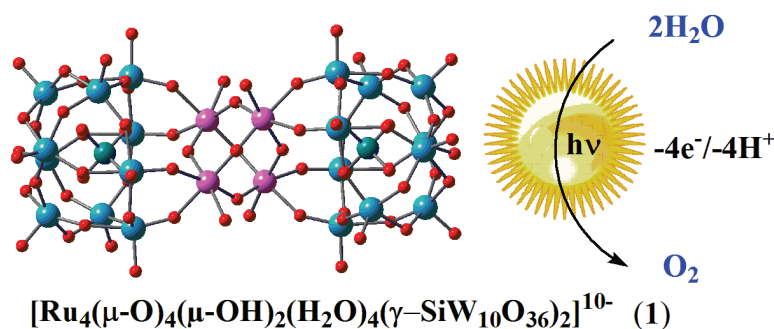
Scheme 1. Water oxidation by photogenerated $Ru(bpy)_3^{3+}$, using **1** as catalyst and persulfate as sacrificial electron acceptor.

In particular, one key parameter is the electron-transfer (ET) rate between the photogenerated $Ru(bpy)_3^{3+}$ and **1**, leading to oxygen evolution (equation 4). While this rate is relatively unimportant in the presence of a sacrificial oxidant, such as persulfate in Scheme 1, it becomes crucial for regenerative systems where the catalyst must be able to scavenge the hole on the photogenerated oxidant in competition with charge recombination. Studies of this type have been used, for instance, by Mallouk to optimize the performance of colloidal IrO_2 as a water oxidation catalyst,[9] prior to its inclusion in a dye-sensitized photoelectrochemical cell for photoassisted water splitting.[10] As it is often the case with water oxidation catalysts, in the IrO_2 case photodriven hole scavenging is relatively slow. Even if the catalyst nanoparticle and the photogenerated oxidant are covalently coupled via malonate groups, hole scavenging takes place in the millisecond time scale and proves to be the main limiting factor towards the function of an efficient cell for the photocatalytic splitting of water.[10] Concerning **1** as catalyst, no direct kinetic information on the reaction with photogenerated $Ru(bpy)_3^{3+}$ is yet available, but the high turnover frequencies observed in oxygen evolution experiments (up to 450 h^{-1})[4] seem to suggest an overall relatively fast behavior.

In this chapter are reported the results of a nanosecond laser flash photolysis investigation on the hole transfer reaction from photogenerated Ru(III) polypyridine

complexes to catalyst **1**. The oxidant species is generated either by quenching with a sacrificial acceptor (Scheme 1) or by charge injection into nanocrystalline TiO_2. In both cases, very fast rates are observed.

6.2 Experimental section

The synthesis and characterization of **1** were performed by Andrea Sartorel in the research group of Dr. Marcella Bonchio at University of Padova (Padova, Italy). Procedures are described in detail in Ref. 4.

Ru(bpy)$_2$(dpb)$^{2+}$, hexafluorophosphate salt, was prepared according to Ref. 11.

Other reagents and spectroscopic-grade solvents were purchased and used as received.

Preparation of sensitized TiO_2 films.

A Dyesol DSL 18NR-T TiO_2 paste was used for the preparation of mesoporous films for photophysical measurements. A small amount of paste was deposited on top of a microscope slide partially covered with two strips of scotch tape as to create a channel of the desired length and width. A microscope slide with a smooth edge, or a glass rod, was used as tool to uniformly distribute the paste dragging it at constant velocity. The films were dried under a stream of warm air and heated in an oven at 450°C for 30'. Dye adsorption was accomplished by putting the films in a crystallizer and covering them with a solution 10^{-3}M of the complex in ethanol. Adsorption is completed within about 24hrs at room temperature or 2 hrs heating the solution near the boiling point. After rinsing with ethanol and drying, the films were stored in a desiccator over silica gel.

The catalyst uptake was performed by contact of the sensitized TiO_2 film (30 min dipping) with 1.0×10^{-3} or 1.0×10^{-2} M aqueous solution of the catalyst, followed by rinsing and drying. The loading of the adsorbed species was estimated spectrophotometrically using the following molar extinction coefficients: Ru(bpy)$_2$(dpb)$^{2+}$, $\varepsilon_{452} = 14710$ M^{-1}cm^{-1}; **1,** $\varepsilon_{452} = 11560$ M^{-1}cm^{-1}, $\varepsilon_{600} = 4290$ M^{-1}cm^{-1}.

Procedures for nanosecond laser flash photolysis.

For flash photolysis in solution, the sample was contained in a 1-cm spectrofluorimeter cell, in a standard 90° excitation/analysis beam configuration.

For flash photolysis of films, the samples were obtained by clamping together a 4 cm x 1 cm glass slide, coated with a 1,5 cm x 1 cm TiO_2 film, with a naked slide of the same size. Peak absorbance values of sensitized films were about 1.5, while at the excitation wavelength they were in the range 0.1-0.2. The solution chosen for the measure was drawn by capillary forces in the thin space between the slides and the assembly was placed diagonally in a 1 cm path length quartz cell at 45 degrees with respect to the optical axis of the spectrometer. Laser excitation pulses at 532nm were defocused by a concave lens in order to reach an energy density of about 18mJ/pulse/cm^2 on the film. The scattered laser light was eliminated by using an interference filter.

6.3 Results and discussion

In a typical experiment, aqueous solutions containing 4.76×10^{-5} M $Ru(bpy)_3^{2+}$, 5.0×10^{-3} M $Na_2S_2O_8$, 1.0×10^{-2} M phosphate buffer (pH = 7), and variable amounts of **1** were excited with 8 ns pulses of 355-nm light from a frequency tripled Nd:YAG laser. In the absence of **1** (Figure 1, trace a), the laser pulse produces an instantaneous bleach of the ground-state MLCT absorption (λ_{max}, 450 nm), indicative of the formation of $Ru(bpy)_3^{3+}$ by reactions 1 and 2 in Scheme 1.[h]
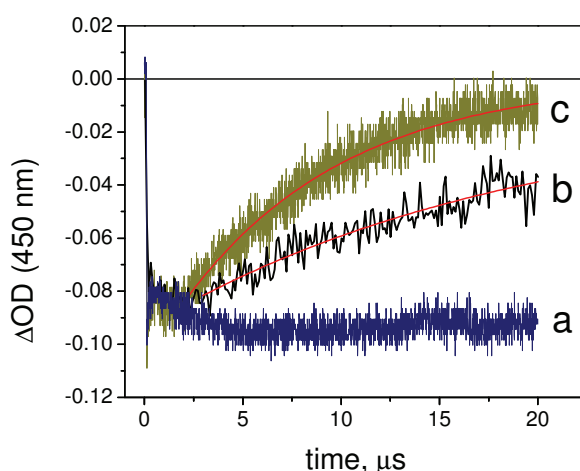
Figure 1. Laser flash photolysis (excitation, 355 nm, FWHM 8ns) of aqueous solutions containing 4.76×10^{-5} M $Ru(bpy)_3^{2+}$, 5.0×10^{-3} M $Na_2S_2O_8$, 1.0×10^{-2} M phosphate buffer (pH = 7), and variable amounts of **1**: (a) 0.0 M, (b) 2.5×10^{-5} M, (c) 4.76×10^{-5} M.

---

[h] The bleach forms within few nanoseconds after the laser pulse, consistent with the efficient quenching observed for the $Ru(bpy)_3^{2+}$ emission.

Then, after a further increase in the few microsecond time scale, assigned to the secondary oxidation reaction 3 in Scheme 1, the bleach remains constant over the whole time scale of the experiment (20 μs). In the presence of **1** (Figure 1, traces b and c), on the other hand, the bleach clearly recovers in the time window of the experiment, showing a kinetic profile dependent on the concentration of **1**. The recovery is attributed to hole transfer from the photo-produced oxidant to the catalyst, generating back the $Ru(bpy)_3^{2+}$ and leading to the one-electron oxidized form of **1**.[i]

$$Ru(bpy)_3^{3+} + \mathbf{1} \rightarrow Ru(bpy)_3^{2+} + \mathbf{1}^+ \qquad (5)$$
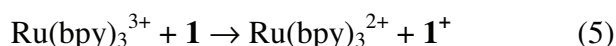
The kinetics (pseudo-first order, expected for [**1**] >> [$Ru(bpy)_3^{3+}$]) yields rate constants of 4.3×10^4 s^{-1} and 1.2×10^5 s^{-1} for [**1**] = 2.5×10^{-5} M and 4.76×10^{-5} M, respectively. This corresponds to an average bimolecular rate constant for process 5 of $(2.1 \pm 0.4) \times 10^9$ M^{-1}s^{-1}. This very high value, within one order of magnitude of diffusion-controlled rate, confirms **1** as a highly promising catalyst for water splitting photochemical cycles.

An alternative way to oxidant photogeneration, more closely related to the design of practical devices for photochemical water splitting,[10] is electron injection from a Ru(II) photosensitizer into an n-type semiconductor (Scheme 2). The ability of **1** to act as hole scavenger in this configuration has been tested by laser flash photolysis measurements. The sensitizer, $Ru(bpy)_2(dpb)^{2+}$ (dpb = 4,4'-diphosphonic-2,2'bipyridine acid), was adsorbed on a layer of nanocrystalline TiO_2 deposited on a glass slide by standard techniques. The sample, examined by laser flash photolysis (λ_{ex}, 532 nm), shows the typical behavior of sensitized semiconductor electrodes (Figure 2 trace a):[12] instantaneous bleach of MLCT absorption (arising from ultrafast electron injection into the semiconductor), is followed by recovery with complex kinetics in the ns-μs time scale as consequence of recombination of the injected electrons with the oxidized sensitizer. The sample was then loaded with **1** by contact (30 min dipping) with 1.0×10^{-3} or 1.0×10^{-2} M aqueous solution of the catalyst, followed by rinsing and drying.

---

[i] In aerated solutions, **1** is known[6] to be present as a Ru_4(V,IV,IV,IV) species. The one-electron oxidized form is likely to be the Ru_4(V,V,IV,IV) state.
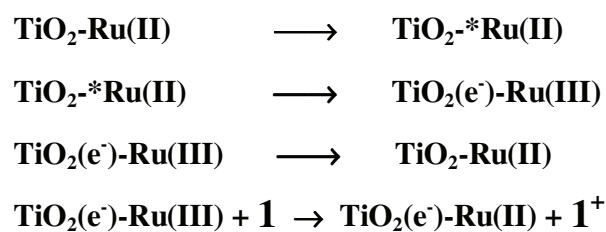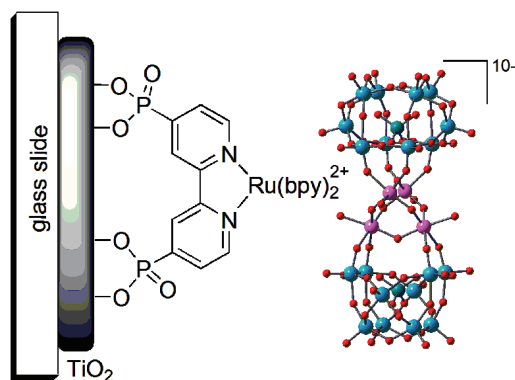
Scheme 2. Reaction of catalyst **1** with Ru(III) species photogenerated by electron injection into nanocrystalline TiO$_2$ layer.

The efficient uptake of the catalyst from the solution (as detected spectrophotometrically) is thought to occur mainly by electrostatic interaction of the negatively charged catalyst with the positively charged photosensitizer (in this regard, the high charge turns out to be a very useful property of **1**).[j]

---

[j] Very efficient ion-pair formation between the sensitizer and the catalyst takes place in solution, as detected by emission quenching measurements. A measurable uptake of the catalyst is also observed by the bare TiO$_2$ layer, but to a smaller extent than in the presence of sensitizer.
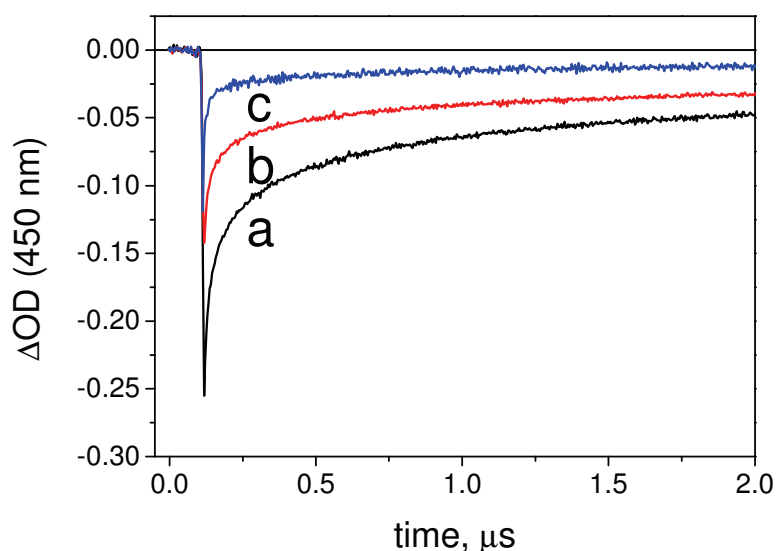
Figure 2. Laser flash photolysis (excitation, 532 nm, FWHM 8ns) of a nanocrystalline TiO_2 layer sensitized with $Ru(bpy)_2(dpb)^{2+}$ (8×10^{-8} mol/cm^2). As such (a), and loaded with 6.6×10^{-9} mol/cm^2 **1** (b) or 3.2×10^{-8} mol/cm^2 **1** (c).

When the catalyst-loaded samples are examined by laser flash photolysis (Figure 2 traces b and c), a clear acceleration of the bleach recovery is observed, increasing with the surface concentration of **1**. At the highest loading (trace c), the fast (ns) component of the recovery becomes almost indistinguishable from the laser pulse, while a long-lived (μs) component of the bleach is still remaining. Considering the molar ratios between sensitizer and **1** (2.5 for trace c), the residual slow component can be very likely assigned to electron-hole recombination for oxidized sensitizer molecules that do not have a catalyst in close proximity. Those that are in an ion-pair situation with a catalyst, on the other hand, undergo very fast (sub-ns) hole scavenging. Ultrafast spectroscopy experiments are needed for the kinetic characterization of this step.

6.4 Conclusions

Nanosecond laser flash photolysis investigation shows that **1** is able to give very fast hole scavenging from photogenerated Ru(III) species, both in homogeneous solution and at a sensitized semiconductor surface. This fast behavior is likely related to a combination of favorable features of catalyst **1**: the high negative charge, that facilitates intimate contact with positively charged oxidants; the low reorganizational energy brought about by the POM ligands that firmly hold and effectively shield from solvent the redox active Ru_4 core. The fast rates of hole scavenging are an excellent premise for the use of the new catalyst in practical water splitting photochemical devices.

6.5 References

[1] (a) C. Herrero, B. Lassalle-Kaiser, W. Leibl, A. W. Rutherford, A. Aukauloo, *Coord. Chem. Rev.*, 2008, **252**, 456-468. (b) M. Hambourger, G. F. Moore, D. M. Kramer, D. Gust, A. L. Moore, T. A. Moore, *Chem. Soc. Rev.*, 2009, **38**, 25-35.

[2] Special issue: *Acc. Chem. Res.* 2009, **42**, 1859-2029.

[3] (a) S. W. Gersten, G. J. Samuels, T. J. Meyer, *J. Am. Chem. Soc.*, 1982, **104**, 4029–4030. (b) F. Liu, J. J. Concepcion, J. W. Jurss, T. Cardolaccia, J. L. Templeton, T. J. Meyer, *Inorg. Chem.*, 2008, **47**, 1727–1752. (c) N. D. McDaniel, F. J. Coughlin, L. L. Tinker, S. Bernhard, *J. Am. Chem. Soc.*, 2008, **130**, 210–217. (d) T. A. Betley, Q. Wu, T. Van Voorhis, D. G. Nocera, *Inorg. Chem.,* 2008, **47**, 1849–1861. (e) R. Tagore, R. H. Crabtree, G. W. Brudvig, *Inorg. Chem.*, 2008, **47**, 1815–1823. (f) R. Zong, R. P. Thummel, *J. Am. Chem. Soc.*, 2005, **127**, 12802–12803. (g) Z. Deng, H.-W. Tseng, R. Zong, D. Wang, R. Thummel, *Inorg. Chem.*, 2008, **47**, 1835–1848. (h) H. Chen, J. W. Faller, R. H. Crabtree, G. Brudvig, *J. Am. Chem. Soc.*, 2004, **126**, 7345-7349. (i) M. W. Kanan, D. G. Nocera, *Science,* 2008, **321**, 1072-1075. (j) R. Brimblecombe, G. F. Swiegers, G. C. Dismukes, L. Spiccia, *Angew. Chem.*, 2008, **47**, 7335-7338. (k) G. La Ganga, F. Nastasi, S. Campagna, F. Puntoriero, *Dalton Trans.* 2009, 9997–9999. (l) F. Jao, H. Frei, *Angew. Chem. Int. Ed.,*. 2009, **48**, 1841–1844.

[4] A. Sartorel, M. Carraro, G. Scorrano, R. De Zorzi, S. Geremia, N. D. McDaniel, S. Bernhard, M. Bonchio, *J. Am. Chem. Soc.*, 2008, **130**, 5006-5007.

[5] Y. V. Geletii, B. Botar, P. Köegerler, D. A. Hillesheim, D. G. Musaev, C. L. Hill, *Angew. Chem. Int. Ed.*, 2008, **47**, 3896-3899.

[6] A. Sartorel, P. Miró, E. Salvadori, S. Romain, M. Carraro, G. Scorrano, M. Di Valentin, A. Llobet, C. Bo, M. Bonchio *J. Am. Chem. Soc.*, 2009, **131**, 16051–16053

[7] Y. V. Geletii, Z. Huang, Y. Hou, D. G. Musaev, T. Lian, C. L. Hill, *J. Am. Chem. Soc.*, 2009, **131**, 7522–7523.

[8] H. S. White, W. G. Becker, A. J. Bard, *J. Phys. Chem.*, 1984, **88**, 1840–1846.

[9] N. D. Morris, M. Suzuki, T. E. Mallouk, *J. Phys. Chem. A*, 2004, **108**, 9115-9119.

[10] J. W. Youngblood, S.-H. A. Lee, Y. Kobayashi, E.A. Hernandez-Pagan, P. G. Hoertz, T. A. Moore, A. L. Moore, D. Gust, T. E. Mallouk, *J. Am. Chem. Soc.*, 2009, *131*, 926–927.

[11] Gillaizeau-Gauthier I., Odobel F., Alebbi M., Argazzi R., Costa E., Bignozzi C.A., Qu P., Meyer G.J. *Inorg. Chem.* **2001**, *40*, 6073-6079.

[12] T. A. Heimer, E. J. Heilweil, C. A. Bignozzi, G. J. Meyer, *J. Phys. Chem. A*, **2000**, *104*, 4256–4262.

Chapter 7

Photophysical Characterization of Multichromophoric Pyridylporphyrin-Rhenium(I) Conjugates.[ξ]
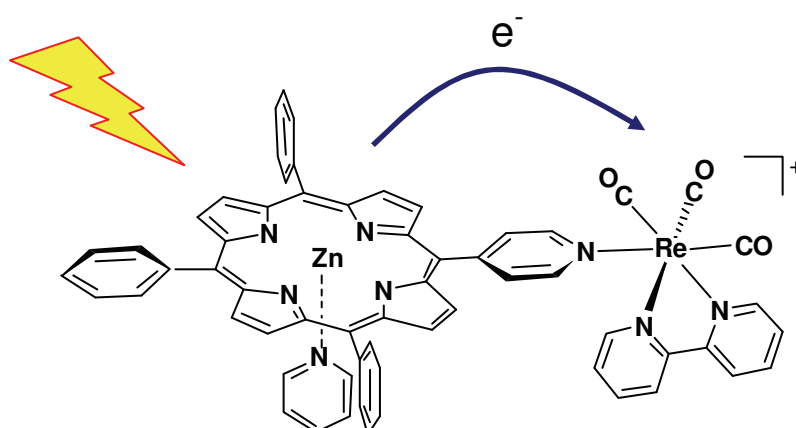
[Re(CO)₃(bpy)]⁺, a fragment capable of catalytic reduction of CO₂, is inserted in supramolecular adducts with Zn-porphyrins and the photophysical properties studied.

The work described in this chapter is the result of a collaboration between the Photochemistry Group at the Department of Chemistry of University of Ferrara (Ferrara, Italy), where i have done my Ph.D., the Inorganic Chemistry Group and the Structural Chemistry Group University of Trieste (Trieste, Italy).

7.1 Introduction

Polypyridine-Re(I)-tricarbonyl complexes show attractive properties from a supramolecular point of view: Re(I) makes strong and inert bonds with pyridyl ligands,[1] opening the possibility to include these complexes in novel assemblies, and the Re(I) fragment has been used in catalytic cycles for the reduction of CO_2.[2] The construction of supramolecular systems where a Polypyridine-Re(I)-tricarbonyl fragment is attached to a chromophore is therefore a topic of interest for photocatalysis purposes.

A photocatalytic system should contain a photoactive unit capable of absorbing light in the visible region and subsequently transfer an electron form its excited state to the Re(I) fragment, making it a powerful reducing agent capable of performing a rapid reduction of the substrate. The catalytic cycle should be closed by a sacrificial electron donor. With this aim, multinuclear compounds in which [fac-Re(CO)$_3$(bipy)]$^+$ units are bound to Ru(II)-polypyridyl or to dirhodium(II) scaffolds have been investigated by Ishitani and coworkers.[2] The connection of organic chromophores, such as porphyrins, to [fac-Re(CO)$_3$(diimine)]$^+$ fragments is expected to afford systems with similar photophysical properties.[3,4]

Recently, our group and the group of Prof. E. Alessio described[5] the photophysical properties of two pyridylporphyrin-Re(I) adducts in which a free base porphyrin is directly coordinated to the Re(I) fragment, namely the dimeric and pentameric compounds [fac-Re(CO)$_3$(bipy)(4'MPyP)](CF$_3$SO$_3$) (**1**) (Figure 1, 4'MPyP = 4'-monopyridylporphyrin) and [fac-{Re(CO)$_3$(bipy)}$_4$(μ-4'TPyP)](CF$_3$SO$_3$)$_4$ (**2**) (Figure 1, 4'TPyP = 4'-tetrapyridylporphyrin).

We found that for **1** and **2**: *i*) no photoinduced electron transfer from the free-base porphyrin to the Re(I)-bipy fragment occurs for thermodynamic reasons (ΔG > 0); *ii*) upon excitation of the porphyrin chromophore the typical fluorescence emission is quenched because of enhanced intersystem crossing induced by the peripheral Re atoms; *iii*) excitation of the Re fragments is followed by partial sensitization of the porphyrin fluorescence, indicating the occurrence of fast inter-component energy and/or electron transfer processes.[5]
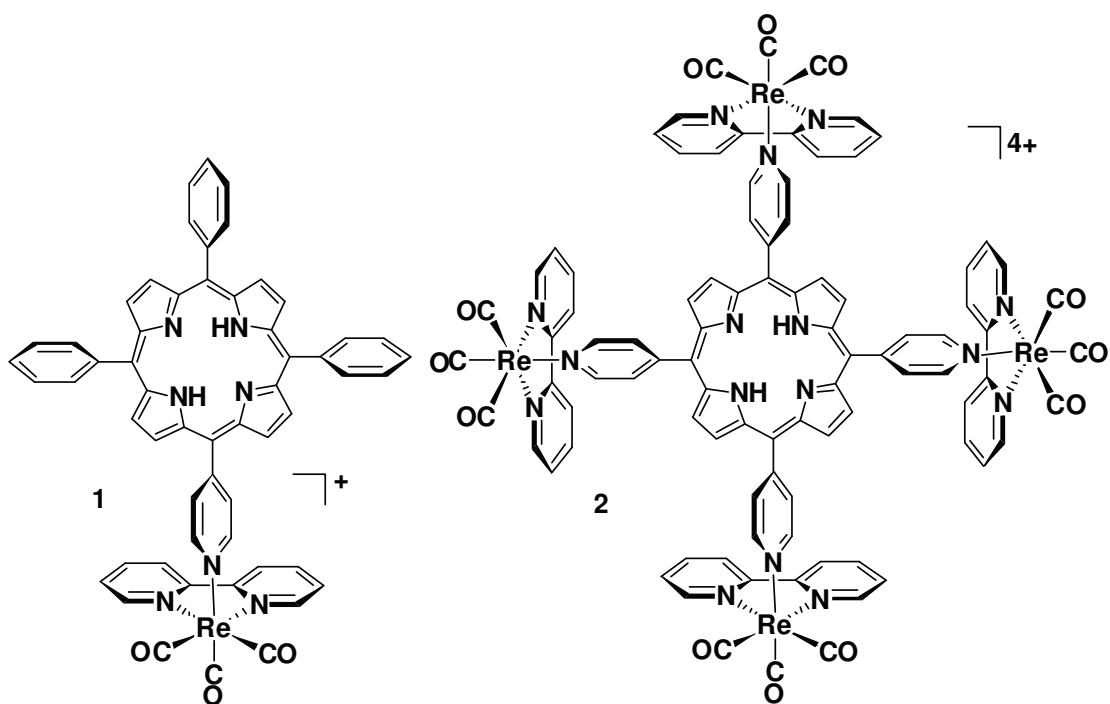
Figure 1. Schematic representation of the cations of [*fac*-Re(CO)$_3$(bipy)(4'MPyP)](CF$_3$SO$_3$) (**1**) and [*fac*-{Re(CO)$_3$(bipy)}$_4$(μ-4'TPyP)](CF$_3$SO$_3$)$_4$ (**2**).

A detailed photophysical investigation of the three zincated derivatives [*fac*-Re(CO)$_3$(bipy)(Zn·4'MPyP)](CF$_3$SO$_3$) (**5**), [*fac*-{Re(CO)$_3$(bipy)}$_4$(μ-Zn·4'TPyP)](CF$_3$SO$_3$)$_4$ (**6**), and [*fac*-Re(CO)$_3$(bipy)(Zn·3'MPyP)](CF$_3$SO$_3$) (**7**) was performed with the aim of establishing: *i*) *how* the photophysical properties of the porphyrin-Re(I) conjugates are affected by insertion of Zn into the porphyrin core: it is known that zincated porphyrins are better electron donors in their excited state compared to the corresponding free bases, thus photoinduced electron transfer from the zinc-chromophore to the Re fragment might become allowed; *ii*) *if* the number of Re-bipy fragments and their relative geometry with respect to the porphyrin (i.e. 3'PyPs *vs* 4'PyPs) have an influence on the photophysical properties of the adducts; *iii*) *how* the photoinduced electron transfer process might be improved (provided that it occurs), for example by axial coordination of ligands to the Zn atom inside the porphyrin.

7.2 Experimental section

The syntheses and characterization of the compounds discussed in this chapter were performed by Massimo Casanova and Elisabetta Iengo in the research group of Prof. Enzo Alessio, and Prof. Ennio Zangrando at University of Trieste (Trieste, Italy). Details can be found in M. Casanova, E. Zangrando, E. Iengo, E. Alessio, M. T. Indelli, F. Scandola, M. Orlandi. *Inorganic Chemistry*, **2008**, *47*, 22, 10407.

Reagents and spectroscopic-grade solvents were purchased and used as received. See Chapter 2 for details on electrochemical and photophysical measurement apparatus and procedures.

7.3 Results

Photophysical Behavior of the zincated pyridylporphyrin-Re(I) conjugates 5-7.

The zincated tetraphenylporphyrin, Zn·TPP, and the rhenium complex [*fac*-Re(CO)$_3$(bipy)(py)][CF$_3$SO$_3$] (**10**),[5] were used as references. Concentration-dependent self-assembly of zincated pyridylporphyrins is known[6] to occur spontaneously in non-coordinating solvents through axial Zn-N(pyridyl). Indeed, the absorption and emission spectra of Zn·4'MPyP and Zn·3'MPyP in CH$_2$Cl$_2$ solutions were found to be concentration-dependent. Reference spectra were taken for concentrations below 10^{-5} M, where no further changes were observed upon dilution. In these conditions, Zn·4'MPyP and Zn·3'MPyP showed spectral patterns and photophysical behaviors almost identical to Zn·TPP, that was therefore selected as reference compound.

For reasons that will be illustrated below, and consistent with previous results,[5] the energetic for the photo-induced electron transfer process is expected to be less favorable for the pentameric species with respect to the dimeric systems. Nevertheless, the pentameric adduct **7** was included in the photophysical investigation as a useful probe to discriminate between different mechanisms (see Discussion).

Absorption Spectra.

The relevant absorption properties of the systems in the visible region are collected in Table 5. As observed for the corresponding free-base compounds **1** and **2**,[5] aside from small red shifts of the porphyrin bands with respect to the parent zinc-porphyrin, the spectra of **5-7** are

good superpositions of those of the molecular components, confirming that the electronic interaction between the zinc-porphyrin and rhenium units is weak.

Compound	Soret	Q_1	Q_2
Zn·TPP	420	547	585
5	421	550	592
6	438	564	605
7	421	550	592

Table 5. Absorption maxima (λ_{max}, nm) of **5-7**, and of the reference compound Zn·TPP in CH$_2$Cl$_2$ solution.

They are dominated in the whole spectral region by the zinc-porphyrin component (Figure 2), with two typical Q-bands between 500-700 nm in addition to the Soret band. The rhenium unit practically does not absorb in the visible region above 350 nm. In the UV region the metal-to-ligand charge-transfer (MLCT) Re→ bipy bands (λ_{max} = 350 nm) are hidden by the porphyrin Soret band, while the intense ligand centered (LC) transitions are evident under 330 nm with a narrow band at 321 nm that can be clearly recognised only in the spectrum of **6**.

Finally, the spectra were not concentration-dependent, suggesting that no aggregation occurs for these compounds in the range of concentrations used.
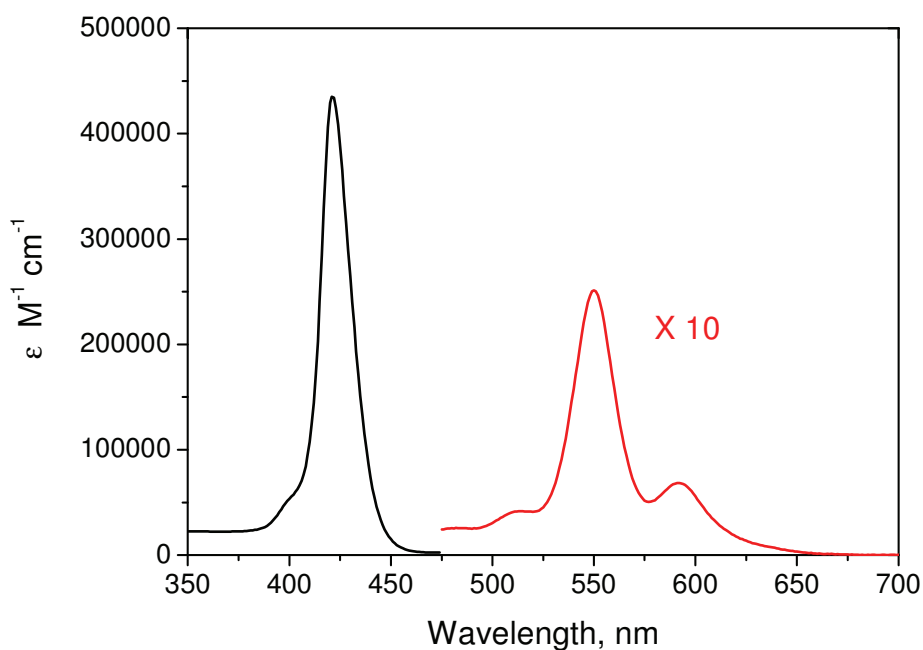
Figure 2. Absorption spectrum of [*fac*-Re(CO)$_3$(bipy)(Zn·4'MPyP)](CF$_3$SO$_3$) (**5**) in dichloromethane solution: Soret band (black line) and Q bands (red line).

Emission.

Emission experiment were performed upon selective excitation of zinc-porphyrin component in the Q-bands region. All the Zn·porphyrin-Re(I) conjugates studied show the typical porphyrin-based fluorescence. The emission spectrum of each compound exhibits two intense sharp bands like that of the zinc-porphyrin model, with a small red-shift with respect to the reference chromophore (see Table 6). Excitation of optically matched solutions of the dyad **5** and of the Zn·TPP reference at the excitation wavelength of 517 nm evidenced a moderate but significant decrease of the emission intensity and lifetime for the rhenium adduct. This effect is more pronounced for the pentad **6**. The data of Table 6 clearly indicate that, in all the adducts studied, the porphyrin fluorescence is affected, but not strongly quenched, by the presence of the peripherally bound rhenium unit(s).

Compound	λ_{max}(em), nm	Φ_0/Φ [b]	τ [c], ns	τ_0/τ [b]
Zn·TPP	599, 645		1.7	
5	607, 650	1.6	0.9	2.0
6	615, 668	3.1	0.5	3.6
7	606, 652	4.0	0.4	4.2
[a] Room temperature. [b] Φ_0 and τ_0 are, respectively, the fluorescence quantum yield and lifetime of the corresponding zinc-porphyrin model. [c] Estimated error: $\pm$ 0.1 ns.				

Table 6. Emission properties of **5-7**, and of the reference compound Zn·TPP in CH_2Cl_2 solution.[a]

In order to evidence effects of solvent polarity on the emission behavior, measurements (emission quantum yield and lifetime) in CH_3CN were also carried out. The results clearly showed that, for these systems, the emission properties are practically unaffected by the solvent polarity.

For **5** emission experiments were also performed in the presence of pyridine (0.5-2 M),[k] that is known to bind axially to the zinc atom.[7] Similarly to what reported by Gust and co-workers for the Zn·TPP chromophore, the addition of pyridine caused small but significant spectral shifts (ca. 15 nm) in the absorption (Q region) as well as in the emission spectra of the dyad **5**, clearly indicating the coordination of pyridine to the zinc center. Remarkably, the presence of pyridine induced a pronounced decrease of the emission intensity of **5**, accompanied by a shortening in the lifetime (from 900 ps to ca. 250 ps), whereas had no effect on the emission behavior (intensity and lifetime) of Zn·TPP.

Emission experiments were also carried out upon excitation in the ultraviolet region (λ_{xc} = 321 nm) where the Re(I)-bipy unit absorbs. As expected on the basis of our previous results with the free base adducts,[5] no rhenium MLCT emission was detected, clearly indicating that its triplet state is efficiently quenched in all the compounds investigated. Although a detailed characterisation of the photophysical behavior following excitation of

---

[k] To ascertain the stability of the compounds in the presence of pyridine, a sample of **5** was dissolved in neat pyridine-*d5*, and its ^{1}H NMR spectrum was monitored in time. Only after one day, very weak signals corresponding to the resonances of free Zn·4'MPyP started to appear, indicating that the Re-PyP bond has an excellent kinetic stability.

the rhenium unit(s) was not attempted, given the energy level diagram of the system (see below) the quenching is likely to occur by intramolecular electron transfer.

Transient absorption.

Transient absorption spectra of **5-7** were measured in deaerated dichloromethane solutions by using nanosecond laser flash photolysis (532 nm laser excitation) in the spectral range 460-520 nm, where the triplet state of the Zn·porphyrin-Re(I) adducts exhibits distinct absorptions.[8] The transient spectra were compared with that of an isoabsorptive solution of Zn·TPP. For all derivatives the transient, that decayed with a lifetime > 20 μs, corresponded to the spectrum of triplet state. The intensity of each transient was very similar to that observed for the reference compound (as an example, the transient spectra of Zn·TPP and of **5** are reported in Figure 3), clearly indicating that in these compounds the yield of triplet formation is the same as in Zn·TPP.
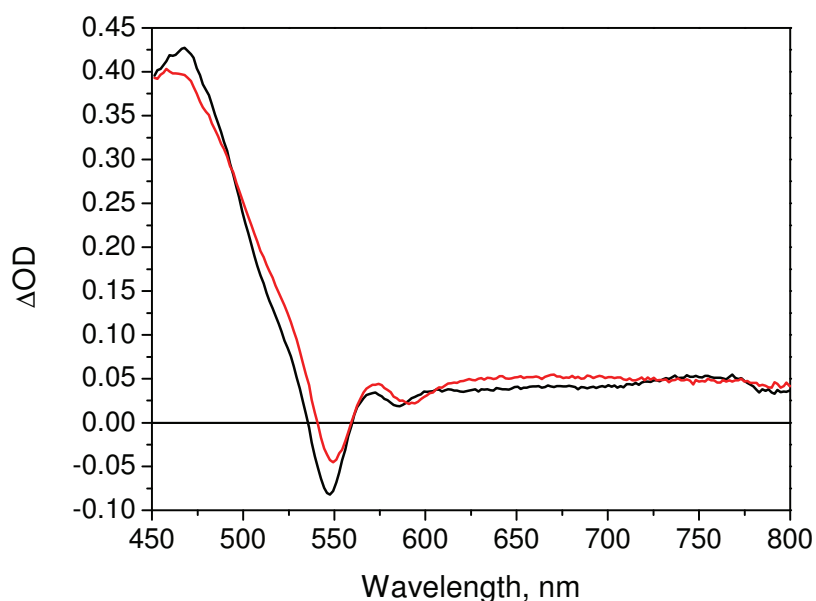
Figure 3. Ttransient absorption spectra of the triplet excited state of Zn·TPP (black line) and of **5** obtained by nanosecond laser photolysis (for details see text).

The photophysical behaviour of each adduct was further investigated by ultrafast spectroscopy using 560 nm excitation. The transient spectral changes of **5** are shown in Figure 4. The initial spectrum, taken immediately after the excitation pulse (1 ps) exhibited the typical zinc-porphyrin S_1 features (a strong broad positive absorption at 460 nm, ground-state bleaching and stimulated emission in the range 590-660 nm). This pattern evolved to a

final spectrum that is practically superimposable to that of the nanosecond experiments and thus corresponds to the triplet spectrum. The evolution of the S_1 spectrum to that of the triplet takes place in ca.1 ns, a time consistent with the singlet lifetime observed in the luminescence decay (see Table 6).

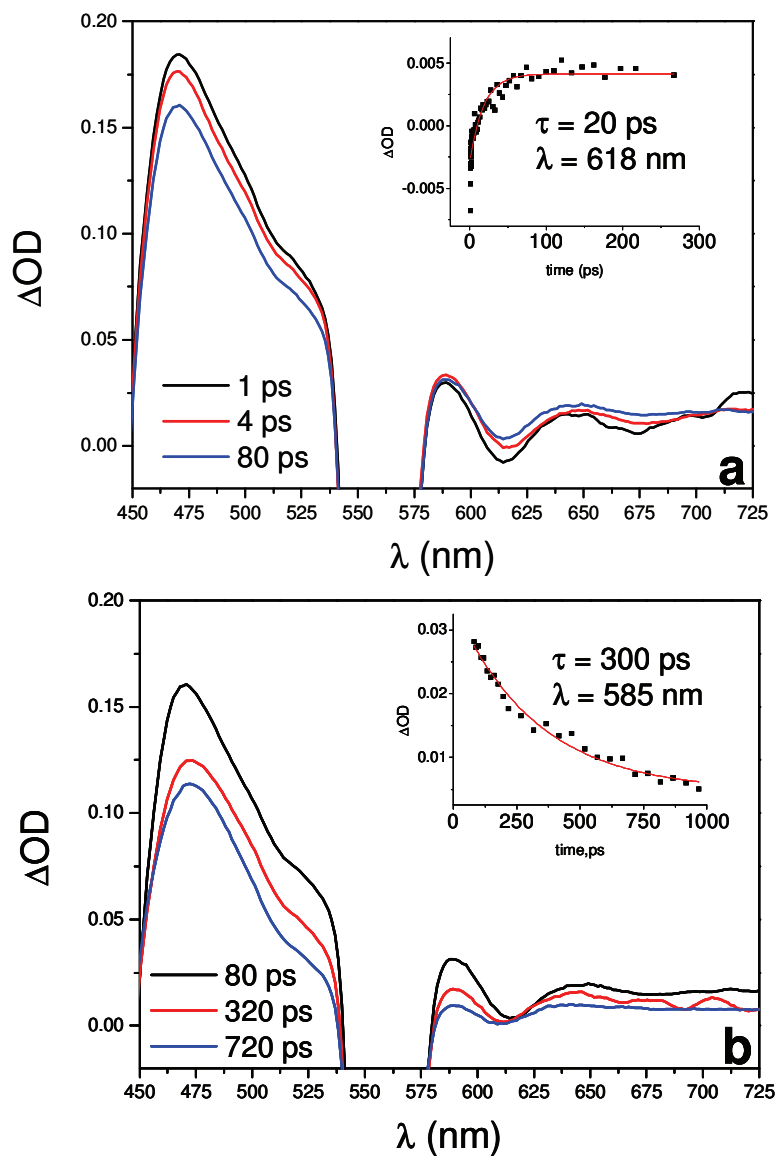**Figure 4.** Transient spectral changes obtained for **5** in CH_2Cl_2 solution. Excitation wavelength: 560 nm.

Ultrafast experiments were also performed in the presence of pyridine. The temporal evolution of spectral changes was substantially different from that observed in absence of pyridine, with a biphasic behaviour taking place for t ≤ 80 ps (Figure 5a) and t ≥ 80 ps

(Figure 5b). Kinetic analysis of the spectral changes at 618 nm yielded a time constant of 20 ps for the first process (Figure 5a) and of 300 ps at 585 nm for the second process (Figure 5b). No clear evidence for the characteristic spectral features of the porphyrin radical cation was detected in the 600-700 nm spectral region.[9] The final spectrum recorded at the end of the temporal window of the experiment (1000 ps) was practically superimposable to the triplet spectrum observed in the nanosecond experiments.

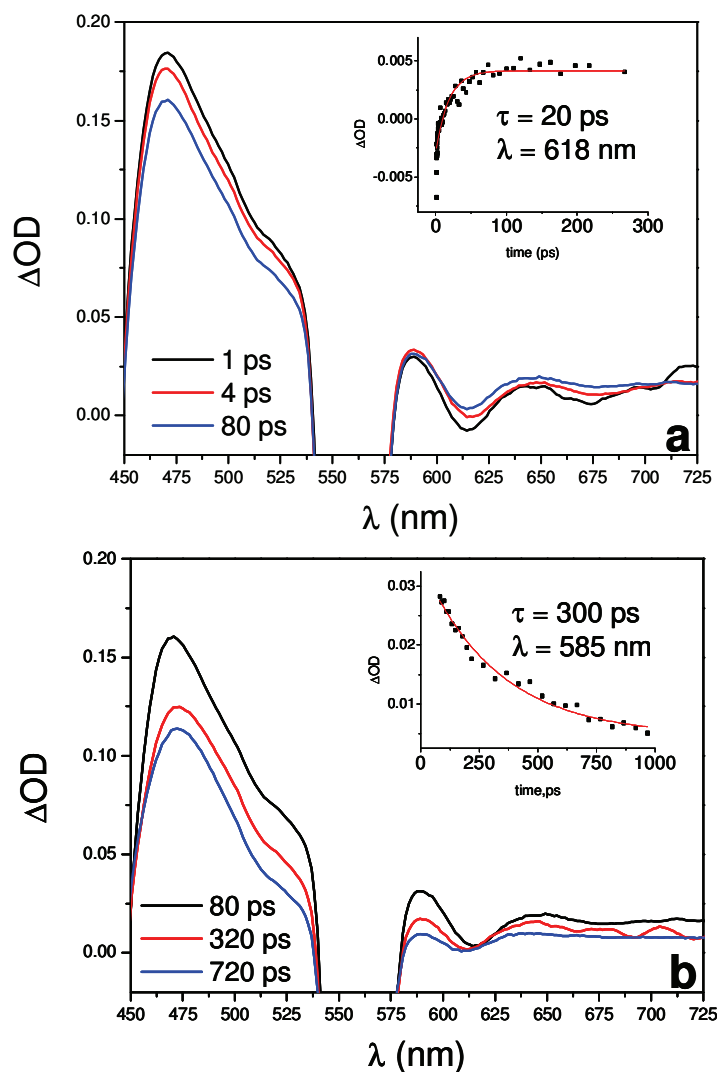**Figure 5.** Transient spectral changes obtained for **5** in CH_2Cl_2 solution in the presence of pyridine (excitation wavelength: 560 nm). (**a**) Spectral changes in the 1-80 ps range; inset: kinetic recorded at 618 nm. (**b**) Spectral changes in the 80-1000 ps range; inset: kinetic recorded at 585 nm.

Electrochemistry.

Cyclic voltammetry measurements on **5**-**7** were performed in deareated CH_2Cl_2. The electrochemical behaviors of Zn·TPP and of **10** were studied in the same experimental conditions for comparison. For mechanistic reasons (see Discussion), attention was focussed on the potential values for the first oxidation and reduction processes. The results are summarised in Table 7: the first oxidation process was assigned to the zinc-porphyrin unit, whereas the first reduction process can be easily attributed to the reduction of the bipy ligand on the rhenium unit.

Compound	$E_{1/2 \, (red)}$, V	$E_{1/2 \, (ox)}$, V	ΔG_{el}, eV
Zn·TPP	-1.38	+0.80	
10[10]	-1.13	+1.74	
5	-1.16	+0.83	-0.05
6	-1.15	+1.10	+ 0.25
7	-1.17	+0.83	-0.04

Table 7. Electrochemical data for **5**-**7**, and for the reference compounds Zn·TPP and [*fac*-Re(CO)$_3$(bipy)(py)][CF$_3$SO$_3$] (**10**). ΔG_{el} = free energy change for intramolecular electron transfer from the excited zinc-porphyrin unit to the bypiridine-rhenium unit calculated assuming $E^{0-0}(S_1) = 2.04$ eV (see Discussion).

7.4 Discussion

The supramolecular nature of the systems studied (as demonstrated by the additive nature of the spectroscopic and electrochemical properties of the molecular components, Tables 5 and 7), allowed us to construct the energy level diagram as a superposition of those of the component units. To this simple picture, possible states of intercomponent charge-transfer character should be added. Given the well known electron accepting properties of the [*fac*-Re(CO)$_3$(bipy)(py)]$^+$ unit,[5,11] a charge transfer state (Zn·porph$^+$-Re(bipy)$^-$), in which an electron is transferred from the zinc-porphyrin to the rhenium-bipy unit, is expected to lie close in energy to the singlet state (S$_1$) of the zinc-porphyrin unit. The energy of this state can be obtained as the difference in the potentials for oxidation of the Zn-porphyrin component and for reduction of Re(bipy) component. In fact, no correction for electrostatic

work terms is required in this case because of the charge shift character of the process involved. The resulting energy diagram for the dimeric species is reported in Figure 12.
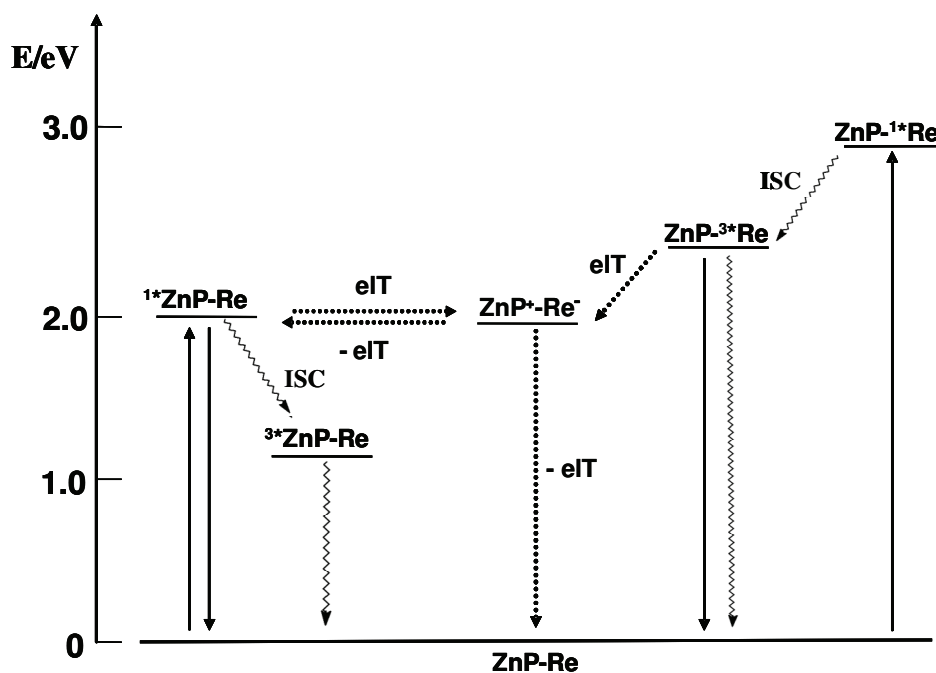

Figure 12. Energy level diagram for **5** in dichloromethane and photophysical processes.

The energy values inferred from electrochemical data (see Table 7) for the Zn·porph$^+$-Re(bipy)$^-$ charge transfer state are 1.99 eV and 2.25 eV for dimeric and pentameric species, respectively. It is worth noting that for **6** it lies significatively higher in energy with respect to the local S$_1$ state of the zinc-porphyrin (E(S$_1$) = 2.05 eV estimated from the fluorescence spectrum), whereas in the case of the dimeric species (**5** and **7**) it is practically isoenergetic with the S$_1$ state. Therefore, conversion from singlet porphyrin to the electron transfer state (eq. 1) is clearly uphill (ΔG = 0.25 eV, Table 7) for the pentanuclear **6** compound, and slightly allowed for the dimeric species (ΔG = -0.05 eV).

^{1}*Zn·porph-Re(bipy) → Zn·porph$^+$-Re(bipy)$^-$ eq. 1

The photophysics was studied by excitation at λ> 500 nm where the light is absorbed selectively by the zinc-porphyrin component. The most interesting observation is that, in all the systems studied, the typical fluorescence of the zinc-porphyrin unit is reduced in intensity and lifetime by the presence of the peripheral rhenium-bipy fragment(s) (Table 6).

118

The differences with respect to the model **10** are not large but clearly outside the experimental error. As far as potential quenching mechanism is concerned, two possibilities should be considered: (*i*) electron transfer quenching, (*ii*) heavy-atom effect.

Nanosecond time-resolved spectroscopy of the Zn·porphyrin-Re(I) dyads showed that the electron transfer quenching is relatively inefficient. Support for this conclusion comes also from the ultrafast absorption experiments where no evidence for formation of the charge transfer product was observed. Evidently, in the present systems, the driving force for the electron transfer (eq. 1) is too small so that the process is not fast enough to compete with the intersystem crossing in the porphyrin unit. Given the strong spin-orbit coupling of the rhenium atom, the most likely explanation for the fluorescence quenching in these systems is the spin-orbit perturbation (heavy atom effect) i.e. the enhancement by spin-orbit coupling of a formally spin-forbidden deactivation process of the singlet state of the porphyrin. In the free-base compounds **1** and **2**, where photoinduced electron transfer from excited porphyrin to rhenium unit is thermodynamically forbidden, we concluded that fluorescence quenching occurs through the heavy atom effect.[5] As discussed in our previous works,[5,12] this effect is a general feature for porphyrin arrays containing peripheral heavy atoms and its magnitude correlates with the number of metal centers connected to the porphyrin core. The observations that also in the present systems the fluorescence quenching is more efficient for pentameric with respect dimeric species, and that it is not affected by the solvent polarity, provide additional evidence for an heavy metal quenching mechanism. Remarkably, the increase of the extent of quenching ($\tau°/\tau$) with increasing the number of rhenium centers from one to four (see Table 6) is the same as that observed for the corresponding free base adducts.[5]

The quenching efficiency is substantially higher for the dyad **7** than for the isomeric dyad **5** (Table 6). Given that the Re-bipy fragment is closer to the porphyrin in **7** than in **5**, this result suggests an effect of the distance on the heavy atom-induced quenching.[13]

Recently Perutz and co-workers reported an interesting and detailed photophysical study of the dyad [*fac*-Re(CO)$_3$(3-pic)(bipy-Zn·porph)]$^+$ (**11**), where two molecular units very similar to those of our systems, a zinc-tetraphenylporphyrin and a rhenium(I)-bipy complex, are covalently linked via an amide bond.[3,4] A complete quenching of the porphyrin fluorescence was observed, together with a drastic shortening of the singlet porphyrin lifetime (24 ps measured in nitrile solvents by time resolved absorption experiments in the visible). In addition, an ultrafast photo-induced electron transfer process from the Zn·porphyrin to the Re(I)-bipy unit was revealed by time-resolved infrared spectroscopy.[4]

Despite the similarity of the molecular component units, the dyads **5** and **7** studied in the present work differ from **11** for the absence of photo-induced electron transfer. The reasons for this different behavior can be analyzed in terms of standard electron transfer theory. In the limit of weak-interaction (non-adiabatic regime), the rate constant for an electron transfer process is given by equation 2:

$$k = \frac{2\pi}{\hbar} H_{DA}{}^2 FCWD$$
<div align="right">eq. 2</div>

where H_{DA} is the electronic coupling between donor and acceptor and *FCWD* is the nuclear term (Franck-Condon weighted density of states) that accounts for the combined effects of the reorganizational energies and driving force. For **11** photoinduced electron transfer ($\Delta G = -0.24$ eV) is substantially more exergonic than for **5** and **7** (Table 7). Thus, as the processes fall in the activated region, electron transfer is predicted to be much faster for **11**. As far as the electronic factor is concerned, it is important to stress that the two types of systems differ in the connection of the two molecular components. At first sight, a better electronic factor could be expected for our systems, where the porphyrin unit is directly coordinated to the rhenium complex via the pyridyl group, whereas an amido bridge is interposed in **11**. However, in **11** the connection takes place at the bipy ligand, i.e. at the site involved in the reduction, whereas in the dyads **5** and **7** bipy is an ancillary ligand of rhenium center. Thus, the effects of the structural differences on the electronic factor are difficult to predict.

We found that, for **5** and **7**, addition of pyridine causes significant increase of the fluorescence quenching, shortening the lifetime from 900 to ca. 250 ps. More interestingly, the biphasic behavior observed by ultrafast spectroscopy experiments (the initial spectrum, taken immediately after the excitation pulse, evolved to a final spectrum through the formation of an intermediate state, Figure 11) is consistent with a picture in which the charge separated state (Zn·porph$^+$-Re(bipy)$^-$) is sufficiently close in energy to the singlet state (S_1) to allow a fast equilibration between them. Thus, in the presence of pyridine: *i*) first, an electron transfer process from the singlet of the zinc-porphyrin to the Re-bpy fragment takes place with a time constant of 20 ps, leading to the charge separated state; *ii*) second, the equilibrium mixture of singlet and charge separated states decays to the triplet state in 300 ps. This value is in good agreement with the lifetime measured in the emission experiment (250 ps). The absence of the absorption features of the charge separated state in the transient spectrum may be attributed to concomitant causes: *i*) at equilibrium the

population of the charge transfer state could be relatively small; *ii*) it is difficult to distinguish the spectrum of the porphyrin radical cation from that of the S_1 and T_1 excited states because they are very similar in the 450-650 region.[4,9]

Similar results were reported by Gust et al. who observed a drastic increase of the rate of intramolecular electron-transfer quenching in a zinc/free-base bis-porphyrin system upon addition of pyridine in CH_2Cl_2. They found that the axial coordination of pyridine to zinc lowers the oxidation potential of the zinc-porphyrin with consequent stabilisation of the interporphyrin charge transfer state and increase of the driving force for electron-transfer.[7] The same conclusions can be drawn in our case: the stabilization of charge separated state $(Zn \cdot porph^+ - Re(bipy)^-)$ caused by the presence of pyridine leads to an increase of the rate constant for the electron transfer that becomes competitive with the intersystem crossing for the deactivation of the singlet state.

7. 5 Conclusions

This study shows that, upon insertion of Zn into the porphyrin core, the photophysical behaviour of the adducts changes appreciably compared to the free-base analogues.[16] In particular, in the dyads **5** and **7** the charge separated state $Zn \cdot porph^+ - Re(bipy)^-$ decreases in energy so that it becomes almost isoenergetic with the excited singlet of the zinc-porphyrin unit. We had no evidence for electron transfer quenching in the dyads as such, whereas the addition of pyridine (that binds axially to zinc) led to a moderately efficient photo-induced electron transfer process. We can conclude that our dyads have a borderline energetic situation in which slight modifications in the porphyrin chromophore and/or in the coordination sphere of the Re(I)-bipy fragment may increase the energy difference between the two states and, as a consequence, the efficiency of the photo-induced electron transfer process. In perspective, both fragments can be separately fine-tuned through an appropriate functionalisation of the bipy ligand and/or of the *meso* phenyl rings of the porphyrin and then connected. This approach will lead to new conjugates that might be suited for being tested in photo-catalytic reactions.

We were also interested to assess how the photophysics of these systems is affected by the number of Re(I) fragments and by their relative positions with respect to the porphyrin chromophore. This work showed that an increase in the number of peripheral Re(I)-bipy fragments is detrimental in that it leads to an increase in the energy of the

charge-separated state and to a more efficient quenching of the porphyrin fluorescence by inter-system crossing. Finally, even though in the Zn·porph-Re(bipy) dyads the energetic for the electron-transfer process is not affected by the geometry of the porphyrin, the heavy-atom induced fluorescence quenching is substantially more efficient for the 3'MPyP than for the 4'MPyP dyad, i.e. it depends on the distance between the two fragments. This result suggests that future work should be focused on 4'PyPs-Re(I) conjugates.

7.6 References

[1] a) R. V. Slone, J. T. Hupp, *Inorg. Chem.* **1997**, *36*, 5422. b) K. E. Splan, M. H. Keefe, A. M. Massari, K. A. Walters, J. T. Hupp, *Inorg. Chem.* **2002**, *41*, 619. c) K. D. Benkstein, C. L. Stern, K. E. Splan, R. C. Johnson, K. A. Walters, F. W. M. Vanhelmont, J. T. Hupp, *Eur. J. Inorg. Chem.* **2002**, 2818. d) K. E. Splan, C. L. Stern, J. T. Hupp, *Inorg. Chim. Acta* **2004**, *357*, 4005. d) J. T. Hupp, *Struct. Bond.* **2006**, *121*, 145.

[2] a) B. Gholamkhass, H. Mametsuka, K. Koika, T. Tanabe, M. Furue, O. Ishitani, *Inorg. Chem.* **2005**, *44*, 2326. b) S. Sato, K. Koike, H. Inoue, O. Ishitani, *Photochem. Photobiol. Sci.* **2007**, 454.

[3] a) C. J. Aspley, J. R. Lindsay Smith, R. N. Perutz, *J. Chem. Soc., Dalton Trans.* **1999**, 2269. b) A. Gabrielsson, F. Hartl, J. R. Lindsay Smith, R. N. Perutz, *Chem. Commun.* **2002**, 950.

[4] A. Gabrielsson, F. Hartl, H. Zhang, J. R. Lindsay Smith, M. Towrie, A. Vlcek Jr, R. N. Perutz, *J. Am. Chem. Soc.* **2006**, *128*, 4253.

[5] M. Ghirotti, C. Chiorboli, M. T. Indelli, F. Scandola, M. Casanova, E. Iengo, E. Alessio, *Inorg. Chim. Acta* **2007**, *360*, 1121.

[6] E. Fleischer, A. M. Shachter, *Inorg. Chem.* **1991**, *30*, 3763.

[7] D. Gust, T. A. Moore, A. L. Moore, H. K. Kang, J. M. DeCraziano, P. A. Liddell, G. R. Seely, *J. Phys. Chem.* **1993**, *97*, 13637.

[8] F. Scandola, C. Chiorboli, A. Prodi, E. Iengo, E. Alessio, *Coord. Chem. Rev.* **2006**, *250*, 1471.

[9] K. M. Kadish, L. R. Shiue, R. K. Rhodes, L. A. Bottomley, *Inorg. Chem.* **1981**, *20*, 1274.

[10] a) J.-P. Collin, V. Heitz, J.-P. Sauvage, *Tetrahedron Lett.* **1991**, *32*, 5977. b) J.-P. Collin, A. Harriman, V. Heitz, F. Odobel, J.-P. Sauvage, *J. Am. Chem. Soc.* **1994**, *116*, 5679. c) A. Harriman, F. Odobel, J.-P. Sauvage, *J. Am. Chem. Soc.* **1995**, *117*, 9461. d) J.-P. Collin, J.-O. Dalbavie, V. Heitz, J.-P. Sauvage, L. Flamigni, N. Armaroli, V. Balzani, F. Barigelletti, I. Montanari, *Bull. Soc. Chim. Fr.* **1996**, *133*, 749. e) L. Flamigni, N. Armaroli, F. Barigelletti, V. Balzani, J.-P. Collin, J.-O. Dalbavie, V. Heitz, J.-P. Sauvage, *J. Phys. Chem. B* **1997**, *101*, 5936. f) L. Flamigni, F. Barigelletti, N. Armaroli, J.-P. Collin, J.-P. Sauvage, J. A. G. Williams, *Chem.-Eur. J.* **1998**, *4*, 1744.

[11] a) D. R. Striplin, G. A. Crosby, *Coord. Chem. Rev.* **2001**, *211*, 163. b) R. A. Kirgan, B. P. Sullivan, D. P. Rillema, *Top. Curr. Chem.* **2007**, *281*, 45.

[12] a) A. Prodi, M. T. Indelli, C. J. Kleverlaan, F. Scandola, E. Alessio, T. Gianferrara, L.G. Marzilli, *Chem. Eur. J.* **1999**, *5*, 2668. b) E. Alessio, S. Geremia, S. Mestroni, E. Iengo, I. Srnova, M. Slouf, *Inorg. Chem.* **1999**, *38*, 869.

[13] P. W. Abegg, T.-K. Ha, *Mol. Phys.* **1974**, *27*, 763.

Chapter 8

Photoswitching of Fluorescence by Intramolecular Electron Transfer in a Diarylethene-Perylene Bisimide Photochromic System.$^\phi$
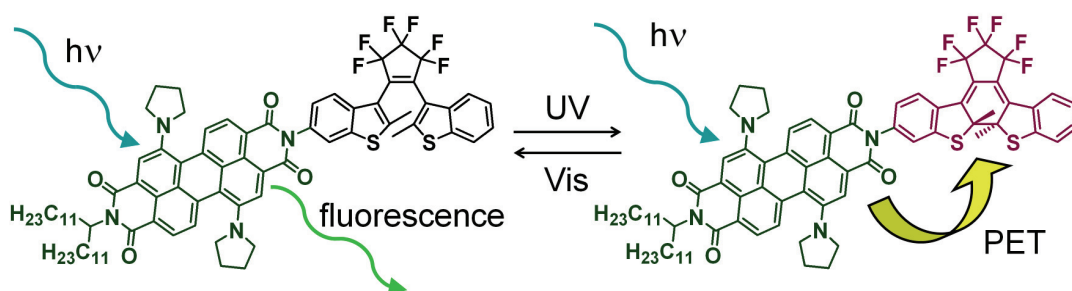
A new prototype optical memory system based on a photochromic diarylethene-perylene bisimide dyad.

The work described in this chapter is the result of a collaboration between the Photochemistry Group at the Department of Chemistry of University of Ferrara (Ferrara, Italy), where i have done my Ph.D., and the Group of Prof. Frank Würthner at the Institute for Organic Chemistry, University of Würzburg (Würzburg, Germany).

8.1 Introduction

Photochromic compounds change their optical and electronic properties upon irradiation due to reversible photochemical reaction and, therefore, they are suitable for manifold tasks.[1] Very recently, application of photochromic compounds for the imaging of living cells by single-molecule photoswitching has been demonstrated.[2] In the past years, diarylethenes (DAEs) have evolved as highly promising photochromic molecules for optical data storage applications because of their durable persistency and thermal irreversibility of closed and open forms.[3]

For DAEs linked to fluorescent dyes, photoswitching of fluorescence has been demonstrated even on the single-molecule level.[4] In these systems, the read-out is based on the fluorescence observed for the open form of diarylethene (DAE_O), whilst fluorescence quenching from the excited dye to the closed form of the diarylethene (DAE_C) takes place by an intramolecular Förster resonance energy transfer (FRET). The drawback of such energy-transfer-based memory systems is that the FRET induces photochromic cycloreversion during reading, and thus destroys the memory.

Such destructive read-out may be circumvented by switching of fluorescence through intramolecular photoinduced electron transfer (PET),[5] if the open and the closed form of the photochromic moieties possess different redox properties.[6] The optimal case would be: (i) if the electron transfer involves oxidation of the dye and reduction of the DAE, as electrochemically induced ring opening/closure has been reported to occur upon oxidation of diarylethenes[7] (in principle, therefore, destructive read-out could not be ruled out with this type of electron transfer quenching) and (ii) the solvent-dependent driving force for PET is exergonic for the DAE_C^--Dye^+ but not for DAE_O^--Dye^+ charge transfer (CT) state (Figure 1).
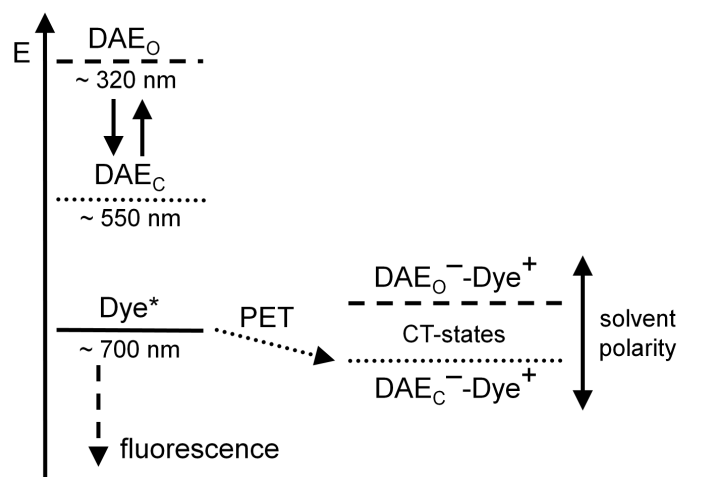
Figure 1. Schematic energy diagram for the fluorescent open form (dashed line) and the non-fluorescent closed form (dotted line) DAE and CT states of DAE-Dye conjugate.

Furthermore, the emission spectrum of the dye should not overlap with the absorption spectrum of any isomer of DAE as in FRET based systems, but needs to be at a higher wavelength. This would facilitate writing, erasing and reading data with light sources of three different wavelengths without destructive read-out.

A photochromic DAE system based on above-mentioned optimized concept is to our knowledge not known, altough the concept has recently been suggested.[8] Thus, we have designed the photochromic system **1o** based on a perfluorinated DAE derivative and a bay-substituted perylene bisimide (PBI) dye (Scheme 1). The fluorescent 1,7-dipyrrolidinylperylene bisimide was chosen because of its low oxidation potential and its absorption maximum in the NIR region, *i.e.*, at around 700 nm.[9]
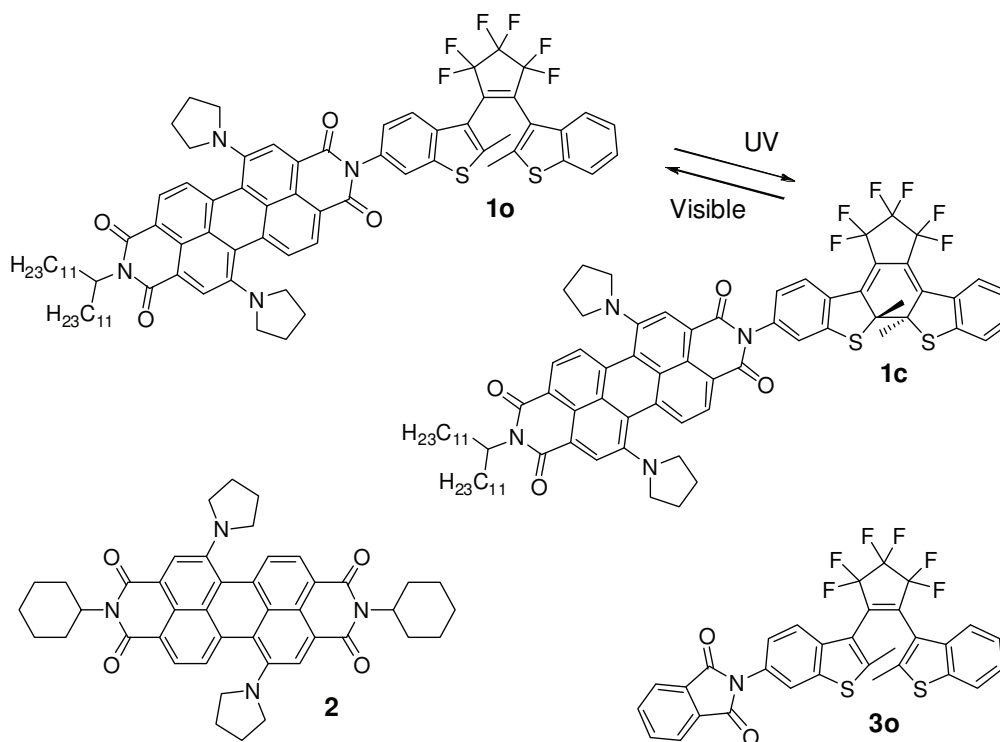
Scheme 1. Photochromic compounds **1o** and **1c**, and reference compounds perylene bisimide dye **2** and DAE **3o**.

8.2 Experimental section

The syntheses and characterization of the compounds discussed in this chapter were performed by Martin Berberich and Ana-Maria Krause in the research group of Prof. Frank Würthner at the Institute for Organic Chemistry, University of Würzburg (Würzburg, Germany). Details can be found in M. Berberich, A.-M. Krause, M. Orlandi, F. Scandola, F. Würthner. *Angew. Chemie Int. Ed.* **2008**, *47*, 6616.

Martin Berberich and Ana-Maria Krause also performed fluorescence quantum yields determination and cyclic voltammetry experiments.

See Chapter 2 for details on spectroelectrochemical and photophysical measurement apparatus and procedures.

8.3 Results and discussion

Compound **1o** is switchable between two photo-stationary states (PS). Upon irradiation with UV light ($\lambda_{max} = 350$ nm) a photostationary state with 66 % of the closed form of the PBI-DAE conjugate **1c** (Scheme 1) is obtained and the latter could be isolated by subsequent column chromatography. The open form can be regenerated almost quantitativly (99 %) by irradiating of a solution of the closed form with visible light ($\lambda > 400$ nm).

The fluorescence quantum yields for **1o** and **1c** were determined in solvents of different polarity with dielectric constants (ε_r) ranging from 2.24 (tetrachloromethane) to 36.71 (dimethylformamide) and divided by the quantum yield of the reference PBI **2** without a DAE moiety (Figure 2 and Table 1). In low polarity solvents such as chloroform ($\varepsilon_r = 4.89$), the quantum yields of **1o** and **1c** are nearly identical with that of the reference dye **2**, which is indicative for no fluorescence quenching by DAE_C or DAE_O moiety. Interestingly, with increasing solvent polarity, quantum yields of **1o** and **1c** differ significantly and in highly polar solvent dimethyl formamide almost complete quenching for closed form **1c** was observed. Fluorescence quenching by FRET from the dye to the closed form of the DAE can be excluded as a deactivation path. Thus, increasing fluorescence quenching for **1c** with increasing solvent polarity is highly indicative for a preferential PET from the dye to the closed form of DAE.

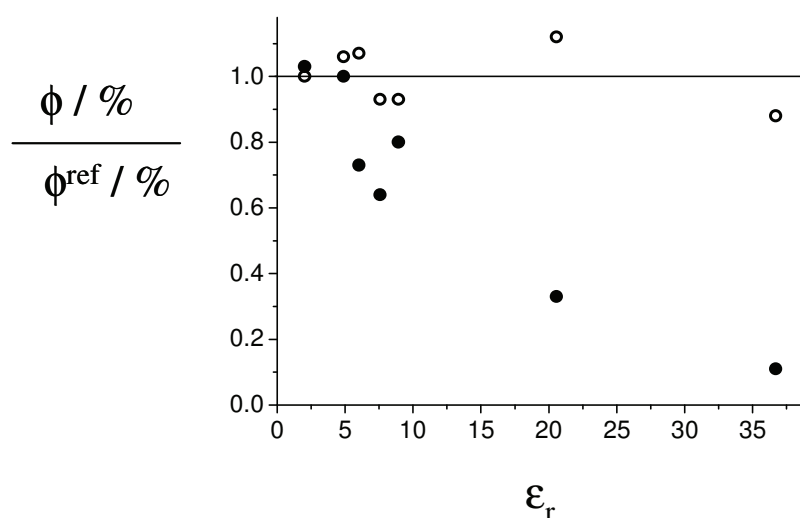**Figure 2.** Fluorescence quantum yields of **1o** and **1c** (ϕ) divided by the quantum yield of reference perylene bisimide **2** (ϕ^{ref}) without DAE moiety as a function of dielectric constants of solvents; open form (○), closed form (●).

solvent	ε_r	$\mathbf{1o}\ \Phi_{fl}$	$\mathbf{1c}\ \Phi_{fl}$	$\mathbf{2}\ \Phi_{fl}$
tetrachloromethane	2.24	39 %	40 %	39 %
chloroform	4.89	18 %	17 %	17 %
ethyl acetate	6.02	16 %	11 %	15 %
THF	7.58	13 %	9 %	14 %
dichloromethane	8.93	14 %	12 %	15 %
acetone	20.56	11 %	3 %	10 %
DMF	36.71	8 %	< 1 %	9 %

Table 1. Fluorescence quantum yields of **1o**, **1c** and **2** in different solvents.

The Gibbs free energy ($\Delta G°$) for an intramolecular charge-separated state in a covalently bonded donor-acceptor system can be estimated by the Rehm-Weller equation (1), where $E_{ox}(D)$ and $E_{red}(A)$ are the respective first oxidation potential of the donor perylene bisimide and first reduction potential of the acceptor DAE.

$$\Delta G^0 = e[E_{ox}(D) - E_{red}(A)] - E_{00} - \frac{e^2}{4\pi\varepsilon_0\varepsilon_S R_{CC}} - \frac{e^2}{8\pi\varepsilon_0}\left(\frac{1}{r^+} + \frac{1}{r^-}\right)\left(\frac{1}{\varepsilon_{ref}} - \frac{1}{\varepsilon_S}\right) \tag{1}$$

E_{00} signifies the spectroscopic excited state energy, while R_{CC} is the distance between the centers of the donor and acceptor moieties. The effective ionic radii of the donor radical cation and acceptor radical anion are labelled as r^+ and r^-, respectively. The dielectric constant of the reference solvent used in electrochemistry is denoted as ε_{ref}, while ε_S is the respective solvent dielectric constant.[10]

Compounds **1o** and **1c** exhibit the characteristic UV/Vis absorption spectra of 1,7-dipyrrolidinylperylene bisimides with an absorption maximum at around 700 nm. For **1c** some additional bands that are attributed to the closed form of DAE (in particular, a broadened absorption band between 450 and 550 nm, see Figure 3) could be observed. From the UV/Vis and fluorescence spectra in dichloromethane a S_0-S_1 excitation energy of 1.71 eV was estimated for **1o** and **1c**.
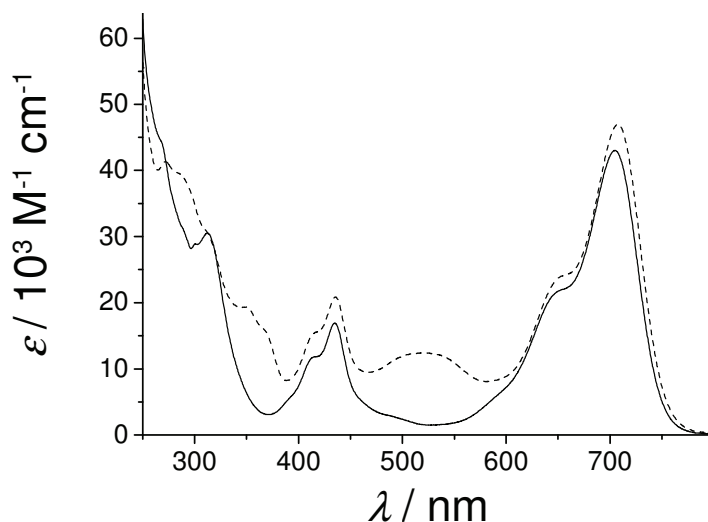
Figure 3. UV/Vis spectra of **1o** (solid line) and **1c** (dashed line) upon irradiation with UV light (λ_{max} = 350 nm) in dichloromethane.

The redox potentials for **1o** and **1c**, and reference compounds (see Table 2) were obtained by cyclic voltammetry measurements in dichloromethane.

	E_{red} (X^{3-}/X^{2-})	E_{red} (X^{2-}/X^-)	E_{red} (X^-/X)	E_{ox} (X/X^+)	E_{ox} (X^+/X^{2+})	E_{ox} (X^{2+}/X^{3+})
2	--	−1.49	−1.39	0.18	0.33	--
1o	--	−1.48	−1.36	0.22	0.36	--
1c	−1.60	−1.43	−1.31	0.21	0.35	1.00
3o	--	--	−1.98	--	--	--
3c	--	−1.90	−1.54	0.95	--	--

All measurements at 298 K, 0.1 M TBA(PF$_6$) as electrolyte, Pt disc as working electrode, Ag/AgCl as reference electrode, Pt wire as counter electrode. Ferrocene (0.46 V vs. SCE)[11] as internal standard.

Table 2. Redox potentials of compounds **1o**, **1c**, PBI **2**, **3o** and **3c** (in V).

The cyclic voltammogram of **1o** is identical with that of the reference dye **2**. Accordingly, additional redox processes due to DAE$_O$ moiety are apparently not given within the available potential window. The first half-wave oxidation potentials of the PBI moiety were observed at 0.22 V and 0.21 V for **1o** and **1c**, respectively. The closed form **1c** showed

additional waves for the DAE moiety in compliance with the reference DAE **3c** compound bearing a phthalic imide residue. The respective first half-wave reduction potential for the open form of DAE **3o** was observed at –1.98 V and that for **1c** at –1.60 V. From optimized[1] geometries of **1o** and **1c** conjugates, donor-acceptor distances of 1.32 nm and 1.24 nm, respectively, were estimated.

Since all our values were determined in dichloromethane, the solvent related term in the Rehm-Weller equation can be neglected for the present case, and by applying the obtained data in this equation, a $\Delta G°$ value of 0.37 eV for **1o** and a slightly exergonic value of –0.03 eV for **1c** in dichloromethane can be calculated. These energy values imply that the electron transfer process, clearly endergonic for the open form, is thermodynamically feasible only for the closed form in dichloromethane. In more polar solvents, such as, e.g. dimethyl sulfoxide (ε_r = 46.68), the CT state for **1c** (DAE_C^{-}-PBI^{+}) becomes more stable and PET is more likely to take place (an approximate value for the driving force, calculated with average molecular radii of ca. 7 Å in the Rehm-Weller equation, is ca. –0.15 eV).

Fluorescence lifetime measurements in dimethyl sulfoxide provided a value of 1.9 ns for **1o** and 0.23 ns for **1c**, revealing that the $S_1{\rightarrow}S_0$ decay is enhanced by ring closure (see Table 3).

solvent	open form (τ/ ns, emission)	closed form (τ/ ns, emission)	closed form (τ/ ps, trans. abs.)
DMF	2.1	ca. 0.29	242
DMSO	1.9	ca. 0.24	228

Table 3. Lifetime of **1o** and **1c** determined by emission and ultrafast absorption spectroscopy in dimethyl formammide (DMF) and dimethyl sulfoxide (DMSO).

Photochromic compounds **1o** and **1c** were also investigated by femtosecond transient absorption spectroscopy in dimethyl sulfoxide by excitation at 680 nm ($S_0{\rightarrow}S_1$ transition of the perylene bisimide dye). For **1o**, an intense bleaching owing to the depopulation of the ground state molecules between 650 and 770 nm and the stimulated emission between 770 and 800 nm is observed as a combined negative signal (Figure 4) that decays with an

---

[1] The geometries of **1o** and **1c** were optimized using MM3 force field with the parameter given in CaChe quantum CaChe workspace 5.04.

approximate lifetime of ca. 1.5 ns. **1c** shows the same qualitative behavior (Figure 5), but with a greatly shortened decay lifetime of 230 ps. The fact that the quenching of the dye S_1 state is not accompanied by a distinctive build-up of electron transfer transient species suggests that charge separation is slower than charge recombination and is the rate-determining step in *PBI-DAE$_C$ deactivation.
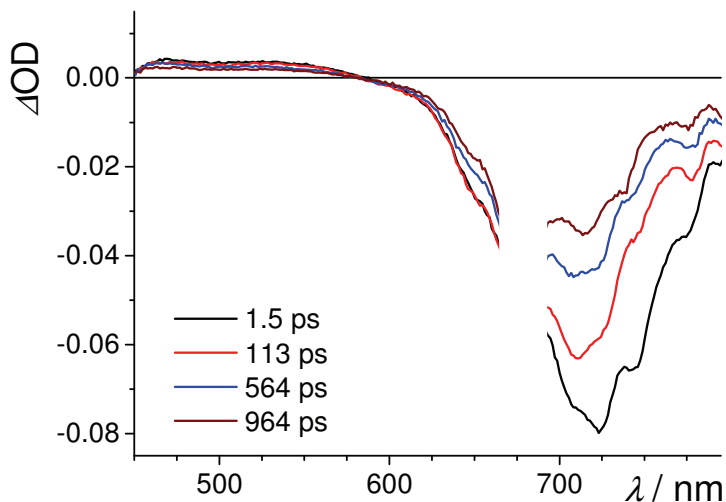

Figure 4. Ultrafast transient absorption spectra in dimethyl sulfoxide of **1o**. λ_{xc} = 680 nm.
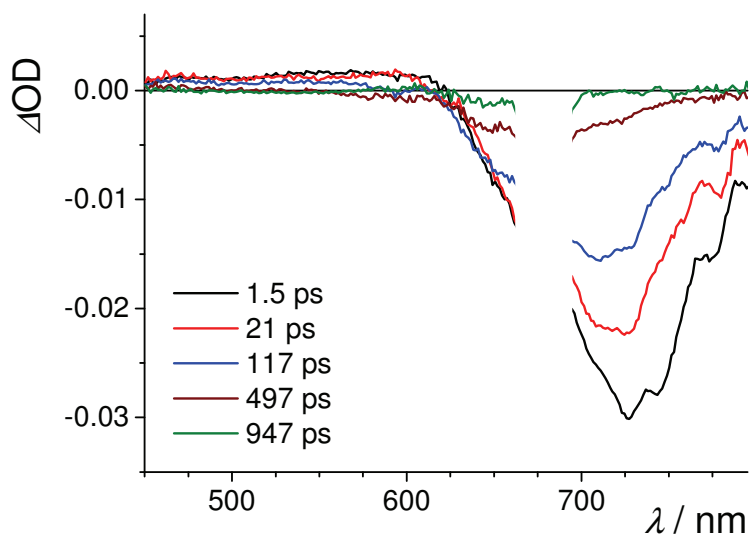

Figure 5. Ultrafast transient absorption spectra in dimethyl sulfoxide of **1c**. λ_{xc} = 680 nm.

A clear evidence for the occurrence of photoinduced electron transfer is obtained in femtosecond transient experiments by excitation at 400 nm ($S_0 \rightarrow S_2$ transition of the dye). In this case, while the behavior of **1o** is virtually identical to that of Fig. 4 (see Figure 6), an

additional short-lived positive absorption band with a maximum centered at 613 nm is observed for **1c** (Figure 7).
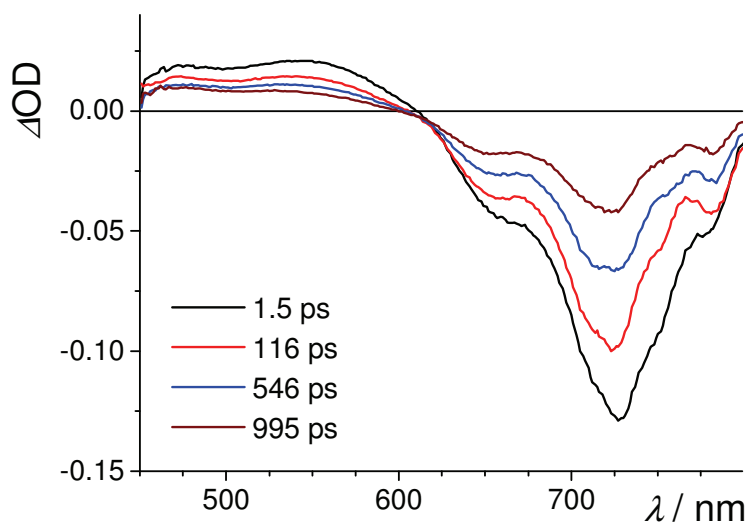

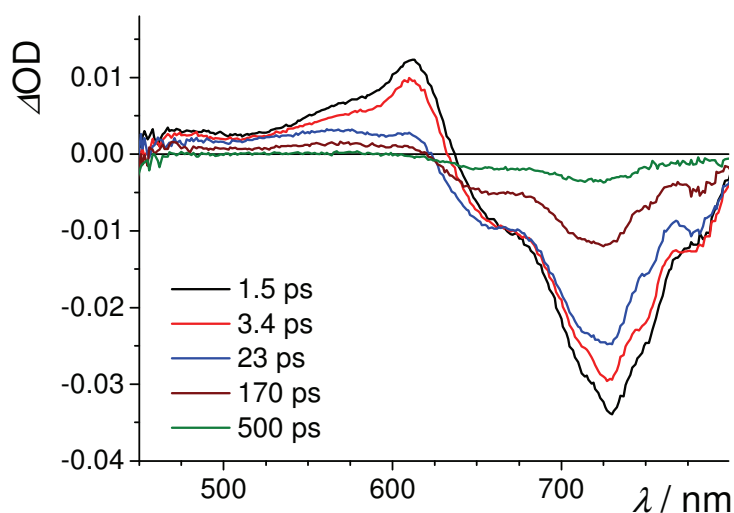**Figure 6.** Ultrafast transient absorption spectra in dimethyl sulfoxide of **1o**; λ_{exc} = 400 nm.

Figure 7. Ultrafast transient absorption spectra in dimethyl sulfoxide of **1c**; λ_{exc} = 400 nm.

The latter can be assigned to the radical cation of 1,7-pyrrolidinylperylene bisimide moiety,[12] as verified by spectroelectrochemistry (Figure 8). In this case, population of the $DAE_C^-\text{-}PBI^+$ state from the upper S_2 state of the dye, rather than from S_1, is fast enough as to lead to appreciable transient accumulation of the product.
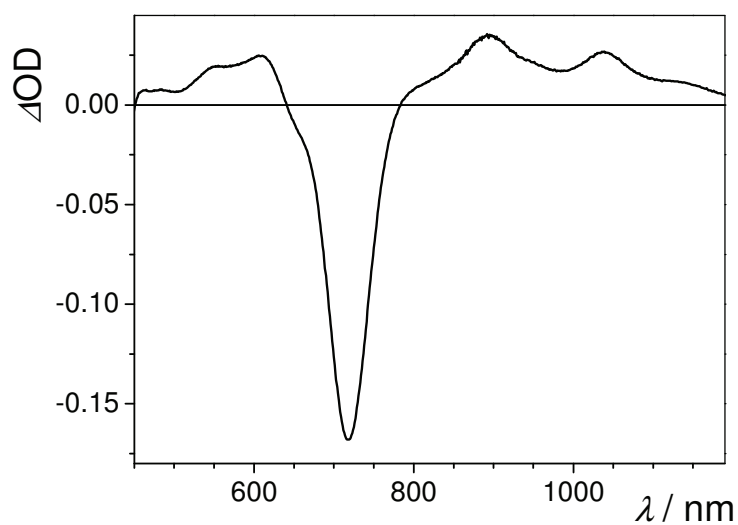
Figure 8. Differential spectrum of reference dye **2** (one-electron oxidized form) upon oxidation in DMSO (0.5×10^{-3} M, 0.1 M Bu$_4$NPF$_6$).[m]

8.4 Conclusions

In summary, the newly designed photoswitch is effective in polar solvents where an intramolecular electron transfer from the excited PBI dye to the closed form of DAE, but not to the open form, takes place, leading to fluorescence quenching by PET mechanism. Thus, a prototype photochromic switch for non-destructive read-out optical memory systems is introduced.

---

[m] Notably, all maxima for the radical cation of **2** are shifted to longer wavelengths compared to the values published for similar compounds in dichloromethane.[12]

8.5 References

[1] a) M. Irie, T. Mrozek, J. Daub, A. Ajayaghosh, Y. Yokoyama, in *Molecular Switches* (Ed. B. L. Feringa), Wiley-VCH, Weinheim, **2001**, p. 37–121; b) *Photochromism: Molecules and Systems* (Eds. H. Dürr, H. Bouas-Laurent), Elsevier, New York, **1990**; c) *Molecular Devices and Machines: A journey into the Nano World* (Eds. V. Balzani, A. Credi, M. Venturi), Wiley-VCH, Weinheim, **2003**; d) B. L. Feringa, *J. Org. Chem.* **2007**, *72*, 6635–6652.

[2] J. Fölling, V. Belov, R. Kunetsky, R. Medda, A. Schönle, A. Egner, C. Eggeling, M. Bossi, S. W. Hell, *Angew. Chem.* **2007**, *119*, 6382–6386; *Angew. Chem. Int. Ed.* **2007**, *46*, 6266–6270.

[3] a) M. Irie, *Chem. Rev.* **2000**, *100*, 1685–1716; b) H. Tian, S. J. Yang, *Chem. Soc. Rev.* **2004**, *33*, 85–97; c) H. Tian, S. Wang, *Chem. Commun.* **2007**, 781–792.

[4] a) M. Irie, T. Fukaminato, T. Sasaki, N. Tamai, T. Kawai, *Nature* **2002**, *420*, 759–760; b) T. Fukaminato, T. Sasaki, T. Kawai, N. Tamai, M. Irie, *J. Am. Chem. Soc.* **2004**, *126*, 14843–14849; c) T. A. Golovkova, D. V. Kozlov, D. C. Neckers, *J. Org. Chem.* **2005**, *70*, 5545–5549; d) G. Jiang, S. Wang, W. Yuan, L. Jiang, Y. Song, H. Tian, D. Zhu, *Chem. Mater.* **2006**, *2*, 235–237.

[5] a) *Supramolecular Photochemistry* (Eds. V. Balzani, F. Scandola), Ellis Horwood, New York, **1991**; b) *Electron Transfer in Chemistry*, (Ed. V. Balzani), Wiley-VCH, Weinheim, **2001**; c) *Fundamentals of Photoinduced Electron Transfer* (Ed. G. J. Kavarnos), VCH Publishers Inc, New York, **1993**; d) N. Mataga, H. Chosrowjan, S. Taniguchi, *J. Photochem. Photobiol. C: Photochem. Rev.* **2005**, *2*, 37–79; e) D. M. Guldi, *Chem. Soc. Rev.* **2002**, *31*, 22–36; f) J. M. Endtner, F. Effenberger, A. Hartschuh, H. Port, *J. Am. Chem. Soc.* **2000**, *122*, 3037–3046.

[6] a) A. J. Myles, N. R. Branda, *J. Am . Chem. Soc.* **2001**, *123*, 177–178; b) Y. Terazono, G. Kodis, J. Andréasson, G. Jeong, A. Brune, T. Hartmann, H. Dürr, T. A. Moore, A. L. Moore, D. Gust, *J. Phys, Chem. B* **2004**, *108*, 1812–1814; c) F. M. Raymo, M. Tomasulo, *Chem. Soc. Rev.* **2005**, *34*, 327–336.

[7] a) T. Koshido, T. Kawai, K. Yoshino, *J. Phys. Chem.* **1995**, *99*, 6110–6114; b) A. Peters, N. R. Branda, *J. Am. Chem. Soc.* **2003**, *125*, 3404–3405; c) A. Peters, N. R. Branda, *Chem. Commun.* **2003**, 954–955; d) B. Gorodetsky, H. D. Samachetty, R. L. Donkers, M. S. Workentin, N. R: Branda, *Angew. Chem.* **2004**, *116*, 2872–2875; *Angew. Chem. Int. Ed.* **2004**, *43*, 2812–2815; e) S. Fraysse, C. Coudret, J. P. Launay, *Eur. J. Inorg. Chem.* **2000**,

1581–1590; f) X. H. Zhou, F. S. Zhang, P. Yuan, F. Sun, S. Z. Pu, F. Q. Zhao, C. H. Tung, *Chem. Lett.* **2004**, *33*, 1006–1007; g) W. R. Browne, J. J. D. de Jong, T. Kudernac, M. Walko, L. N. Lucas, K. Uchida, J. H. van Esch, B. L. Feringa, *Chem. Eur. J.* **2005**, *11*, 6414–6429; h) W. R. Browne, J. J. D. de Jong, T. Kudernac, M. Walko, L. N. Lucas, K. Uchida, J. H. van Esch, B. L. Feringa, *Chem. Eur. J.* **2005**, *11*, 6430–6441; i) G. Guirado, C. Coudret, M. Hliwa, J. P. Launay, *J. Phys. Chem. B* **2005**, *109*, 17445–17459; j) Y. Moriyama, K. Matsuda, N. Tanifuji, S. Irie, M. Irie, *Org. Lett.* **2005**, *7*, 3315–3318.

[8] a) Y. Odo, T. Fukaminato, M. Irie, *Chem. Lett.* **2007**, *2*, 240–241, b) M. Berberich, Master Thesis, University of Würzburg, Würzburg (Germany), **2007**.

[9] F. Würthner, *Chem. Commun.* **2004**, 1564–1579.

[10] A. Z. Weller, *Z. Phys. Chem.* **1982**, *133*, 93–98.

[11] Connelly, N. G.; Geiger, W. E. *Chem. Rev.* 1996, *96*, 877 -910.

[12] a) A. S. Lukas, Y. Zhao, S. E. Miller, M. R. Wasielewski, *J. Phys. Chem. B* **2002**, *106*, 1299–1306; b) M. J. Ahrens, M. J. Tauber, M. R. Wasielewski, *J. Org. Chem.* **2006**, *71*, 2107–2114.

List of Publications

M. Orlandi, R. Argazzi, A. Sartorel, M. Carraro, G. Scorrano, M. Bonchio, F. Scandola.
Chem. Comm. **2010**. In press.

M. T. Indelli, C. Chiorboli, M. Ghirotti, M. Orlandi, F. Scandola, H. J. Kim, H.-J. Kim.
J. Phys. Chem B. **2010**. ASAP Article.

D. Streich, Y. Astuti, M. Orlandi, L. Schwartz, R. Lomoth, L. Hammarström, S. Ott.
Chem. Eur. J., **2010**, *16*, 60.

M. Casanova, E. Zangrando, E. Iengo, E. Alessio, M. T. Indelli, F. Scandola, M. Orlandi.
Inorganic Chemistry, **2008**, 47, 22, 10407.

M. Berberich, A.-M. Krause, M. Orlandi, F. Scandola, F. Würthner.
Angew. Chemie Int. Ed. **2008**, *47*, 6616.

Acknowledgements

Sincere gratitude goes to all the people who spent their time on the projects described in this thesis: it's been a pleasure working with you all.

Then, i would like to express special gratitude to the following people:

My supervisor, Prof. Franco Scandola. His enormous reservoir of patience and ability in handing down a precious wealth of knowledge sometimes made me feel like Dante following Virgil in a wondrous adventure.

Dr. Sandro Fracasso, The Wise Old Man, his feet are both on the ground but his head is often well above the fog that surrounds mine (or at least he pretends it).

Dr. Roberto Argazzi, The Wise Very Old Man, for always being patient the countless times i stepped into his office and for teaching me how to deal with The Strange Machinery in the lab.

Dr. Marcella Ravaglia, for tons of discussions on every possible subject, often ending with a laugh and, unfortunately, for granting me the rights upon her old desk.

Prof. Maria Teresa Indelli for all her help and in particular for keeping under control the entrophy levels in the lab.

Dr. Claudio Chiorboli, in particular for teaching me some very useful practical sense.

All the people at the Chemistry Department at University of Ferrara, for enduring this annoying guy wandering in their corridors.

Prof. Leif Hammarstrom for giving me the opportunity to spend a training period in his group, an experience not only very important for me but also funny and rewarding.

Dr. Erik Goransson, for all the keen and pointed discussions we have on everything and for all the experiences we share, as friends and colleagues.

Dr. Daniel Streich, for his companionship during my period in Uppsala and for sharing with me his enthusiasm.

All the people at the Photochemistry and Molecular Sciences Department at Uppsala University, they make the department a nice and friendly place.

Dr. Elisabetta Iengo, for a collaboration enriched by advice, exchange of toughts and good time spent toghether.

To my friends, for being able of knotting ropes so tight that they resist time and space.

A tutta la mia grande famiglia, per avermi sempre supportato e spesso sopportato (...Laura).

A mio nonno Sergio e mio zio Liviano, per avermi insegnato a fare le cose fatte bene, anche se non sempre ci riesco.

Finally, to my wife Angela, we walk toghether and every step is a joy.